

Master's thesis

NTNU
Norwegian University of
Science and Technology
Faculty of Engineering, Science and Technology
Department of Marine Technology

Kristian Dahl

Hybrid Model Testing of Deep- water Moored Structures by Active Control of Line Forces

Trondheim, June, 2010

THESIS DESCRIPTION SHEET

Name of the candidate:	Kristian Dahl
Field of study:	Marine control systems
Thesis title (Norwegian):	Hybrid modelltesting ved aktiv styring av simulerte strengkrefter for djupvannsførtøydde strukturer.
Thesis title (English):	Hybrid model testing of deep-water moored structures by active control of simulated line forces.

Background

The main reason for use of model tests in the design of floating production units is the need for reliable prediction of motions caused by the combined actions of waves, wind, and current. Since wind and higher order wave effects give load frequencies in the same regime as in-plane motion eigenfrequencies, damping and all nonlinear effects should be adequately represented in the model. Mooring lines and risers will represent nonlinear restoring forces and also add to inertia and damping. These elements must hence be included.

The model scale for hull and waves should preferably not be smaller than 1:40. A test facility with 10 meters water depth will hence have a full scale depth limitation of 400 meters, while water depth for offshore oil production now has passed 2000 meters. In order to have a reasonable scale for the floater hull on this water depth, the mooring and riser system must be truncated. The challenge is hence to make a truncated model that has identical static and dynamic properties as for the real system.

The idea to be investigated in this project is to design a test system using a control system that induces correct resulting forces and moments from simulated mooring lines, in real time for all degrees of freedom of motion, onto the model vessel. This multidiscipline project requires contributions from hydrodynamics, structural dynamics, and automatic control.

Work description

From the student project, fall 2009, it was concluded to use a motor-winch-wire setup for actuating the simulated line forces. Focus has been on the motor-winch-wire control system and the following:

1. Make an assessment of bandwidths and necessary sampling frequency of the continuous time responses for a vessel in model scale due to force influence on the vessel.
2. Development of a simulation model of a simplified 1-DOF dynamic system, consisting of a mass and a spring corresponding to the mass and restoring force of a realistic model ship, where the mass-spring are influenced by a typical regular wave motion.
3. Development of a simulation model of the electrical motor, including realistic motor parameters.
4. Perform engineering and procurement of parts for the experimental system.
5. Development of control laws for the motor-winch-wire system.
6. Set up of a 1-DOF experimental system and testing of the motor control on the simplified mass-spring system for the vessel, according to typical reference sequences.
7. An assessment of pros and cons of the test system, including an analysis of the closed-loop performance, assessment of bandwidths, and time constraints.
8. Write the thesis report, including conclusions and proposed future work.

Guidelines

The scope of work may prove to be larger than initially anticipated. By the approval from the supervisor, described topics may be deleted or reduced in extent without consequences with regard to grading.

The candidate shall present his personal contribution to the resolution of problems within the scope of work. Theories and conclusions should be based on mathematical derivations and logic reasoning identifying the various steps in the deduction.

The report shall be organized in a rational manner to give a clear exposition of results, assessments, and conclusions. The text should be brief and to the point, with a clear language. The report shall be written in English (preferably US) and contain the following elements: Abstract, acknowledgements, table of contents, main body, conclusions with recommendations for further work, list of symbols and acronyms, references and (optional) appendices. All figures, tables, and equations shall be numerated. The original contribution of the candidate and material taken from other sources shall be clearly identified. Work from other sources shall be properly acknowledged using a Harvard citation style (e.g. DCU). Any plagiarism is taken very seriously by the university, and any such practice will have consequences.

The thesis shall be submitted in 2 printed copies, each signed by the candidate. The final revised version of this project description must be included. The report must appear in a bound volume or a binder. Computer code and a PDF version of the report should be included electronically.

A 15 min. presentation (conference style) on your main results is desired to be delivered upon request.

Start date: 1 February, 2010 **Due date:** As specified by administration.

Supervisor: Professor Roger Skjetne

Co-advisor(s): Professor Carl M. Larsen and affiliated professor Anne Marthine Rustad.

Abstract

Increased activity in deeper water areas, in connection with oil and gas exploration, has resulted in a steadily increased demand for model testing technology to predict reliable behavior of floating offshore structures at deep water. Common model testing technology, developed for more shallow water, must be modified to meet the challenges that deep water model testing poses. The approach using active control of line forces to replace the mooring and riser system seems promising. Actuators should induce the same resulting forces as calculated by numerical methods on to the vessel in real time.

This master's thesis has its focus on the development of an experimental setup to investigate the performance of the control system inducing desired forces on to a simplified vessel model. To simplify the complexity with an experiment using a vessel moving in 6 degrees of freedom (DOF), a simplified vessel model with motion only in the heave direction is considered. Active control of the line force connected to the vessel, moving only in heave direction, is launched to investigate if the actuator or motor-winch system, manage to induce the correct calculated mooring force for a measured heave motion.

Necessary procurement of parts to the experimental setup has been obtained. Reasonable values for the maximum and minimum top tension for one mooring line has been used to find an appropriate actuator. A Faulhaber electrical motor was chosen to meet the specifications. The drive electronics controlling the electrical motor has a wide variety of control options, and control of the motor shaft torques, necessary to obtain desired forces, is possible.

A mathematical model describing the experimental setup was developed. A model of the DC motor dynamics and the mass dynamics are mathematically derived. The unknown parameters in the model have been found using measurement data from experiment. The measurement data are established using a pretensioned spring connected to the DC motor shaft, as well as a freely running shaft.

In the experiments two test cases are considered. In test case one a spring and line, representing the active mooring line, is connected in-between the vessel model, or oscillating actuator, and a motor-winch system. The motor-winch, or DC motor, will then try to pull the line and spring till it reaches the desired reference. The measured heave motion to the oscillating system is utilized to calculate the mooring force references, the active mooring line will then try to induce the same forces as calculated. The calculated forces are only available for a given heave motion.

A second test case is performed with a vessel model represented as a mass. The mass, or vessel, is connected to the oscillating system actuator with a spring. The oscillating system actuator will represent the wave motion, while the spring should represent the water plane stiffness. A rope, or line, connected in-between the mass and the motor-winch system will represent the active mooring line. Different sinusoidal references, as well as piecewise constant signals are used to test if the active mooring line is able to induce the desired forces on to the mass real time.

The results show that for the given heave motion the motor-winch setup will be able to actuate the desired mooring line forces on to the oscillating body. Sinusoidal force references are also possible to follow. There is however a constraint in the frequency, and a high

oscillating system frequency will be a limitation. By decreasing the oscillating frequency less noise in the measured signal will occur.

To avoid a lot of noise in the measured forces filtering the signal was necessary. An observer has been developed to remove this noise. The filtered signal (estimated force) can then be used as feedback to the controller.

A vessel model considered in three DOF is used to find an appropriate sampling frequency. The real time response measurements to the vessel need to be sampled in order to calculate desired mooring forces. A study is therefore conducted to find the bandwidth, or highest frequency, in the system to conclude which sampling frequency that is needed to recreate the response signals without loss of information. The results show that 50 Hz sampling frequency will be necessary to recreate the continuous time signals for the specific case considered.

Acknowledgment

This master's thesis has been carried out within the Faculty of Engineering Science and Technology under the Department of Marine Technology (IMT) at the Norwegian University of Science and Technology (NTNU).

This thesis work has been supervised by Professor Roger Skjetne, Professor Carl M. Larsen and affiliated Professor Anne Marthine Rustad. My main supervisor, Roger Skjetne, deserves a special thank for his inspiration and enthusiastic encouragement, and his helpful feedback and guidance during our meetings and discussions. I would also like to thank Anne Marthine for her motivation, positive enthusiasm and helpful feedback. Finally, I would like to thank Carl M. Larsen for his valuable input this is much appreciated.

The aid and assistance offered by Torgeir Wahl during the experimental testing were essential for the outcome of the experiments. Much of the installation of the equipment and setup could easily turned out different without his helpfulness.

I would also like to thank the staff working at MARINTEK and my Co. student Stian Garlid for their help and fruitful discussions.

Kristian Dahl
Trondheim 14.06.2010

Notation

Characters:

Roman

\mathbf{M}_{rb} Mass matrix
 \mathbf{M}_a Added mass matrix
 \mathbf{D} Potential damping matrix
 \mathbf{G} Elastic stiffness matrix
 \mathbf{f} Force vector
 x_b longitudinal axis (directed from aft to fore)
 z_b transversal axis (directed to starboard)
 u surge velocity
 w heave velocity
 q angular velocity in pitch
 X force input surge
 Z force input heave
 M moment in pitch
 D draught
 L length
 B breath
 u_{ai} voltage
 f_{ref} reference force
 T_s settling time
 z vertical motion
 A_{33} hydrodynamic added mass in heave
 B_{33} linear damping coefficient
 C_{33} spring coefficient
 g gravitational constant
 f_m measured force
 \hat{f}_m estimated force
 k_1 spring stiffness
 f_L load force from wire
 f_{k1} spring force
 u_a voltage
 R_a resistance
 L_a inductance
 e_a back electromotive force
 K_T torque constant
 i_a current
 K_E voltage constant
 K_f viscous friction coeff.
 J_m inertia rotating masses
 w disturbance
 u input
 e error

Greek

θ_b Rotation about the y-axis (pitch,trim)
 η displacement
 $\dot{\eta}$ velocity vector
 $\ddot{\eta}$ acceleration vector
 ζ_a wave amplitude & heave amplitude
 λ model scale & wave-length
 ω angular velocity
 τ torque
 τ_L load torque
 θ pulley angle
 ω_0 target angular velocity
 η_3 vertical motion in heave
 ρ density of water
 ω_b bandwidth frequency
 ω_s sampling frequency
 η_s safety factor

Abbreviation:

ATLAS	Active Truncated Line Anchoring Simulator
COG	Center of Gravity
CONTMOD	Continuous Mode
cRIO	Compact Reconfigurable I/O
DC gain	Low frequency (DC) gain
DC motor	Direct Current motor
DOF	Degrees of Freedom
DNV-RP	Det Norske Veritas – Recommended Practice
HLA	High Level Architecture
I/O	Input output
LTI	Linear-time invariant
MARINTEK	The Norwegian Marine Technology Research Institute
MARIN	Maritime Research Institute Netherlands
MC lab	Marine Cybernetics Laboratory
P1Z	One pole one zero transfer function
P2	Two pole transfer function
PI	Proportional Integral
PID	Proportional Integral Derivative
PWN	Pulse Width Modulation
RS232	Recommended Standard 232
SNAME	Society of Naval Architects and Marine Engineers
SOR	Source For Velocity
TF	Transfer Function
UDP	User Datagram Protocol

Contents

Abstract	i
Acknowledgment	iii
Notation	v
Contents.....	vii
1 Introduction	1
1.1 Background and Motivation	1
1.2 Previous Work in Model Testing.....	1
1.2.1 Active Control of Line Forces.....	3
1.2.2 Published Literature	4
1.3 Main Contributions.....	4
1.4 Outline of Thesis	5
2 System Overview	7
2.1 Presentation of the Project.....	7
2.1.1 Prerequisites and limitations	8
2.2 Outline of the Method.....	8
3 Modeling of Vessel Dynamics	15
3.1 Coordinate Systems	15
3.2 Froude Scaling	17
3.3 Description of Case	17
3.3.1 Equation of Motions.....	18
3.3.2 Equation of motion in model scale.....	19
3.3.3 Frequency response	20
3.3.4 Determination of Sampling Frequency	22
4 Experimental Setup	25
4.1 Determination of DC motor.....	25
4.2 Necessary Equipment	28
4.2.1 Servo motor / winch	30
4.2.2 Precision Gearhead.....	31
4.2.3 Motion Controller.....	32
4.2.4 Sensors Specifications	33
4.2.5 Power Supply	34
4.2.6 Oscillating System.....	34
4.3 Discussions	35
5 Mathematical Models of Experimental Setup	37
5.1 Mass Dynamics.....	37
5.2 Motor Dynamics	40
5.2.1 Transfer Functions.....	43
5.3 1 DOF Dynamic Model	45
5.4 Motion Controller	46
6 System Identification.....	53
6.1 Parameter Identification in the Model from Analog Voltage to Target Velocity	53
6.2 Parameter Identification in the Model from Target Velocity to Current and Actual velocity.....	55
6.2.1 Determination of the Control Gains	55
6.2.2 Determination of the DC motor parameters	57

6.3	Relationship between measured voltage and actual force	59
6.4	Discussion.....	61
7	Model Validation.....	63
7.1	Model Validation between Analog Voltage to Target Velocity	63
7.2	Model Validation from Target Velocity to Current and Actual Velocity	64
7.3	Comparison between the Simulated Force and Measured Force	66
7.4	Discussion.....	68
8	Control Design	69
8.1	Control Design.....	69
8.2	Observer Design	70
8.3	Mooring Line Calculations	72
9	Experiments.....	75
9.1	Case 1	75
9.2	Case 2	80
9.3	Discussion.....	85
9.3.1	Challenges	85
10	Conclusions	87
10.1	Conclusion	87
10.2	Recommendations for Further Work	88
11	Bibliography.....	91
12	Appendix A	93
12.1	Motion controller and Computer Software	93
12.2	Parameter DC motor Calculations using System Identification Toolbox.....	95
12.3	Sesam	97
12.4	Piecewise Constant References.....	99
12.5	Frequency Responses	102

1 Introduction

This chapter gives an overview of model testing in the design of floating structures in general, the use of such methods on deep water floating systems, and a proposed method for how the problem can be solved. The second section reviews some of the available literature that is relevant for this master's thesis. The chapter ends with a presentation of the contributions of this master's thesis, and an outline of the report.

1.1 Background and Motivation

Floating production systems have been accepted by the offshore industry as reliable and economic solution for oil production. Today, the possibility of discovering new oil and gas resources within deep water fields continue to push technology forward.

Oil companies have invested a considerable amount of money in the research and development in order to utilize oil, gas and ore deposits in deep water fields, and thus have played an important role in the development of methods for model testing deep water floaters. According to Buchner et al., Wichers & de Wilde (1999), approximately 25 % of the future deepwater fields will be deeper than 1000 m.

Model testing in the design of floating production systems has been performed to find reliable prediction of motions caused by the combined actions of waves, wind and current. Model testing is also used when testing new concepts, numerical software and when finding operational limits for existing structures.

The model testing facilities for offshore structures have a typical water depth limitation of 10 meters. The model scale for hull and waves should preferably not be smaller than 1:40. The existing test facilities will therefore limit the full scale water depth to 400 meters. The testing of floating structures on very deep water must therefore apply an approach using a truncated model of the mooring and riser system. The challenge is hence to make a truncated model with identical static and dynamic properties as for the real system.

The approach using active control of line forces to replace the mooring and riser system seems promising. The active lines should actuate the same forces on to the vessel as calculated by numerical methods. The numerical calculation of the mooring and riser system must be done real time and preferably correspond to the full-scale dynamic forces. The force calculations are computed from measured vessel motion and waves.

1.2 Previous Work in Model Testing

Different methods for model testing deep water structures already exist. However, on very deep waters problems with the existing methods occur. Several different approaches are presented in the following subsections.

Ultra-small scale testing

Normally model testing is done by scaling the floating production system. Hence, scaling a deep water system seems like a reasonable approach especially since the testing is carried out geometrically complete and correct. However, the existing model test facilities for offshore structures have a typical water depth limitation of 10 meters. When simply scaling the deep water system, the model will become undesirable small. With small models, uncertainties in the results especially mooring line forces become significant. Scaling a deep water system will therefore limit the prototype water depth to about 1000 m at reasonable scales MARINTEK and Chevron (2008). This will result in a 1:100 in model scale. However, with 1:100 in model scale the current is difficult to include. This is not optimal and a larger model scale must preferably be used.

In Buchner et al. et al. (1999) ultra small scale testing is defined as scales smaller than 1:100. Since the loads scale with λ^3 uncertainties in the result at smaller scales may be expected. In Moxnes & Larsen (1998) it is shown that to generate environmental forces at these scales become problematic. Especially the waves are difficult to generate since they are significantly influenced by surface tension.

Active equivalent mooring system

When it comes to development of technology for deep water model testing, MARIN in the Netherlands and MARINTEK in Trondheim have been some of the main driving forces. In recent years, different possible approaches have been suggested. Buchner et al. et al. (1999) shows one example, the ATLAS (Active Truncated Line Anchoring Simulator) model testing method. The focus to this system has been to use an active equivalent mooring system.

The active equivalent mooring system, described in Buchner et al. et al. (1999), is a setup using robot arms placed on the basin floor. The function of these robot arms is to actuate the same forces as the truncated riser and mooring system above the basin floor. The virtual mooring lines and risers below the basin floor is simulated and coupled to the real mooring lines in the test basin. With a system like this larger model scales are possible, and simulations of the full dynamic behavior of the mooring and riser system are possible. However, as Buchner et al. et al. (1999) states a system like this will require heavy computational power to simulate the mooring and riser system real time.

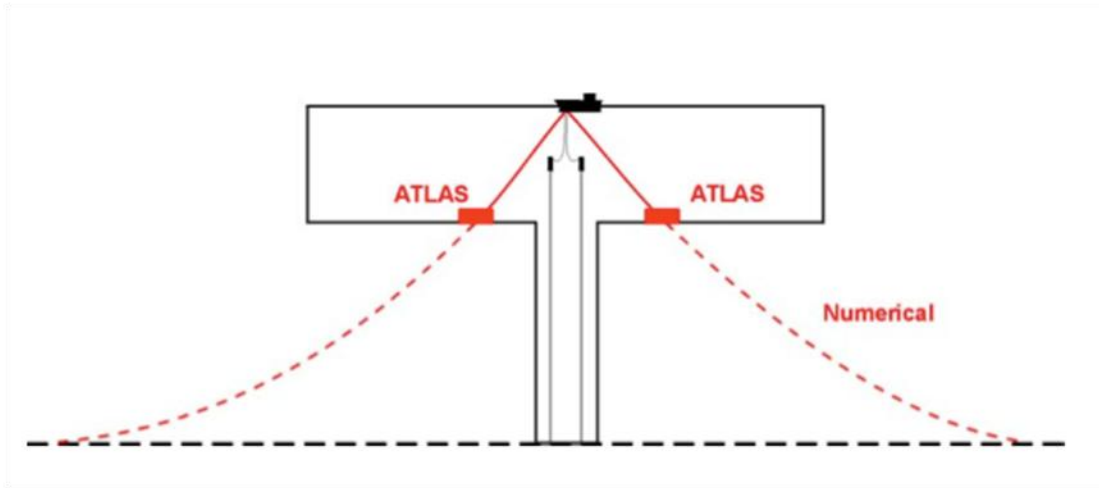


Figure 1.1: Schematic setup of the active equivalent mooring system given in Buchner et al. et al. (1999).

Truncated systems with off-line numerical simulations

An alternative approach is to use a truncated mooring and riser system, usually in combination with computer simulations. Some examples are given in Stansberg, Ormberg & Øritsland (2002), Buchner et al. et al. (1999) and Stansberg, Karlsen, Ward, Wichers, & Irani (2004). This hybrid approach uses a passive truncated mooring system modeled to be as similar as possible to the real deepwater system. However, the full depth mooring line and riser dynamics, as well as damping, cannot be modeled accurately. Coupled mooring analysis is needed to calibrate the test results from the truncated setup to the real deepwater system. A numerical program representing the physical system is calibrated using the truncated model-test results. By using relevant information to the reduced depth system the numerical program can be extrapolated to fit the full basin depth. Hence, the results can be scaled up to full scale.

In Buchner et al. (1999) the main disadvantage with an approach like this, is that numerical calculations are necessary to determine design values. This is due to the fact that the mooring and riser system cannot be modeled correctly using a passive system.

Outdoor model testing

Outdoor model testing is another possibility as mentioned in Stansberg et al. (2004). The idea of the method is to do the model testing in a quiet fjord or lake as an alternative to the existing facilities. In Huse, Kleiven and Nielsen (1998) tests using a 90 m long model of deep sea risers were performed in a Norwegian fjord. The problem with this approach, also mentioned in Stansberg et al. (2004), is that the environmental conditions given in nature are non-controllable.

1.2.1 Active Control of Line Forces

The active control of line forces method is proposed so that the full depth mooring and riser system can be replaced by active controlled lines. This can be done by calculating real time desired mooring and riser forces. A control system should then actuate the same equivalent forces onto the floating unit using the active lines.

This method will add several new uncertainties such as delays in the numerical calculations, or delays in the control system actuating the desired forces. The system will depend on actuators that accurately impose the correct forces. Technical issues regarding this will be investigated in this thesis.

1.2.2 Published Literature

There has been extensive work trying to describe the problem related to deep water model testing. Hybrid approaches using truncated mooring and riser systems together with model tests have been presented in Buchner et al. et al. (1999), Stansberg et al. (2002) and Watts (1999).

In Watts (1999) a hybrid approach is proposed as an alternative to the construction of deeper, more expensive wave basins. The article describes the problems related to numerical calculations, especially for smaller scales since the computational time accelerate. This is because time is scaled with the square root of the model scale.

The hybrid approach explained in Watts (1999) uses a physical model of the floater interfaced with a numerical model of the mooring and riser system by means of an actuator. According to Watts (1999) alternative designs are currently being evaluated, and it is likely that calculated desired forces will be used and actuated on to the floater using servo motors that follow the floater motion.

Buchner et al. (1999) describe that the wave, wind and current generation systems have a large impact on the reliability to the model test results. Using the present facilities at MARIN in the Netherlands, puts a limitation on the model scales for water depths deeper than 1000 m.

In addition a recent article published in the Oil and Gas magazine by Argyros Langley and Ahilan (2009) present a new study that aims to simplify mooring analysis for deepwater systems. An analytical truncation procedure presented allows a rapid assessment of line dynamics.

1.3 Main Contributions

The overall objective of this master's thesis is to find a control strategy able to actuate reliable and accurate forces on to the vessel, using active control of line forces replacing the mooring and riser system. To achieve this goal, this thesis contribution is the development of a simplified 1 DOF experimental setup moving only in the heave direction. Necessary equipment has been procured, and experiments using one active mooring line attached to the simplified vessel have been performed. The work carried out in order to achieve this objective can be summarized as follows:

- A simplified model of the offshore vessel is developed. The bandwidth and necessary sampling frequency to recreate the continuous time responses for the vessel moving in three degrees of freedom (DOF) is proposed. The necessary sampling frequency is found using a specific case.

- A one DOF case only looking at the heave motion is modeled mathematically and the unknown parameters in the model has been found using system identification. The DC motor dynamics and mass dynamics are derived.
- A control system is designed in order to induce desired forces in the one DOF case. Velocity control of the motor shaft is proposed as a solution to actuate the desired forces on to the vessel. An observer that filters the disturbance found in the measured actuated force is proposed. The estimated filtered force signal is then used as feedback to the controller.
- The experimental setup consistent with the one DOF model together with the control system is made, and experimental testing of the system is preformed. A Faulhaber engine is proposed as an actuator to induce the desired forces.

1.4 Outline of Thesis

Chapter 2 gives a system overview of the method using active control of line forces to replace the mooring and riser system. The chapter proposes a solution for how the problem can be solved for a vessel moving in 6 DOF. A motor-winch configuration using an actuator solution to induce the correct resulting forces, calculated from numerical methods in real time, is proposed. The chapter ends with suggesting the simplified motor-winch configuration setups for the one DOF case considered in this thesis.

Chapter 3 presents the simplified vessel dynamics for a 3 DOF case. The vessel is considered to be a barge exposed to a given regular wave. The equation of motion is presented in model scale using calculated data from Hydro-D. The equation of motion is then used to establish transfer functions from the force inputs to the response output. The bandwidth, or highest frequency in the system is the determined, and the necessary sampling frequency in order to recreate the continuous time responses is suggested.

Chapter 4 introduces the experimental setup built in the marine cybernetics laboratory. The choice of actuator, or Faulhaber DC motor, is elaborated and key equipment in order to build the simplified 1 DOF model is discussed and presented.

Chapter 5 gives a detailed mathematical description of the 1 DOF simplified system. Mathematical models for the mass dynamics and motor dynamics are derived. Velocity control of the engine shaft is discussed as a method for actuating the desired forces. The motion controller implemented on the Faulhaber drive electronics is explained.

Chapter 6 presents a method for establishing the unknown parameters in the model. The DC motor parameters, control gains in the model, as well as parameters to describe the Faulhaber motion controller are determined.

Chapter 7 compares the simulated outputs in the derived model with the measured data from experiment. The parameters used in the model are found in the previous chapter.

Chapter 8 presents the control design. An observer is presented in order to filter the measured force signals. A control strategy that minimizes the difference between a filtered measured force signal (estimated force) and force reference is presented.

Chapter 9 gives a presentation of the results found from the experiments and a discussion regarding the experimental setups used in the marine cybernetics laboratory.

In chapter 10 the report is concluded and the most important findings are presented.

The Appendix contains some of the detailed data used in this thesis.

2 System Overview

As oil is becoming more scarce, developments of fields at more inaccessible places will be necessary. In the design and operation of floating oil production vessels, reliable prediction of the behavior is important. Model testing of the floating structures plays an important role in this evaluation.

Currently, methods for model testing at deepwater depths have significant shortcomings. There are several drawbacks to small-scale model testing and model testing using a truncated mooring and riser system. A promising solution is to replace the mooring and riser system with active control of line forces. This chapter starts with a general presentation of a possible solution, before the main principles behind the method are discussed in more detail.

2.1 Presentation of the Project

In this thesis, solutions for model testing of deepwater moored structures using active control of line forces, will be investigated. In this method, the mooring and riser systems are replaced by a set of lines connected to torque controlled motors actuating mooring and riser forces. The objective of the control system is to actuate the same equivalent forces as the simulated mooring and riser system. It will be necessary to investigate if the control system will be able to actuate these forces and still be able to give reliable motions for the floater. In addition reasonable mooring and riser forces within a sufficient range needs to be determined and tested.

The time delay in the control system and signal communication needs to be found. Too large time delay will give undesirable effects in the resulting behavior of the floater. Hence, the acceptable delay, and corresponding bandwidth (speed) of the control system, must be determined.

Simplified models of the floating structure will be designed in order to evaluate the control system. A simple one DOF model setup using a motor, spring, mass, wave effects and typical mooring forces will be designed. In addition a method for solving a three DOF case is proposed.

The one DOF model together with the control system will be mathematically modeled. In addition an assessment of the necessary sampling frequency to reconstruct the continuous time responses to a vessel moving in three DOF, exposed to force inputs, will be investigated.

A physical model reflecting the target system in the model test basin, will be designed, consisting of a motor, line, controller, spring, communication, and gear. This physical model will be tested using the designed control setup in loop. The goal is to make an assessment of the performance of the system using a real physical experimental setup.

2.1.1 Prerequisites and limitations

The 10 meter basin water depth makes it difficult to perform small-scale model testing using existing methods. However, it may be possible to apply larger model scales by simulating the riser and mooring forces and actuating them on to the vessel using active control of line forces.

The prerequisite assumption is that the mooring force simulator and communication system is fast enough such that time delays will not result in unacceptable distortions of the vessel responses.

Limitations

- The test strongly depends on the accuracy of the simulated numerical mooring and riser forces that controls the electronic equipment.
- The line forces will only be able to exert strain forces, and the force will always be positive.
- The simulation of mooring forces must be done in real time.
- The time delay between the simulated forces and the corresponding actuated line forces will have a limit.

2.2 Outline of the Method

As previously mentioned various methods for model testing of moored floaters exist today. However, as discussed earlier the existing methods are inadequate when using model tests in the design of ultra deep water floaters. The “active control of mooring line forces” method is proposed as a solution.

The idea of this method is that calculated resulting mooring line forces are forced onto the floater using a control system. To solve the problem by actuating forces onto the floater three possible solutions are proposed:

- Hexapod
- “Sea bed” robot arm
- Motor-winch configuration

The hexapod is a solution using robot arms directly connected to the hull of the floater and a carriage. The robot arms to the hexapod are placed such that all 6 degrees of freedom can be actuated. The main disadvantage with this method is that the system will involve large inertia due to the robot arm masses and the robot arm motion may be too slow. This method will not be further evaluated in this thesis.

“Sea bed” robot arms placed on the model tank bottom can be used to actuate desired forces through a set of lines. The approach will demand advanced equipment and high knowledge about the robot arm dynamics. This method will not be further evaluated in this thesis.

The motor-winch configuration approach consists of motors directly connected to lines actuating forces onto the floater. Hence, resulting desired forces can be forced onto the floating structure. The dynamics to a system like this will be much easier to model than it would for a robot arm, or hexapod, solution. The equipment to such a system will be much cheaper and easier to acquire.

The motor-winch configuration method uses thin lines coupled to torque controlled motors. The lines are only able to exert tension forces, and thus need to be directly connected to the hull of the floater. Necessary knowledge about the dynamics and effects of the lines in water may be needed.

Figure 2.1 shows the overall system containing a mooring line simulator, controller, motor-winch system and a vessel. From the vessel motion the mooring line simulator will calculate the desired forces. The controller will use this input and give command to the motor winch system. Control signals will then tell the motor winch system to actuate forces onto the vessel. The actuated forces will affect the vessel and give new vessel motion.

The numerical mooring simulator uses the measured data from the vessel motion and waves to calculate full-scale dynamic forces in the anchor and riser system. Motion sensors and HLA communication is used to gather the measured data. The mooring simulator passes on the corresponding model scale forces to the controller using Ethernet, user datagram protocol (UDP), or some other communication. A customized input output (I/O) protocol in LabVIEW® connected to some hardware, typically a Compact Reconfigurable I/O (cRIO) module, can then be configured to receive the desired force reference signals.

The calculated resulting forces from the anchor and riser system are then used as reference in the control system. A control allocation scheme will distribute the desired resulting forces among the set of actuators, in this case the motor-winch. Optimal setpoints are commanded to each motor-winch in order to actuate the same resulting forces as calculated by the mooring simulator. Force rings connected in-between the vessel and the active lines measures the force actuated by each motor.

To command the engines analog voltage signals can be applied. Alternatively, a pulse width modulation (PWN) signal can be used. Recommended standard 232 (RS232) communication is another possibility.

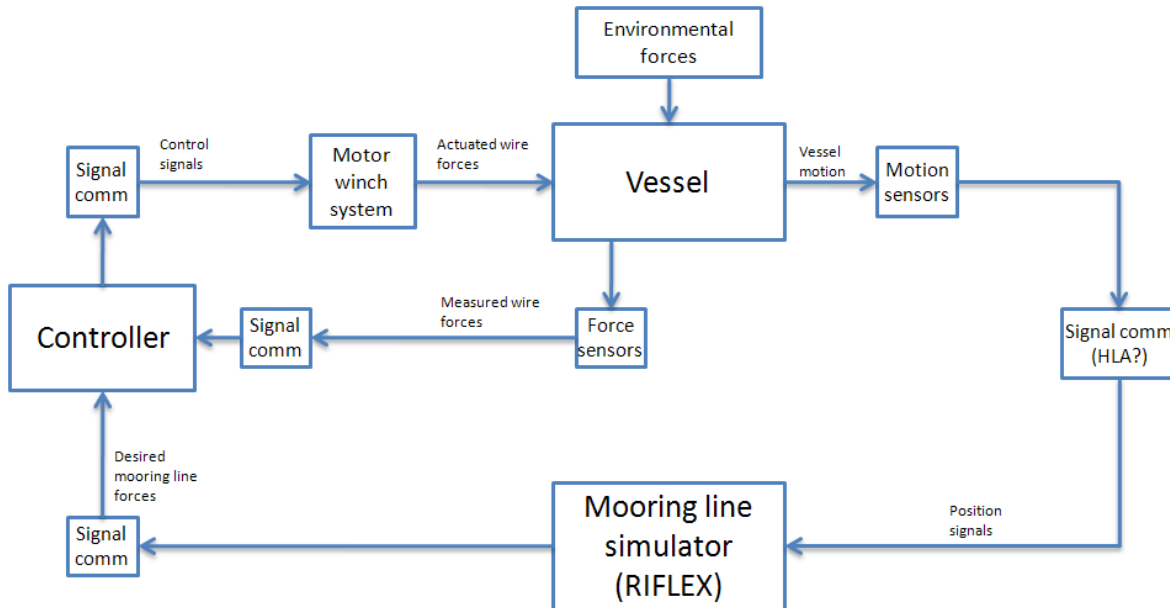


Figure 2.1: Main topology showing the key elements in the active control of lines method.

The problem is divided in two parts. The first subproblem will look closer at the mooring line simulator, and work will be done in order to find reliable mooring line forces fast enough. Co MSc. student Stian Garlid will look closer at this problem. The second subproblem will be the design of the controller and motor winch system.

The core of the system first subproblem must be a real time simulator for computation of full-scale dynamic forces in the anchor and riser system. The vessel motion and waves are used real-time to calculate the resulting forces using the computer software Riflex. Riflex receive the motion from vessel and waves using high level architecture (HLA) communication. The calculated forces are then used as input in the vessel model. New vessel motions and wave signals are then used to calculate the the next set of desired forces.

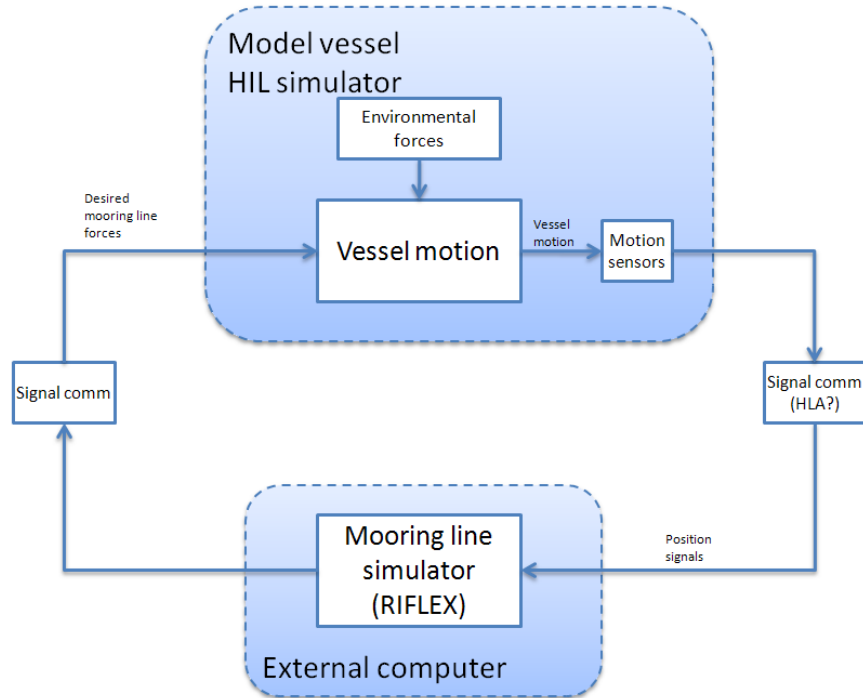


Figure 2.2: Sub-HIL simulator topology.

This thesis will look at the second subproblem, presented in Figure 2.3. The hardware in the loop (HIL) simulation is a technique that is used in the development and test of complex real-time embedded systems. For this problem this technique will be used to test the design of the control system setup.

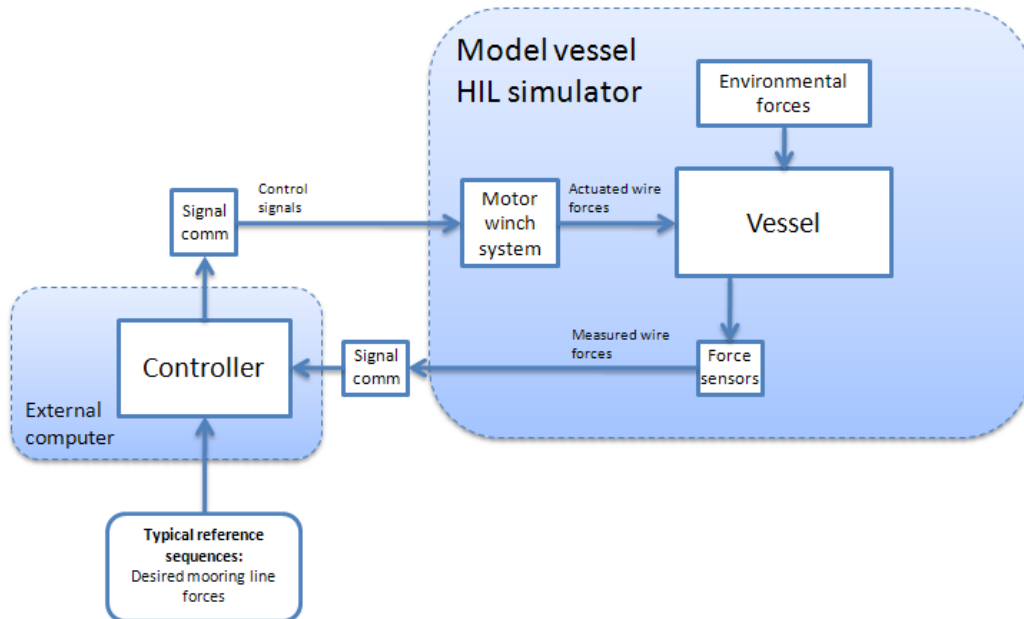


Figure 2.3: Sub-HIL simulator topology with control system in loop.

A motor-winch configuration for a six DOF case is proposed in Figure 2.4 as one possible schematic setup. The box shaped body will represent the vessel, the circles marked as M represent the motor-winch actuators and the zigzag lines represent the passive springs. Force rings are placed in-between each connection point to the vessel to measure the actual forces on the vessel. A control system, using appropriate allocation algorithms, should then actuate the same resulting forces in each degree of freedom as calculated by the mooring simulator.

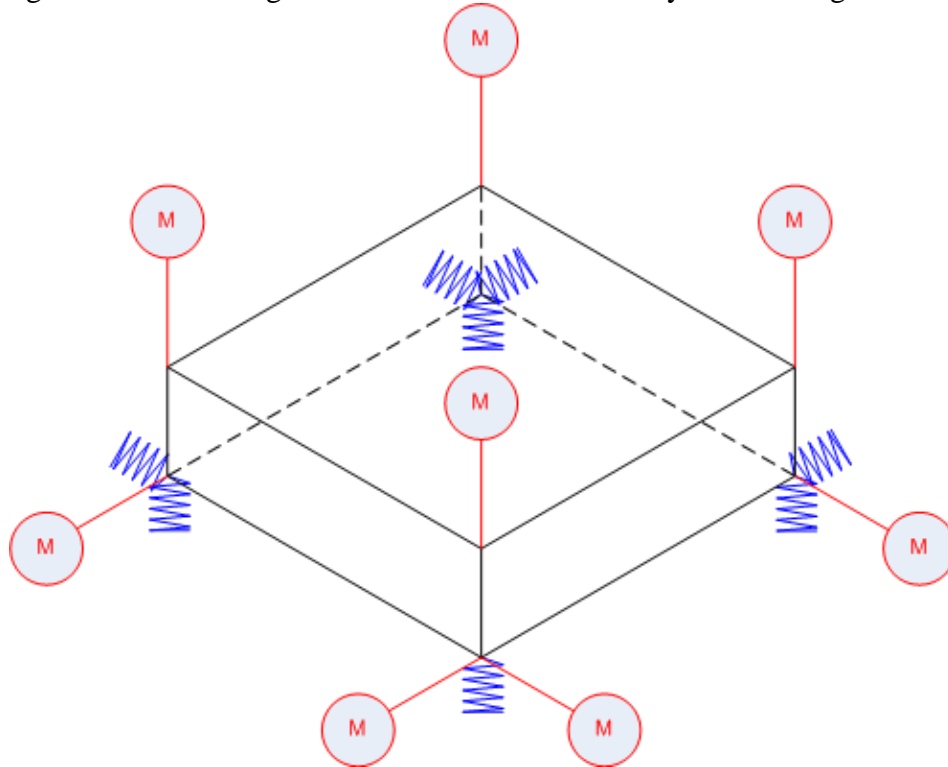


Figure 2.4: Experimental setup for a six DOF case, courtesy Stian Garlid (2010).

If less DOFs are included, a different motor-winch configuration setup will be needed. A schematic setup for a three DOF case is shown in Figure 2.5. The figure shows the required setup needed to successfully control three DOF. For the schematic setup presented the focus is of control in the vertical plane i.e. surge, heave and pitch.

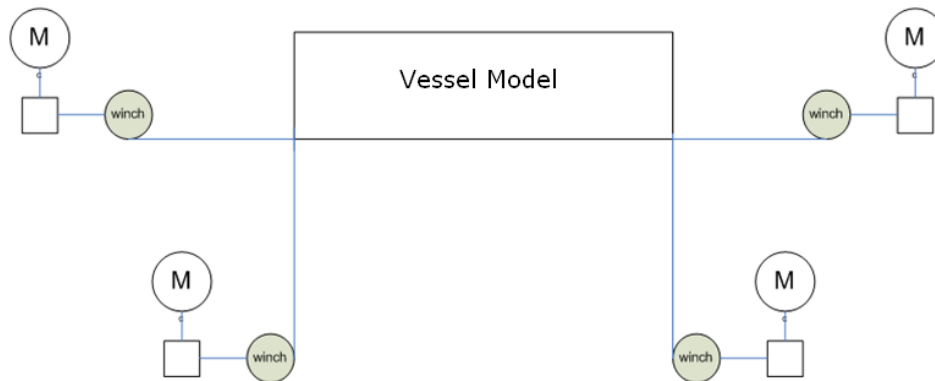


Figure 2.5: Configuration of motors and winches.

The problem will be divided into subproblems using an experimental setup. The vessel in Figure 2.5 will then be replaced by a simplified one DOF mass-spring model in heave. The idea is to test the controller together with this setup.

The schematic for the 1 DOF setup is presented in Figure 2.6. A mass-spring system together with the controller will first be mathematically modeled. The physical simplified model, according to Figure 2.6, will be built, and the control setup will be experimentally tested on this system.

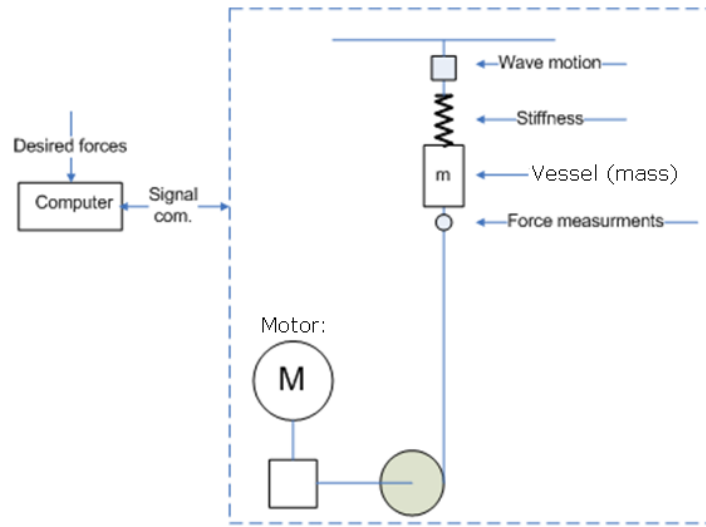


Figure 2.6: One DOF mass-spring system.

In the experiments a second test case will be conducted, shown in Figure 2.7. The vessel will now be the oscillating system represented as the wave motion in previous figure. The active mooring line will be the line with spring connected to the oscillating body.

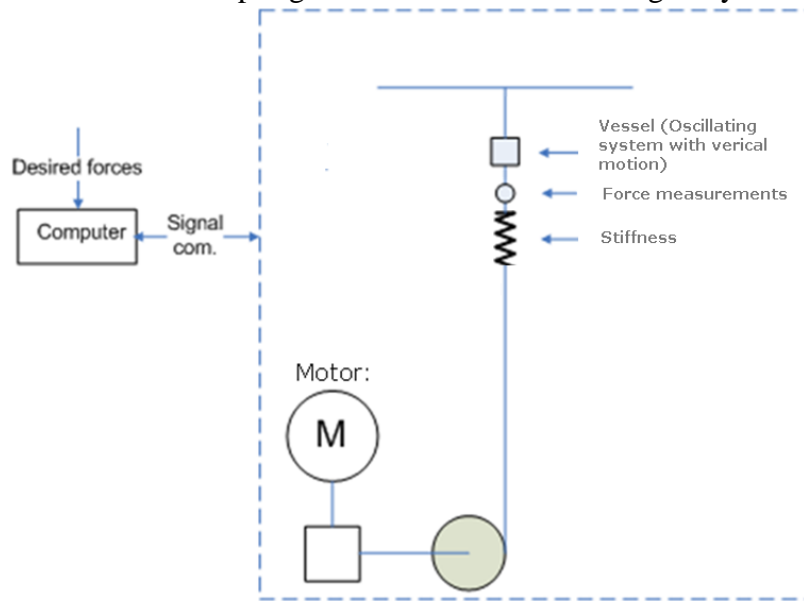


Figure 2.7: One DOF experimental setup.

3 Modeling of Vessel Dynamics

In this chapter a model for the vessel dynamics in a three DOF case will be introduced. The vessel will be a simple rectangular barge. The equation of motion to this barge is presented for a given case both in full scale and model scale. Since the focus in the schematic setup presented in Figure 2.5 is of control in the vertical plane, the responses are given in surge, heave and pitch. In the model testing experiments, real time measurement of the vessel responses are needed to calculate desired mooring line forces. An assessment of the necessary sampling frequency to recreate the measured analog signal, without loss of information, is therefore desired.

In order to recreate the signal a frequency response analysis is performed between the different force inputs to the response outputs to determine the bandwidth in the system, or highest frequency. The necessary sampling frequency required to successfully recreate the continuous signal is then determined.

3.1 Coordinate Systems

The positions, motions and accelerations are described by coordinate systems. The coordinate systems follow the standard right-hand rules. The coordinate system is illustrated in Figure 3.1 and Figure 3.2.

The notation to Society of Naval Architects and Marine Engineers (SNAME), for marine vessels, is used and given in Table 3.1. The DOF is indicated in the left column with its respective notation for “forces and moments”, “linear and angular velocities” and for “position and Euler angles”.

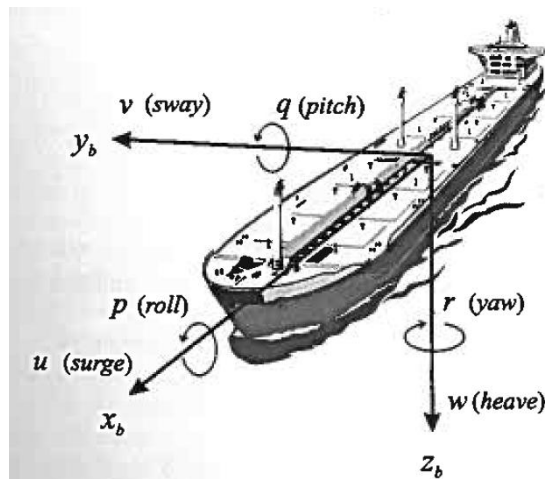


Figure 3.1: Motion of variables for marine vessels (SNAME, 1950).

The coordinate system to the vessel shown in Figure 3.1 can be expressed using the following notation:

DOF		Forces and Moments	Linear and angular velocities	Positions and Euler angles
1	Motions in the x-direction (surge)	X	u	x
2	Motions in the y-direction (sway)	Y	v	y
3	Motions in the z-direction (heave)	Z	w	z
4	Rotation about the x-axis (roll,heel)	K	p	ϕ
5	Rotation about the y-axis (pitch,trim)	M	q	θ
6	Rotation about the z-axis (yaw)	N	r	ψ

Table 3.1: The notation of SNAME (1950) for marine vessels.

The global and body coordinate system to a floating vessel is explained below and illustrated for a three DOF case in Figure 3.2.

Global coordinate system: This coordinate system is fixed in the mean water level. Coordinates with respect to this coordinate system are denoted (x_g, y_g, z_g) . This coordinate system is assumed to be the inertial reference frame.

Body fixed coordinate system: The floater coordinate system is a moving reference frame fixed to the vessel. The origin of the coordinate system coincides with the floater center of gravity (COG). The body axis x_b , y_b and z_b coincide with the principal axes of inertia and are defined as in Fossen (2002) as:

- x_b - longitudinal axis (directed from aft to fore)
- y_b -transversal axis (directed to starboard)
- z_b -normal axis (directed from top to bottom)

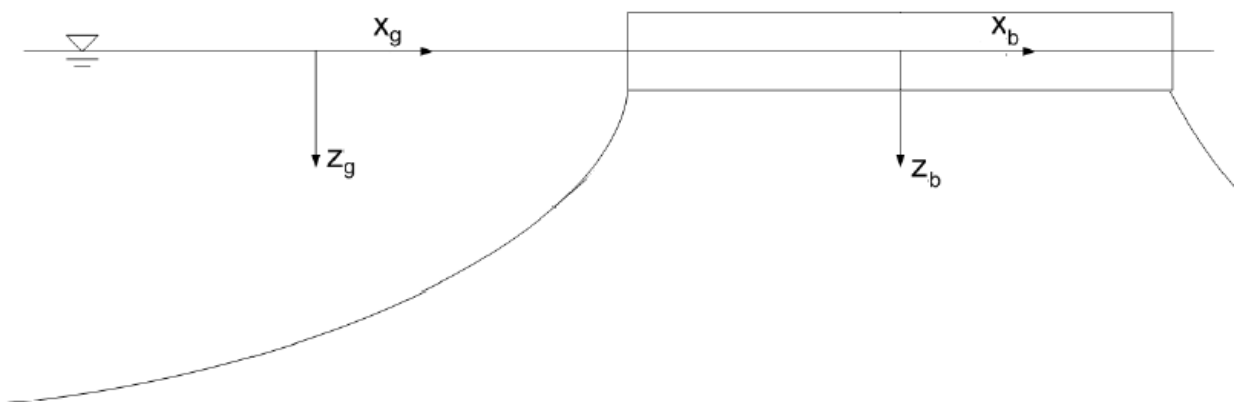


Figure 3.2: Coordinate systems.

3.2 Froude Scaling

Depending on the problem, different scaling methods are used. For problems where the volume forces dominate, Froude scaling of the wave kinematics and responses is mostly used. This is the most common way to scale model tests since the forces on large volume bodies mainly come from volume forces. If viscous forces dominate, Reynold scale of the model should be used. Large volume bodies that also are influenced by viscous forces can be modeled in a corrected Froude scale as stated in DNV-RP-C205 (2007), Section 10.9.2.1. However, it is most typical to use pure Froude scaling in model tests. In DNV-RP-C205 (2007) the scaling factor relations between full-scale and model scale, shown in Table 3.2, are given.

Parameter	Scaling factor	Model unit (typical)	Full scale unit (typical)
Length	λ	m	m
Velocity	$\lambda^{1/2}$	m/s	m/s
Linear acceleration	λ^0	m/s ²	m/s ²
Angular acceleration	λ^{-1}	deg/s ²	deg/s ²
Angle	λ^0	degrees	deg
Force	$\lambda^3 1.026$	N	kN
Moment	$\lambda^4 1.026$	Nm	kNm
Stiffness	$\lambda^2 1.026$	N/m	kN/m
Linear Damping	$\lambda^{2.5} 1.026$	kg/s	kg/s
Time	$\lambda^{1/2}$	s	s

Table 3.2: Froude scaling law.

3.3 Description of Case

The floater is chosen to be a simple barge with specifications given by Table 3.3. The barge will be a box-shaped floating body with length L , breath B and draught D is subjected to regular sinusoidal waves that propagate along the negative x -axis shown in Figure 3.3. The wave-length is λ and the wave amplitude is ζ_a .

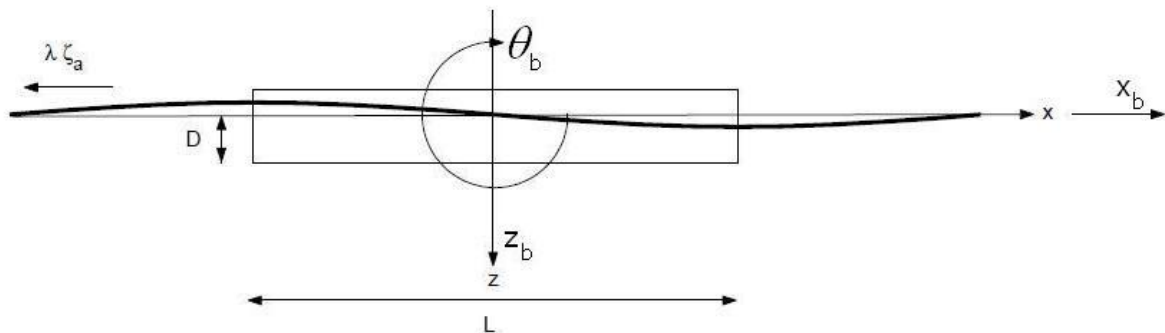


Figure 3.3: Schematics of the floating barge.

Dimension	Abbreviation	Value	Unit
Length	L	91	m
Beam	B	27	m
Depth moulded	Dm	6	m
Depth	D	3	m
Mass	M	7555	ton
Radius of gyration		$r_4 = 1, r_5 = 1, r_6 = 1$	m
Centre of gravity		$x_{b,COG} = 0, z_{b,COG} = 0, \theta_{b,COG} = 0$	m
Wave amplitude	ζ_a	2	m
Wave period	T	7	s

Table 3.3: Case specifications and barge dimensions.

3.3.1 Equation of Motions

The coupled equations of motion for the three DOF system can be written

$$(\mathbf{M}_{rb} + \mathbf{M}_a)\ddot{\eta} + \mathbf{D}\dot{\eta} + \mathbf{G}\eta = \mathbf{f}(t), \quad (3.1)$$

where \mathbf{M}_{rb} is the rigid body mass matrix, \mathbf{M}_a is the added mass matrix, \mathbf{D} is the damping matrix, \mathbf{G} is the stiffness matrix, \mathbf{f} is the force vector and η is the displacement vector. $\dot{\eta}$ and $\ddot{\eta}$ are the 1st and 2nd derivative of the displacement with respect to time.

Defining

$$\mathbf{x} = \begin{bmatrix} \eta \\ \dot{\eta} \end{bmatrix}, \quad (3.2)$$

The state space representation, with $\mathbf{u} = \mathbf{f}(t)$, of the equation of motion can be written as

$$\dot{\mathbf{x}} = \mathbf{A}\mathbf{x} + \mathbf{B}\mathbf{u} \quad (3.3)$$

$$y = \mathbf{C}\mathbf{x} \quad (3.4)$$

where

$$\mathbf{A} = \begin{bmatrix} \mathbf{0}_{3 \times 3} & \mathbf{I}_{3 \times 3} \\ -(\mathbf{M}_{rb} + \mathbf{M}_a)^{-1}\mathbf{G} & -(\mathbf{M}_{rb} + \mathbf{M}_a)^{-1}\mathbf{D} \end{bmatrix}, \quad \mathbf{B} = \begin{bmatrix} \mathbf{0}_{3 \times 3} \\ (\mathbf{M}_{rb} + \mathbf{M}_a)^{-1} \end{bmatrix} \quad (3.5)$$

$$\mathbf{C} = [1 \ 0 \ 0 \ 0 \ 0 \ 0]. \quad (3.6)$$

The motions of the vessel are given in 3 DOF $\eta = [x_b \ z_b \ \theta_b]^T$ where x_b is the surge displacement in x -direction, z_b , is the heave displacement in z -direction and θ_b it the rotation about the z -direction (pitch). The derivative to η is defined as $\dot{\eta} = [u \ w \ q]^T$ where u is the surge velocity, w is the heave velocity and q is the angular velocity in pitch. The input will be $\mathbf{u} = F(t) = [X \ Z \ M]^T$, where X is the force input in surge, Z is the force input in heave and M is the moment in pitch.

The matrices are calculated in Sesam Hydro-D for a wave amplitude $\zeta_a = 2$ [m] and wave period $T = 7$ [s], see Appendix 12.3. The added mass matrix is calculated as

$$\mathbf{M}_a = \begin{bmatrix} 7.7760 \cdot 10^5 & 1.7430 & 7.9350 \cdot 10^6 \\ -2.0790 \cdot 10 & 2.2190 \cdot 10^7 & 3.1740 \cdot 10^3 \\ 8.2720 \cdot 10^6 & 2.1710 \cdot 10^3 & 1.3910 \cdot 10^{10} \end{bmatrix}. \quad (3.7)$$

The matrix will change depending on the period we use. The potential damping matrix is also found and it is given as

$$\mathbf{D} = \begin{bmatrix} 3.3870 \cdot 10^5 & 5.8920 & 3.0510 \cdot 10^7 \\ 1.2520 \cdot 10^1 & 1.1510 \cdot 10^7 & 1.8990 \cdot 10^3 \\ 3.0270 \cdot 10^7 & 1.7850 \cdot 10^3 & 5.8990 \cdot 10^9 \end{bmatrix}. \quad (3.8)$$

This matrix will also change depending on the wave period. The constant water plane stiffness matrix is calculated as

$$\mathbf{G} = \begin{bmatrix} 0 & 0 & 0 \\ 0 & 2.4700 \cdot 10^7 & -3.0010 \cdot 10^2 \\ 0 & -3.0010 \cdot 10^2 & 1.6930 \cdot 10^{10} \end{bmatrix}. \quad (3.9)$$

while the body mass matrix is found to be

$$\mathbf{M}_{rb} = \begin{bmatrix} 7.5550 \cdot 10^6 & 0 & 4.0260 \cdot 10^{-8} \\ 0 & 7.5550 \cdot 10^6 & 9.4160 \cdot 10^{-8} \\ 4.0260 \cdot 10^{-8} & 9.4160 \cdot 10^{-8} & 7.5550 \cdot 10^6 \end{bmatrix}. \quad (3.10)$$

3.3.2 Equation of motion in model scale

The previous matrixes are given in full-scale and it will therefore be necessary to scale them to model scale. Table 3.3 gives the scaling factors.

The terms in the matrices must therefore be multiplied with the scale corresponding to its units. The terms multiplied with the pitch rotation, i.e. third column, needs to be scaled with an extra λ factor. This is because angles are scaled with 1 and “meter” is scaled with λ according to Table 3.3.

In the added mass matrix the terms, in kg, are scaled with $\lambda^3 1.026$. The terms multiplied with the rotation will have denomination $[kg \cdot m]$ and therefore a scaling factor $\lambda^4 1.026$. With a 1:70 as model scale the added mass matrix can be written as

$$\mathbf{M}_{aM} = \frac{1}{\lambda^3 1.026} \begin{bmatrix} \mathbf{M}_{a11} & \mathbf{M}_{a13} & \mathbf{M}_{a15} \frac{1}{\lambda} \\ \mathbf{M}_{a31} & \mathbf{M}_{a33} & \mathbf{M}_{a35} \frac{1}{\lambda} \\ \mathbf{M}_{a51} & \mathbf{M}_{a53} & \mathbf{M}_{a55} \frac{1}{\lambda} \end{bmatrix} = \begin{bmatrix} 2.2096e+000 & 4.9529e-006 & 3.2211e-001 \\ -5.9076e-005 & 6.3054e+001 & 1.2884e-004 \\ 2.3505e+001 & 6.1691e-003 & 5.6466e+002 \end{bmatrix},$$

with a wave period $T_M = 7 / \sqrt{\lambda} = 0.8367$ [s] and a wave amplitude $\zeta_{aM} = \zeta_a / \lambda = 2.86$ [cm].

The body mass will be

$$\mathbf{M}_{rbM} = \frac{1}{\lambda^3 1.026} \begin{bmatrix} \mathbf{M}_{rb11} & \mathbf{M}_{rb13} & \mathbf{M}_{rb15} \frac{1}{\lambda} \\ \mathbf{M}_{rb31} & \mathbf{M}_{rb33} & \mathbf{M}_{rb35} \frac{1}{\lambda} \\ \mathbf{M}_{rb51} & \mathbf{M}_{rb53} & \mathbf{M}_{rb55} \frac{1}{\lambda} \end{bmatrix} = \begin{bmatrix} 2.1468e+001 & 0 & 1.6343e-015 \\ 0 & 2.1468e+001 & 3.8223e-015 \\ 1.144e-13 & 2.6756e-013 & 3.0669e-001 \end{bmatrix}.$$

The third column is multiplied with the pitch acceleration. In Table 3.2 potential damping is scaled with $\lambda^{2.5} 1.026$ and can therefore be written as

$$\mathbf{D}_M = \frac{1}{\lambda^{2.5} 1.026} \begin{bmatrix} \mathbf{D}_{11} & \mathbf{D}_{13} & \mathbf{D}_{15} \frac{1}{\lambda} \\ \mathbf{D}_{31} & \mathbf{D}_{33} & \mathbf{D}_{35} \frac{1}{\lambda} \\ \mathbf{D}_{51} & \mathbf{D}_{53} & \mathbf{D}_{55} \frac{1}{\lambda} \end{bmatrix} = \begin{bmatrix} 8.0524e+000 & 1.4008e-004 & 1.0362e+001 \\ 2.9765e-004 & 2.7364e+002 & 6.4496e-004 \\ 7.1965e+002 & 4.2437e-002 & 2.0035e+003 \end{bmatrix}.$$

The water plane stiffness matrix in model scale will be

$$\mathbf{G}_M = \frac{1}{\lambda^2 1.026} \begin{bmatrix} \mathbf{G}_{11} & \mathbf{G}_{13} & \mathbf{G}_{15} \frac{1}{\lambda} \\ \mathbf{G}_{31} & \mathbf{G}_{33} & \mathbf{G}_{35} \frac{1}{\lambda} \\ \mathbf{G}_{51} & \mathbf{G}_{53} & \mathbf{G}_{55} \frac{1}{\lambda} \end{bmatrix} = \begin{bmatrix} 0 & 0 & 0 \\ 0 & 4.9131e+003 & -8.5276e-004 \\ 0 & -5.9693e-002 & 4.8108e+004 \end{bmatrix}.$$

The matrices derived can be used in the equation of motion given by (3.1) to find the velocities in surge and heave as well as angular velocity in pitch. The displacements and rotation given in three DOF, i.e. surge, heave and pitch, can also be found from given force inputs.

3.3.3 Frequency response

The transfer functions between given inputs and outputs can be established by using the state space representation of the system given by (3.3) to (3.4). The corresponding frequency response can then be found for different transfer functions. Hence, the bandwidth can be determined.

The transfer function from the force input in surge X to the velocity output in u can be expressed as

$$\frac{u}{X}(s) = \mathbf{C}(s\mathbf{I} - \mathbf{A})^{-1}\mathbf{B}. \quad (3.11)$$

Using the “ss2tf” function in Matlab® the transfer function is found to be

$$\frac{u}{X}(s) = \frac{-004226s^4 - 02867s^3 - 654s^2 - 2036s - 209.2}{s^6 + 709s^5 + 1564s^4 + 530.9s^3 + 5084s^2 + 1684s} \quad (3.12)$$

The frequency response for this transfer functions can be found using the “freqs” function in Matlab®. “freqs” evaluates the polynomials at each frequency point, then divides the

numerator response by the denominator response, ref MathWorks. $s = i\omega$ and “freqs” calculates the response using the “polyval” equation for desired frequencies.

The low frequency (DC) gain is defined as

$$K = \mathbf{D} + \mathbf{C}(\mathbf{I} - \mathbf{A})^{-1}\mathbf{B}, \quad (3.13)$$

where K is the transfer function value at $z=1$ ($s=0$ in continuous time).

The bandwidth to the system can then be defined as the first frequency where the gain drops below -3 dB of the DC gain, ref (The MathWorks). The bandwidth can also be found using the Matlab® function “bandwidth”.

The frequency response from u to X (velocity in surge to force input in surge) is plotted together with its discrete transfer function in Figure 3.4. The figure shows that the discretization, using zero-order hold sampling time $T_s = 0.1$ [s], of the transfer function affects the frequency response. The plot also shows that the discrete system will get unstable for higher frequencies.

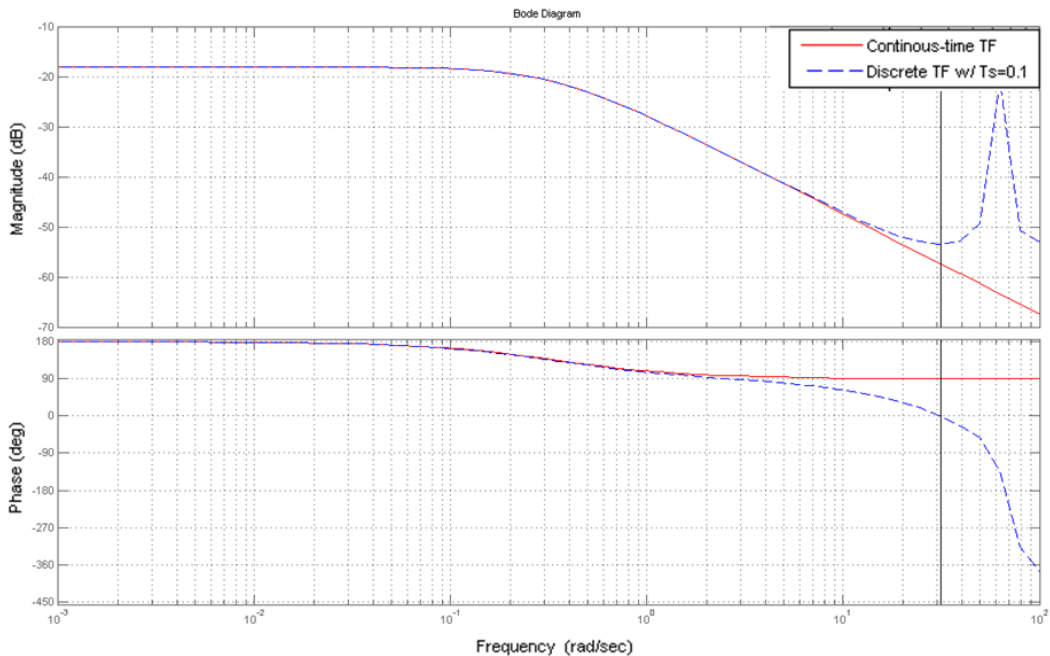


Figure 3.4: Frequency response to the continuous time transfer function from force input in surge to the surge velocity, shown together with its discrete transfer function.

In Figure 3.4 the steady state low frequency (DC) gain will be

$$K = -0.124 \quad (3.14)$$

The system, with poles and zeros given by Figure 3.5, will be stable since all its poles are in the left half plane (L.H.P). This makes sense since the system investigated is a general $\dot{x} = -ax + u$ model. However, the input output stability for the outputs x_b, z_b and θ_b (positions and Euler angle), will only be marginal stable.

The frequency response and bandwidths from the inputs $\mathbf{u} = [X \ Z \ M]^T$ to the surge velocity u , heave velocity w and angular pitch velocity q are given in Appendix 12.5. As a

result the bandwidth from force input X in surge to the surge velocity u is used in the determination of sampling frequency.

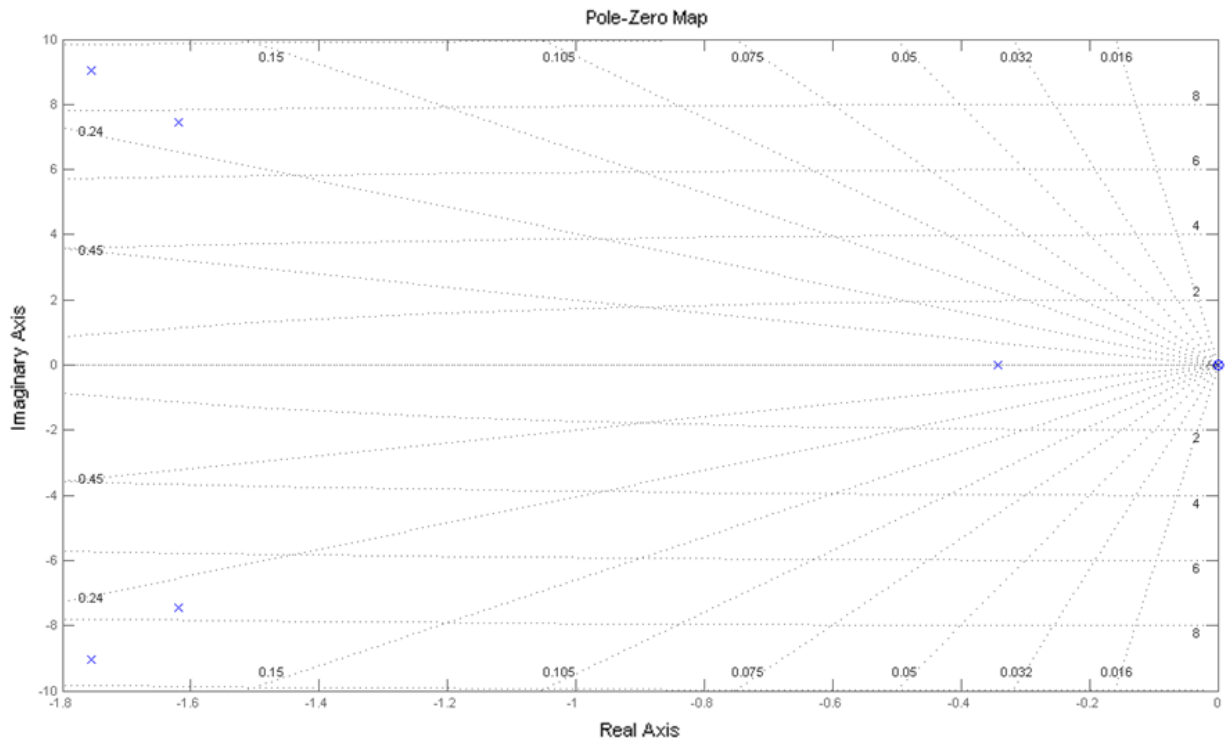


Figure 3.5: Poles 'x' and zeros 'o' for the system with surge velocity as output.

3.3.4 Determination of Sampling Frequency

In order to reconstruct the continuous time signal perfectly it is possible to use sampling instants that are sufficiently close. However, much of the signal will be lost if the sampling instants are too far apart, and if the sampled signal is changing too fast. It may therefore be of importance to find the highest frequency of the continuous time signal. This frequency is often referred to as the bandwidth frequency to the system, (Hüche, 1996). The value can be found by investigating where the transfer functions magnitude drops 3 dB below its DC gain value, ref Mathworks. The DC gain is the transfer function magnitude at $s = 0$ (frequency equal to zero).

To avoid getting the phenomena called aliasing, meaning that the sampled signal is interpreted as a lower frequency signal, the necessary sampling rate needs to be determined. According to Nyquist's sampling rule (Aastrom, 1997) the signal can be reconstructed if we sample with a frequency at least two times higher than the highest frequency to the system. The bandwidth frequency ω_b , often referred to as the Nyquist frequency ω_N , must therefore be

$$\omega_b < \frac{\omega_s}{2}, \quad (3.15)$$

where ω_s is the sampling frequency.

From the frequency response analysis of the system the design bandwidth frequency to the system should be chosen to be $\omega_b = 0.3415$ [rad/s]. This is the highest frequency to the transfer function from the input force X to the velocity output in surge u .

In practice a much faster sampling frequency than the bandwidth frequency is necessary. As a rule of thumb (Perdikaris, 1991) suggest a sampling rate that is 10-20 times larger than the frequency bandwidth to the system.

The sampling frequency should therefore be selected to be

$$\omega_s = 2 \cdot \omega_b \cdot \eta_s = 2 \cdot 0.3415 \cdot 2\pi \cdot 10 = 42.91 \text{ [Hz]}, \quad (3.16)$$

where η_s is the safety factor. To recreate the continuous time signal and avoid losing information, a sampling time of 0.023 [s] should be selected.

4 Experimental Setup

The 3 DOF vessel model can be simplified by neglecting the surge and pitch motion. By only looking at the heave motion of the vessel it will be easier to establish an experimental model. The experimental model consists of a DC motor that needs to be able to actuate necessary forces onto the simplified vessel model.

The simplified 1 DOF model, Figure 4.1, show a DC motor, with precision gear head, connected to a line actuating forces onto the simplified vessel model. The system communicates with a computer, giving commands to the motor. The DC motor will then actuate the necessary force to reach its desired reference.

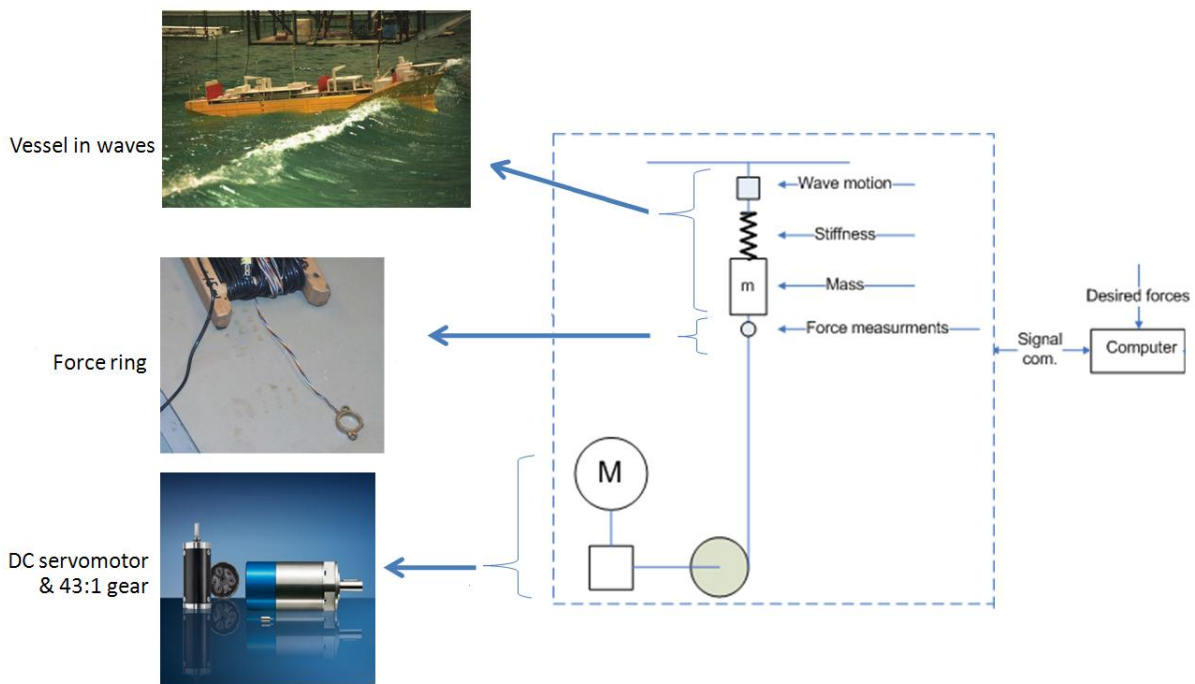


Figure 4.1: Overview of the 1 DOF system and its key components.

In this chapter, the necessary equipment for the experimental setup will be introduced. First, a discussion regarding the choice of DC motor is presented. Finally, the overall key equipment is explained. The chapter ends with a discussion regarding the installation of the equipment.

4.1 Determination of DC motor

In order to find an appropriate DC motor for the simplified vessel model, the maximum range for the expected mooring line forces, and responses, is needed. A reasonable estimate can be found by investigating the maximum and minimum top tension in one mooring line. To find the expected deflection amplitude to the simplified vessel model it is possible to look at the maximum and minimum heave response.

In J.M. Heurtier et al. (2001) a fully coupled analysis is presented wherein the motions of the floater, mooring lines and risers are computed. In the fully coupled analysis a test case proposed by Ormberg H. and Larsen (1998) is reproduced. The analysis deals with the dynamic response to environmental sea loads of a Floating Production and Storage Offloading

vessels (FPSO). The FPSO analyzed in the paper is anchored at 2000 m water depth using eight mooring lines connected to a rotating turret in the bow.

The maximum and minimum heave movement, presented in J.M. Heurtier et al. (2001), is found to be -9 m and 11 m, see Figure 4.2. The values give a reasonable assumption for what to expect of the maximum, and minimum, vertical motion of the top node for one mooring line.

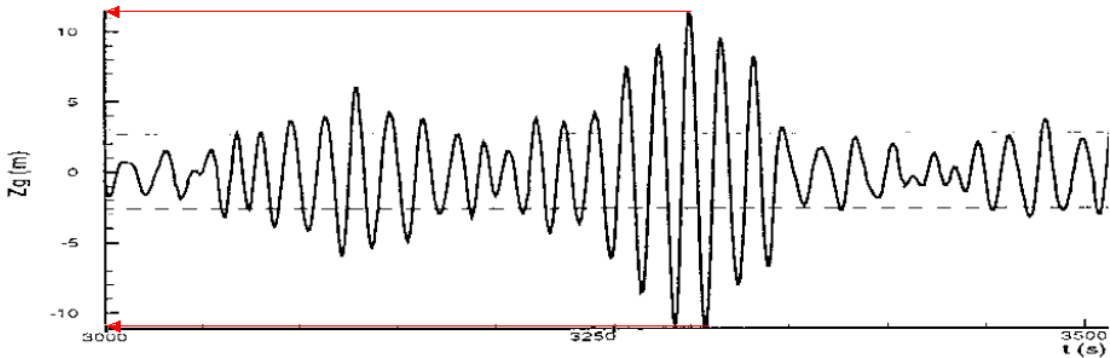


Figure 4.2: Heave motion versus time, zoom near peak (J.M. Heurtier, 2001).

It will also be necessary to suggest an appropriate estimate on how large, or small, a mooring line force is. The result in J.M. Heurtier et al. (2001), present the top tension in the most loaded line. The results over the complete simulation give a maximum top tension of 4800 kN, and a minimum of 800 kN, see Figure 4.3.

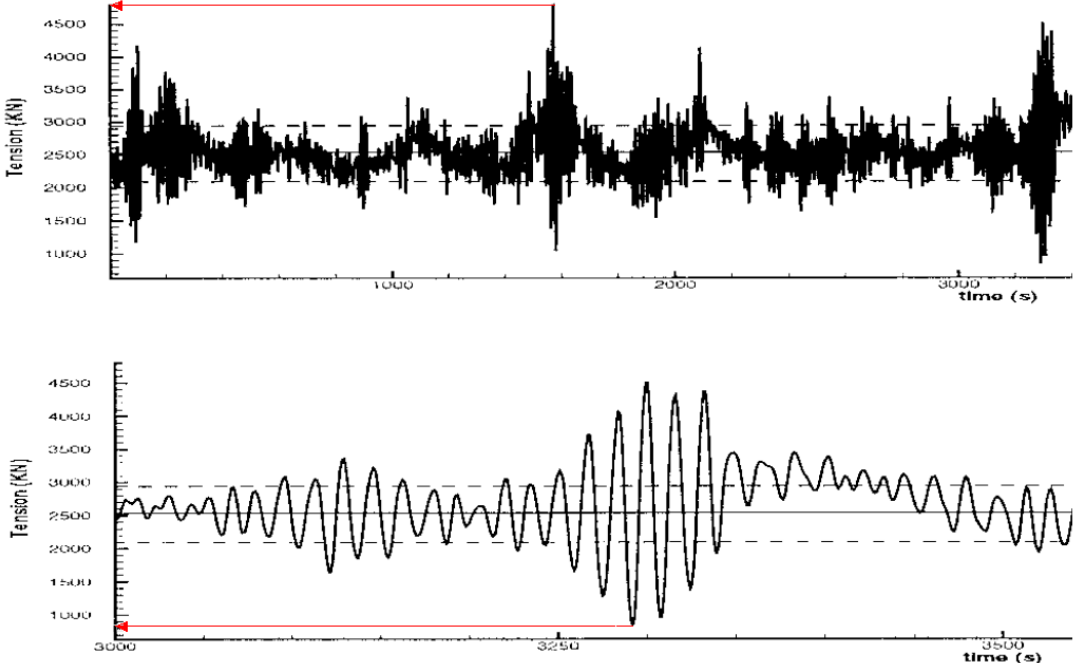


Figure 4.3: Top tension in the most loaded line versus time. Top: complete simulation. Bottom: zoom near a peak (J.M. Heurtier, 2001).

Using Figure 4.3, it will be possible to find the top tension and heave motion in model scale. According (DNV, 2007), the typical model scales for shallow water mooring tests are

between 1:30 and 1:100. The scaled top tension, using selected scales in this interval, for one mooring line will then be:

Model Scale	Maximum top tension model scale force (full scale 4800 kN).	Minimum top tension model scale force (full scale 800 kN)	Unit
1:30	182.4	30.4	N
1:50	39.4	6.6	N
1:70	14.4	2.4	N
1:90	6.8	1.1	N
1:100	4.9	0.8	N

Table 4.1: Model scale maximum expected top tension in one mooring line.

Hence, the maximum and minimum vertical motion of the top node, for one mooring line, will most likely not exceed the following values:

Model Scale	Maximum heave motion in model scale (full scale 11 m).	Maximum heave motion in model scale (full scale -9 m).	Unit
1:30	0.36	-0.30	m
1:50	0.22	-0.18	m
1:70	0.16	-0.13	m
1:90	0.12	-0.10	m
1:100	0.11	-0.09	m

Table 4.2: Model scale maximum expected heave motion.

The necessary maximum model scale force is dramatically cut down when the model scale is reduced from 1:30 to 1:70. Selecting a 1:70 model scale will therefore reduce the power demand to the machine actuating the maximum force. A much more practical, cheaper and smaller engine can then be selected. Another reason to select 1:70 as the model scale is that the top node vertical motion will be smaller than with a 1:30 as model scale. Hence, the wave generator does not need to have large deflection amplitudes.

A 1:70 in model scale should however be avoided when model testing in the ocean basin facilities. Preferably a 1:40 in model scale or larger should be used, reducing the margin of error and making it easier to implement environmental disturbances.

The top node of the mooring line, using 1:70 as model scale, will have vertical motion between 0.16 m and -0.13 m. In order to just have one revolution of the wheel connected to the DC motor shaft, the following radius will be necessary

$$O = 2\pi r \rightarrow r = \frac{O}{2\pi} = \frac{0.16 \text{ m} - (-0.13 \text{ m})}{2\pi} = 0.05 \text{ m}, \quad (4.1)$$

The obtained maximum and minimum values give us appropriate design specifications for the DC motor. The DC motor needs to actuate the necessary forces onto the vessel. With a 5 cm moment arm, the DC motor has to be able to actuate the following torques

$$\begin{aligned}
&0.05 \text{ m} * 2.39 \text{ N} = 0.12 \text{ Nm} \\
&0.05 \text{ m} * 14.36 \text{ N} = 0.72 \text{ Nm} \\
&0.12 \text{ Nm} < \text{torque} < 0.72 \text{ Nm}
\end{aligned}
\tag{4.2}$$

Hence, an engine that is able to actuate the calculated torques must be used in the experimental setup in order to reproduce the maximum and minimum top tension. The data from J.M. Heurtier (2001) is scaled using a 1:70 in model scale to reduce the engine torque demand.

Table 1 in Watts (1999) shows that the expected mooring line peak tension, in the most loaded line, is measured to be 23.54 [N]. A model scale 1:80 of a turret moored concrete FPSO with four mooring lines are experimental tested in Watts (1999). The comparison between random wave test and simulated tensions in mooring lines are presented. In our calculation the 14.4 N peak tension will be smaller than the value presented in Watts (1999). A higher peak tension is however expected since the FPSO is moored using four mooring lines instead of eight.

4.2 Necessary Equipment

Figure 4.4 shows an overview of the key equipment used in the experimental setup. The equipment consists of several parts and an overview is shown in the figure. The experimental setup use a DC motor to actuate forces onto the vessel model using velocity control of the engine shaft. Analog voltage signals are used as input to the Faulhaber motion controller to control the shaft velocity. The cRIO-9074 module is used to transmit the analog voltage signals; hence the shaft velocity can be preset. Force measurements can then be used as feedback to control the torque actuated by the motor.

The computer is communicating with the cRIO module using TCP/IP and the computer software LabVIEW®. The cRIO-hardware I/O are mapped to its respective ports in the compiled Simulink® model utilized by LabVIEW®. The Simulink® model can therefore be used to control the shaft velocity using force measurements as feedback.

The Faulhaber motion manager is used to set the configuration to the motion controller. The Faulhaber drive electronic is connected directly to the computer using a RS232 cable. The RS232 communication is used together with the Faulhaber motion manager to configure the motion controller implemented on the drive electronics.

The Simulink® model must be compiled in order to run together with the LabVIEW® software. The model must be compiled to a “dll” file using the Real-Time Workshop. Further, the real-time workshop toolbox I/O blocks must be used at the ports in the Simulink® model that are mapped to the cRIO module. The solver and fundamental sample time is set in the “configuration parameters” panel. The fundamental sampling time is set to be 0.01 s, or 100 Hz.

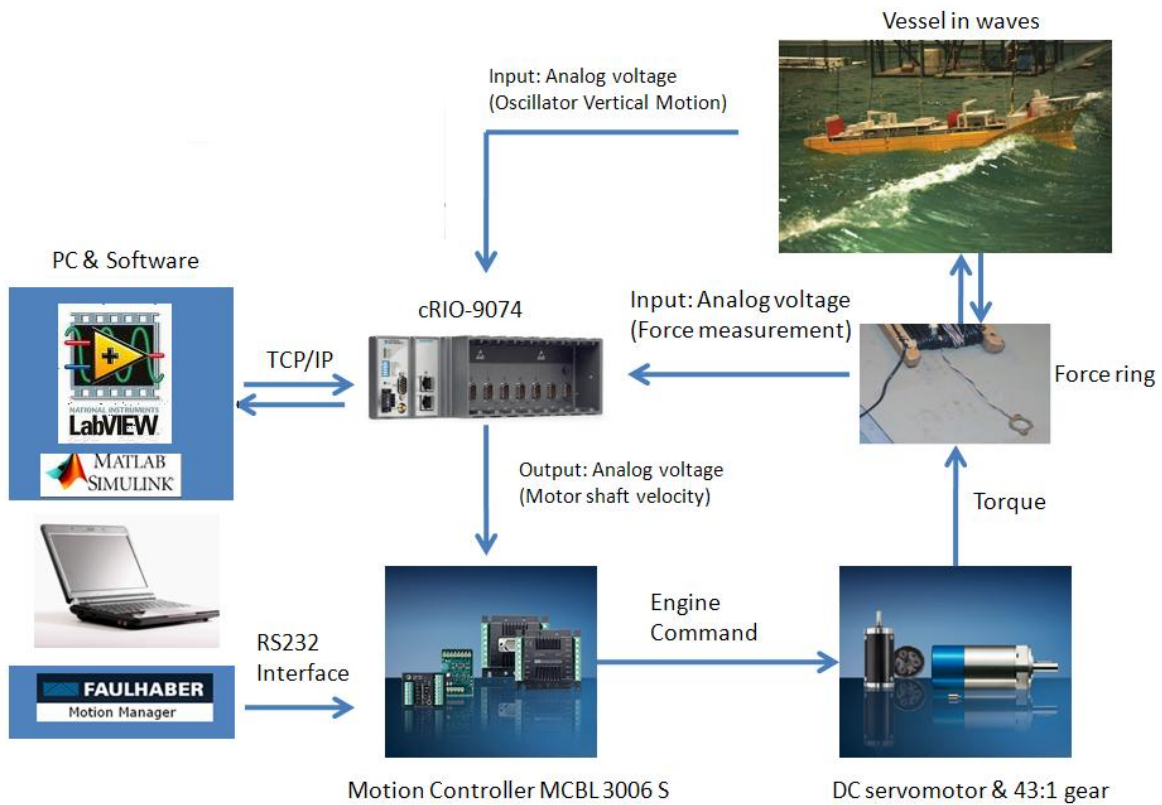


Figure 4.4: Experimental setup of the 1 DOF system.

The connections to the Faulhaber drive electronics are illustrated in Figure 4.5. The figure show the cables connected to its respective ports on the motion controller. The engine is connected to the motion controller using eight small cables. The RS232 communication is used by the Faulhaber motion manager to configure the motion controller. The velocity to the shaft can then be preset via analog voltage input by enabling the motion controller in speed mode.

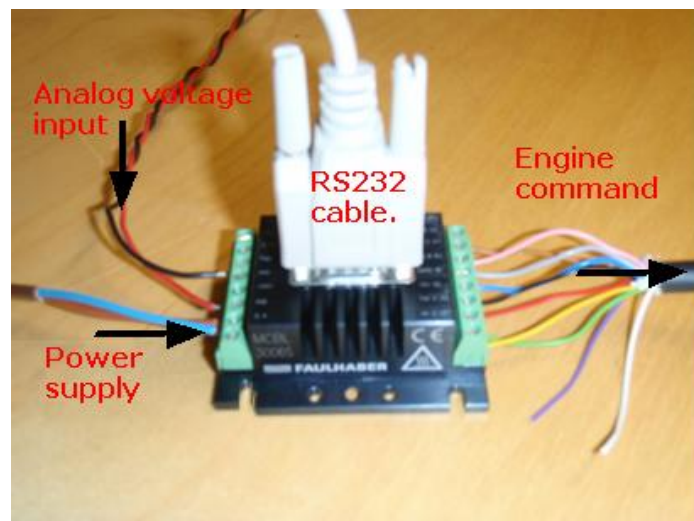


Figure 4.5: Faulhaber MCBL 3006 S motion controller connections.

The cRIO module is shown with its cables connected in Figure 4.6. The cRIO module is used to transmit analog voltage signals to the motion controller in order to command the shaft

velocity of the engine. The TCP/IP port shown in the figure is used to communicate with LabVIEW®.

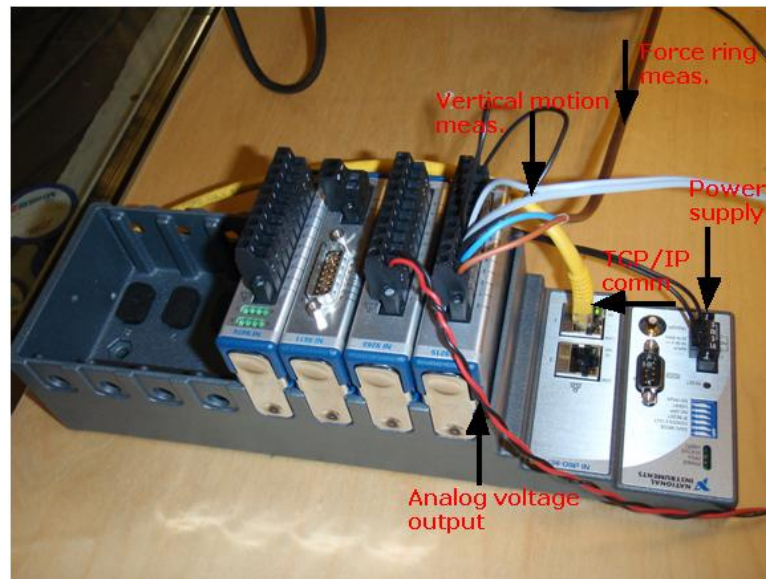


Figure 4.6: cRIO-module connections.

4.2.1 Servo motor / winch

A brushless DC servomotor, 3564 k024B-k1155, from Faulhaber was chosen in order to meet the specifications. The engine will be able to actuate the necessary mooring line forces in model scale. Staubo Elektro-Maskin-AS, situated in Oslo, was used as dealer¹. The key technical data are:

Description	Value	Unit
Diameter	35	mm
Length	64	mm
Stall torque	371	mNm
Torque up to	44	mNm

Table 4.3: DC Servomotor key technical data , ref (DC Motor Specifications).

¹ Contact person: Morten Sjøgaard, Tlf. 22 75 35 26/41 67 92 65, E-mail: morten.sogaard@staubo.no

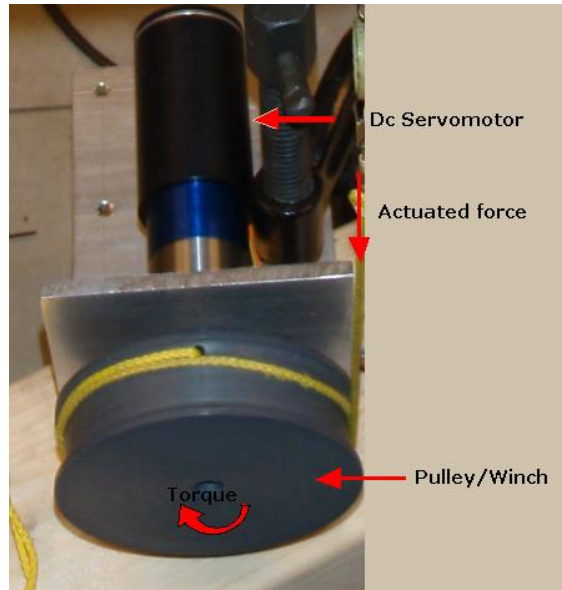


Figure 4.7: Brushless DC servomotor/winch setup.

4.2.2 Precision Gearhead

In order to achieve the appropriate torque the planetary precision gearhead, 30/1 S-34:1, from Faulhaber is chosen in order to meet the specifications. The key gearhead data are:

Description	Value	Unit
Shaft Diameter	8	mm
Diameter	30	mm
Length	43,1	mm
Efficiency	70	-
Reduction ratio	43:1	-

Table 4.4: Precision gear head technical data.



Figure 4.8: Planetary gearhead, ref. (Gear Specifications).

With the brushless DC-Servomotor in Figure 4.7 the engine will be able to actuate the following torque:

Engine: Maximum torque	44 mNm
Gearhead: Reduction ratio	43:1
Gearhead: Efficiency	70 %
Max available torque	$44\text{mNm} \cdot 43 \cdot 0.7 = 1.3 \text{ Nm}$

Table 4.5: Maximum available DC motor torque.

With a reasonable choice of radius, a 14 N peak force will be possible. With a 4 cm radius the estimated expected forces should be well covered, without reaching the 1.3 Nm limit. Using the radius directly from the gear shaft a peak force at $1.3\text{Nm}/0.004 \text{ m} = 325 \text{ N}$ will be possible.

4.2.3 Motion Controller

The Faulhaber motion controller is designed for control of the DC motor. The controller has numerous functions and operating modes which enable flexible adjustment to the respective drive function. The motion controller can be set in speed, position and torque control. The flexible connection option opens up a wide range of application areas. In addition the motion controller parameters can be adjusted in the Faulhaber motion manager.

The motion controller MCBL 3006 S from Faulhaber, in combination with the brushless DC-Servomotor, has the following control options

Control nr.:	Control option:
1	Torque control
2	Speed control
3	Position control

Table 4.6: Control options.

The Faulhaber motion controller is equipped with an integral current controller, which enables torque limitation. In the instruction manual, (Instruction Manual), on page 39, 53 and 58, current regulation is explained. It is possible to switch to “analog target current presetting”, page 39, with the source for velocity (SOR) command. The SOR command with argument 3 makes it possible to set the current target value via analog input. Since the current is proportional to the torque, it will be possible to follow a torque reference.

The engine can also run in speed mode and the angular velocity to the engine shaft can be preset via analog voltage input. Force measurements can then be used as feedback to control the desired torque actuated by the motor. The motion controller should then be set in continuous mode (CONTMOD) using the SOR command with argument 1.



Figure 4.9: Drive electronics, ref. (Instruction Manual)

4.2.4 Sensors Specifications

To measure the actuated forces the MARINTEK² force ring is used. An amplifier is used to amplify the measured force ring signal. The amplifier is shown in Figure 4.11.

The measured force will include white noise; filtering the signal will therefore be necessary before using it as feedback.

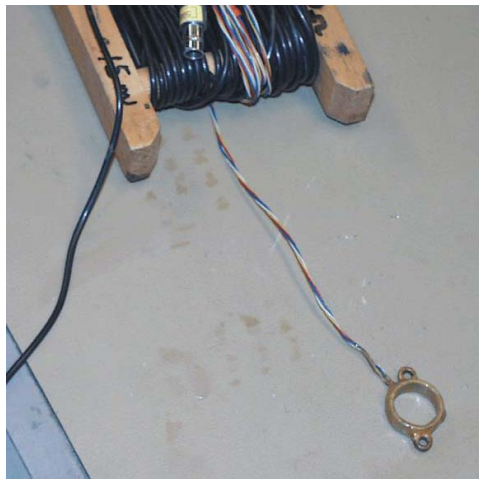


Figure 4.10: Marintek force ring.

² Contact person: Torgeir Wahl, Tlf. 73 59 57 44/ 92 86 34 28, E-mail: torgeir.wahl@ntnu.no

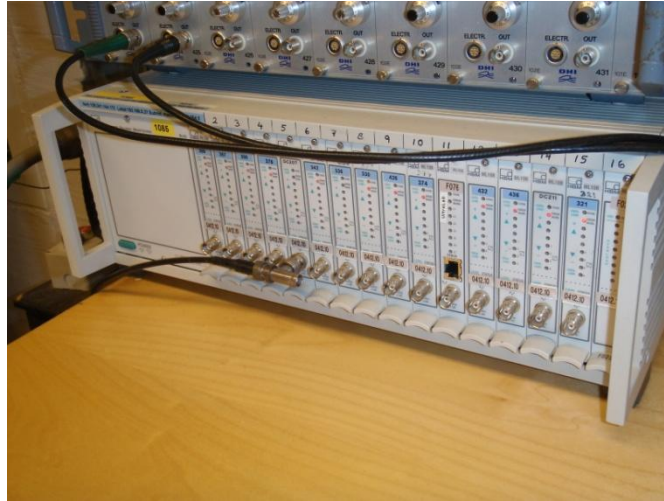


Figure 4.11: Force measurements amplifier.

4.2.5 Power Supply

The cRIO module and motion controller is connected to individual 24 volt power supplies.

4.2.6 Oscillating System

The oscillating system can be set to create desired vertical motion. The vertical motion is controlled using an external computer. The frequency and amplitude to the sinusoidal motion generated can be changed in the LabVIEW® interface controlling the device. Measurements of the vertical motion are sent as voltage signals to the cRIO module.

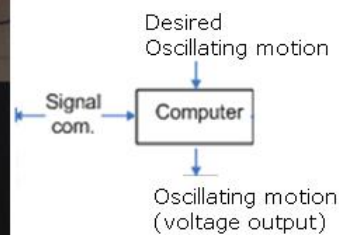
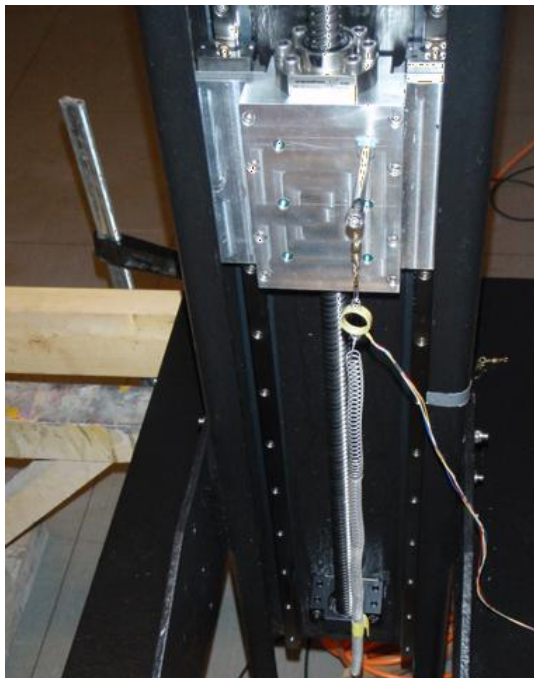


Figure 4.12: Oscillating system generating sinusoidal vertical motion.

The program in LabVIEW® used to control the actuator is shown in Figure 4.13.

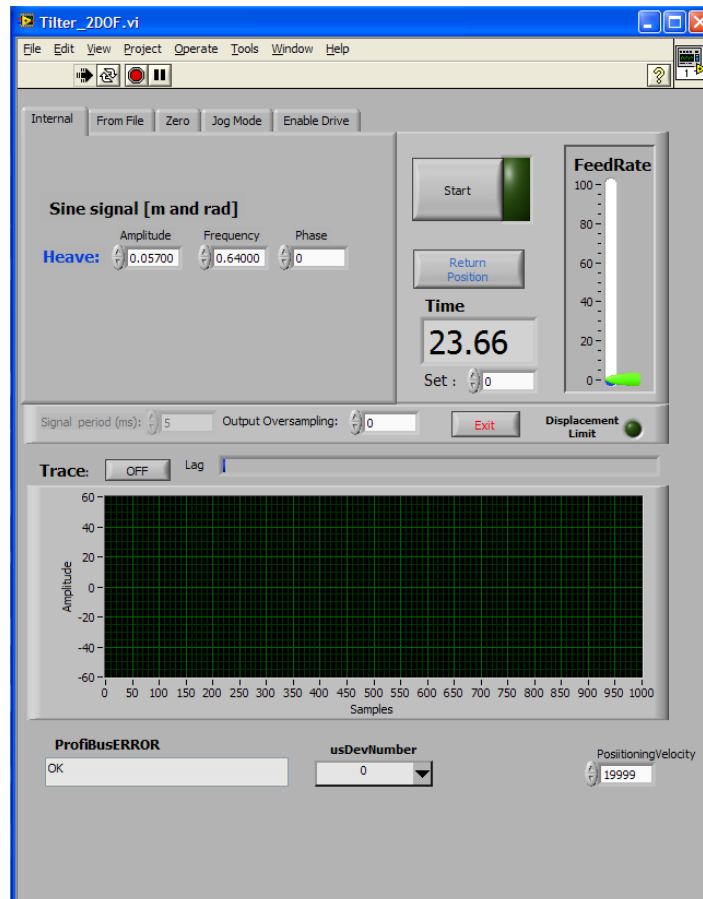


Figure 4.13: LabVIEW® interface used for control of the oscillating system actuator.

4.3 Discussions

At first torque control with current limitation was carried out. An analog voltage at the motion controller input will then correspond to a current limitation in the DC motor. The relationship between torque and current is proportional, and a current limit will then correspond to a given torque. Hence, the desired reference force can be achieved. However, with current limitation used as set point the motor shaft will try to keep its position. If a torque higher than the current limit is applied at the motor shaft the pulley will turn, with lower torque the position will be maintained. The motor shaft needs to have a sinusoidal motion in order to follow the vessel vertical motion. A high positive angular velocity of the motor shaft is therefore set as target in the controller. If the torque, or current set point limit, is set to be high in the Faulhaber motion controller, the pulley will turn until it reaches its current limit. If the torque or current limit is set to be a low value the shaft will release its pull until the new current limit is reached. This control option will however be too slow and the pulley will not release its pull fast enough due to the friction in the gear. Another control option will therefore be needed.

According to the Faulhaber Instruction Manual velocity control with high requirements on synchronous operation and minimal torque fluctuations can be utilized. A PI velocity controller ensures that the target velocities are maintained. The velocity to the engine shaft can then be preset using analog voltage input. Force measurement can be applied as feedback to ensure that desired force references are achieved by controlling the shaft velocity.

The engine shaft maximum speed can be set to run at rpm values all the way up to 22 000. The maximum speed at the gear shaft will however be lowered to about 360 rpm with a 43:1 reduction rate and 70 % efficiency. Meaning that the gear shaft can turn 6 rounds each second. The engine should therefore have no problem following an oscillating vertical motion. In addition the engine has no problem inducing a 14 [N] peak mooring line force, larger forces can be actuated without any problem.

5 Mathematical Models of Experimental Setup

In this chapter, a model for the 1 DOF system will be introduced. First, a detailed model of the mass dynamics is explained. Special attention is given to the modeling of the vessel, or mass, connected to a spring and oscillator. A simplified model of the motor dynamics and its corresponding transfer functions is then presented. This model is used together with the derived mass dynamics to represent the total model. Finally, the motion controller included on the Faulhaber drive electronics is explained. Velocity control of the motor shaft is discussed as a method for controlling the force actuated onto the vessel. The total model of the mass and motor dynamics is used to describe the Faulhaber system with velocity control.

5.1 Mass Dynamics

A floating vessel in heave is described by the following uncoupled equation of motion (Pettersen, 2007):

$$(M_{33} + A_{33})\ddot{\eta}_3 + B_{33}\dot{\eta}_3 + C_{33}\eta_3 = F_3(t) \quad (5.1)$$

where η_3 is the heave position, $F_3(t)$ is the external forces in heave and:

$$\begin{aligned} m &= \text{mass of the vessel (kg)} \\ A_{33} &= \text{hydrodynamic added mass in heave (kg)} \\ B_{33} &= \text{linear damping coefficient} \\ C_{33} &= \text{spring coefficient} \end{aligned}$$

$F_3(t)$ is defined as all the forces acting on the body mass in vertical direction (or the 3-direction). The spring force term $C_{33}\eta_3$ is position dependent, and it is given as the difference between the body's buoyancy force and the gravity force. If the body is brought out of its equilibrium position the force will be the result of the change in buoyancy (Pettersen, 2007). The spring coefficient can therefore be written using the equation in (Pettersen, 2007) as

$$C_{33} = \rho g A_{wp}, \quad (5.2)$$

where A_{wp} is the area of water plane (m^2) with

$$\begin{aligned} \rho &= \text{density of water (kg / m}^3\text{)} \\ g &= \text{acceleration of gravity (m / s}^2\text{)} \end{aligned}$$

In order to emulate the heave motion of a floating vessel the setup in Figure 5.1 is introduced.

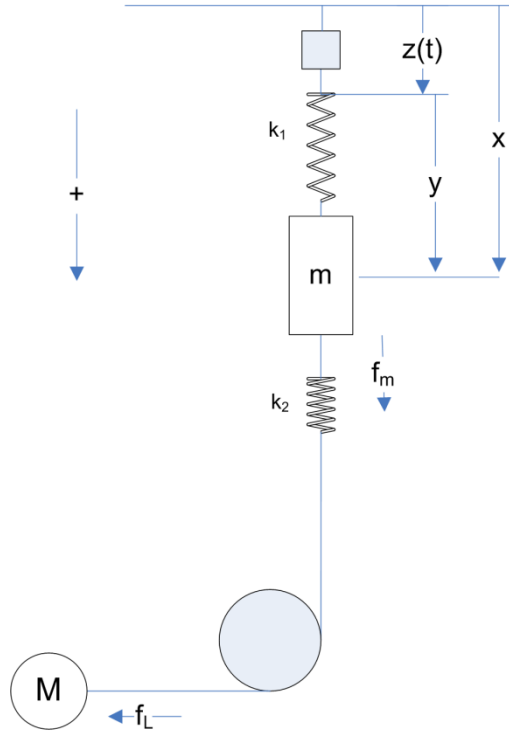


Figure 5.1: Simplified vessel model

The simplified model should have properties similar to (5.1) describing a floating vessel in heave. f_m is the measured force, or the force actuated onto the system from the motor. f_L is the load force from the wire (tension) on the motor shaft. Further, k_1 should equal the water plane stiffness given by the coefficient C_{33} , and m should equal the body mass M_{33} of the floating vessel in model scale. When the vessel is considered to be a rectangular barge the mass is defined in (Pettersen, 2007) as

$$M_{33} = \rho L B d , \quad (5.3)$$

where B is the breadth, L is the length and d is the draught to the barge. k_2 is the stiffness to the force ring measuring the force actuated onto the body mass from the direct current (DC) motor, shown as M in Figure 5.1.

To introduce a wave force on the body mass a “wave generator” is introduced. The “wave generator” is connected to the spring k_1 and the roof. An engine will cause the spring connection point to move up and down, emulating a wave force on the body mass. The vertical motion, caused by this engine, can be written as a harmonic function

$$z(t) = a + b \sin(\omega t) , \quad (5.4)$$

where a and b are some constants and ω is the frequency.

From the setup we also have the relationship

$$x(t) = z(t) + y(t) . \quad (5.5)$$

The following sign convention is adopted (see Figure 5.1)

- $z(t)$ Distance from the fixed roof to the fastening point of the spring (positive downwards). $z(t) = a - b$ is the minimum value, and $z(t) = a + b$ is the maximum value. Hence, a must be larger than b , where a and b is given in (5.4).
- x Distance from the fixed roof to the COG of the moving mass. (positive downwards)
- x_0 Equilibrium position of the pretensioned starting position of the mass m , or the distance from the fixed roof to the center of gravity (COG) of the mass at rest when $z(t) = a + b$ and $f_m = 0$.
- y Distance from the fastening point of the spring (k_1) to the COG of the moving mass m (positive downwards).
- y_0 Distance from the spring fastening point to the COG of the mass when $f_{k1} = f_m = mg = 0$, where f_{k1} is the spring force due to the stiffness k_1 . In other words the equilibrium position of the mass when the system is at rest with $z(t)$ stationary and no gravity acting on the mass.

In the simplified vessel model the damping and added mass is neglected. Since the body mass is oscillating in air, added mass will not be included here as it would in an experiment in water. Also damping is neglected in this simplified model, and hence some accuracy lost. However, the simplified model will give a good indication of the bandwidth to the control system actuating the simulated mooring force onto the vessel. The behavior to the vessel, proposed in the simplified model, will therefore be satisfactory.

Hook's law describes the opposing force exerted by the spring

$$f_{k1} = -k_1 d_1 \quad (5.6)$$

where, k_1 , is the spring constant, and d_1 is the total distance the spring is disturbed from its position at relaxation. The spring force is then given as

$$f_{k1} = k_1 (y(t) - y_0) = k_1 (x(t) - z(t) - y_0), \quad (5.7)$$

and d_1 is given as

$$d_1 = x(t) - z(t) - y_0. \quad (5.8)$$

The spring force will be a simple linear approximation, and in most instances Hook's law is not precise. For metal springs, linear model is only valid in the region where the spring behavior is elastic, beyond that the model breaks down.

The equations describing the mass dynamics becomes

$$m\ddot{x} = mg + f_m - f_{k1}. \quad (5.9)$$

Inserting (5.6) into (5.9) give

$$m\ddot{x} = mg + f_m - k_1 (x - z(t) - y_0), \quad (5.10)$$

where g is the gravitational constant and m is the mass. The equilibrium to the dynamic equation will be $(\dot{x}, x) = (0, \frac{mg}{k_1} + z_0 + y_0)$ which shows that the mass falls to rest when $f_{k1} = mg$, with $f_m = 0$ and $z(t) = z_0$.

Assuming the second spring, k_2 , is infinitely stiff so that it may be disregarded and there is no slack in the wire, then the mass system and the rotating motor dynamics, will be coupled. The revolution or distance, x_m , of the pulley on the motor shaft can then be written as

$$x_m = r(\theta - \theta_0) = x - x_0, \quad (5.11)$$

where θ is the pulley angle, θ_0 is the initial angle, r is the radius of the pulley connected to the motor shaft.

For convenience, the initial motor angle could be selected as $\theta_0 = 0$, such that

$$\begin{aligned} r\theta &= x - x_0 \\ r\dot{\theta} &= \dot{x} = r\omega \end{aligned} \quad (5.12)$$

where ω is the angular velocity of the pulley connected to the motor shaft. x_0 can be selected to

$$x_0 = \frac{mg}{k_1} + a + b + y_0 + \delta, \quad (5.13)$$

where $\delta > 0$ ensures that $x = x_0$ is at a pretensioned position for all $z \in [a - b, a + b]$ when $\theta_0 = \theta = 0$.

5.2 Motor Dynamics

The equivalent electrical circuit of the DC motor is illustrated in Figure 5.2. It can be represented by a voltage source u_a across the coil of the armature, see (Egeland, 1993). The resistance is denoted by R_a , and the armature inductance of the circuit by L_a . The induced voltage due to the applied voltage source is referred to as e_a , or the back electromotive force (emf). It is generated by the rotation of the electrical coil through the flux lines of the permanent magnets.

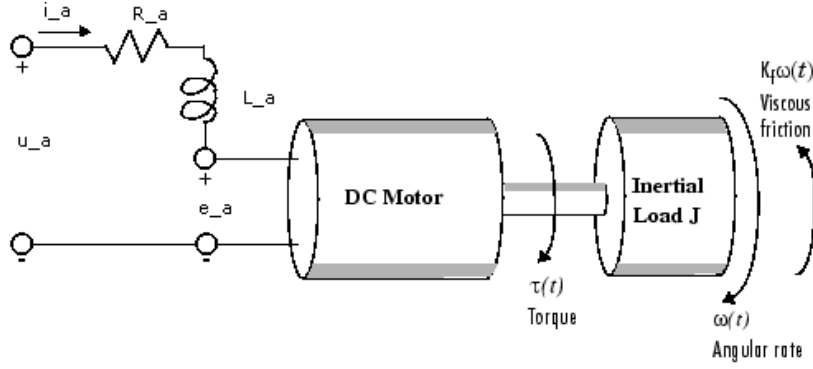


Figure 5.2: Electrical representation of a DC motor, ref (The MathWorks).

The torque, τ , seen at the shaft of the motor is proportional to the current induced by the applied voltage

$$\tau(t) = K_T i_a, \quad (5.14)$$

K_T is the torque constant and dependent on the flux density of the magnets, the number of turns around the armature winding, ref. (The MathWorks). The back induced electromotive force can be written, in compliance with Faraday's law, as

$$e_a = K_E \omega, \quad (5.15)$$

where ω is the angular velocity and K_E is the voltage constant dependent on the physical properties of the motor. The sum of all the torques around the shaft, using Newton's law, can be written as in (Egeland, 1993)

$$J_m \frac{d\omega}{dt} = \sum \tau_i = -K_f \omega(t) + K_T i(t) - \tau_L, \quad (5.16)$$

where $K_f \omega_m$ is a linear approximation for viscous friction, J_m is the inertia of the rotating masses, and τ_L is the load torque. Further, Kirchhoff's voltage law states that the sum of all voltages around a loop must equal zero, giving

$$u_a - e_a - i_a R_a - L_a \frac{d}{dt} i_a = 0. \quad (5.17)$$

Substituting (5.15) into (5.17) give the following differential equation

$$L_a \frac{di_a}{dt} = -R_a i_a(t) - K_E \omega(t) + u_a(t). \quad (5.18)$$

A differential equation for the torque can be found by inserting (5.14) into (5.18), giving

$$L_a \dot{i}_a = -R_a i_a - K_E \omega + u_a(t) \quad (5.19)$$

Further, the differential equation for the angular velocity can be found, using (5.14) and (5.16), as

$$J_m \dot{\omega} = -K_f \omega + K_T i_a - \tau_L. \quad (5.20)$$

The equations given by (5.19) and (5.20) describe the DC motor dynamics. Hence, a state space representation of the motor dynamics can be expressed as

$$\begin{bmatrix} \dot{i}_a \\ \dot{\omega} \end{bmatrix} = \begin{bmatrix} -\frac{R_a}{L_a} & -\frac{K_E}{L_a} \\ \frac{K_T}{J_m} & -\frac{K_f}{J_m} \end{bmatrix} \begin{bmatrix} i_a \\ \omega \end{bmatrix} + \begin{bmatrix} \frac{1}{L_a} \\ 0 \end{bmatrix} u_a + \begin{bmatrix} 0 \\ -\frac{1}{J_m} \end{bmatrix} \tau_L \quad (5.21)$$

and

$$y = \begin{bmatrix} 0 & 1 \end{bmatrix} \begin{bmatrix} i_a \\ \omega \end{bmatrix}, \quad (5.22)$$

which is expressed symbolically as

$$\frac{d}{dt} \mathbf{x} = \mathbf{A}\mathbf{x} + \mathbf{B}_1 u_a + \mathbf{B}_2 \tau_L \quad (5.23)$$

and

$$y = \mathbf{C}\mathbf{x} \quad (5.24)$$

where the applied voltage u_a is the control input, τ_L is the load disturbance, $\mathbf{x} \in \mathbb{R}^2$ is the state vector and $y = \omega$ is the output.

In (Hesphana, 2009) the controllability matrix for a linear time-invariant (LTI) system is given as

$$Co = [B \quad AB \quad A^2B \quad \cdots \quad A^{n-1}B]_{n \times (kn)} \quad (5.25)$$

for a n -by- n matrix \mathbf{A} , and an n -by- k matrix \mathbf{B} . In the LTI system, (5.23), the \mathbf{B} matrix is a 2-by-1, and the \mathbf{A} matrix a 2-by-2. This will give the following controllability matrix

$$Co = [B \quad AB_1] = \begin{bmatrix} \frac{1}{L_a} & -\frac{R_a}{L_a^2} \\ 0 & \frac{K_T}{J_m L_a} \end{bmatrix} \quad (5.26)$$

The reduced row echelon form of the controllability matrix, using Gauss Jordan elimination, will be

$$\begin{bmatrix} 1 & 0 \\ 0 & 1 \end{bmatrix} \quad (5.27)$$

This corresponds to two linearly independent columns, or rows, of the controllability matrix Co , resulting in full rank. The controllability matrix test, or Theorem 38 in (Hesphana, 2009), states that a LTI system is controllable if and only if $rank(Co) = n$. Since $n = 2$ the LTI system in (5.23) is controllable.

Using the duality Theorems in (Hesphana, 2009) Section 15.8 it is possible to conclude that a pair (\mathbf{A}, \mathbf{C}) is observable if and only if the pair $(\mathbf{A}', \mathbf{C}')$ is controllable. Using (5.25), on the pair $(\mathbf{A}', \mathbf{C}')$, the following controllability matrix is obtained

$$Co = [C' \quad A'C' \quad (A')^2C' \quad \cdots \quad (A')^{n-1}C'] = Ob'$$

where, Ob' , denotes the observability matrix of the LTI system, defined by

$$Ob = \begin{bmatrix} C \\ CA \\ CA^2 \\ \vdots \\ CA^{n-1} \end{bmatrix}_{(kn) \times n}$$

Since $rank(Co) = rank(Ob') = rank(Ob)$ Theorem 59 in (Hesphana, 2009) states that the LTI system is observable if and only if $rank(Ob) = n$.

$$Ob = \begin{bmatrix} C \\ CA \end{bmatrix} = \begin{bmatrix} 0 & 1 \\ \frac{1}{J_m} & -\frac{K_f}{J_m} \end{bmatrix}$$

This matrix will also have full rank, or rank equal to two, giving an observable LTI system.

5.2.1 Transfer Functions

A block diagram for the motor dynamics can be developed from the differential equations. Taking the Laplace transform of each equation gives

$$s i_a(s) - i_a(0) = -\frac{R_a}{L_a} i_a(s) - \frac{K_E}{L_a} \omega(s) + \frac{1}{L_a} u_a(s)$$

$$s \Omega(s) - \omega(0) = \frac{K_T}{J} i_a(s) - \frac{K_f}{J} \omega(s) - \frac{1}{J} \tau_L(s)$$

The initial conditions converges to zero, and all the variables become some change around a reference state, if we consider perturbations around some steady state value. The equations can then be rewritten into the following form:

$$i_a(s) = \frac{u_a(s) - K_E \omega(s)}{L_a s + R_a} \quad (5.28)$$

$$\omega(s) = \frac{K_T i_a(s) - \tau_L(s)}{J_m s + K_f} \quad (5.29)$$

The block diagram, using (5.28), and (5.29), is shown in Figure 5.3.

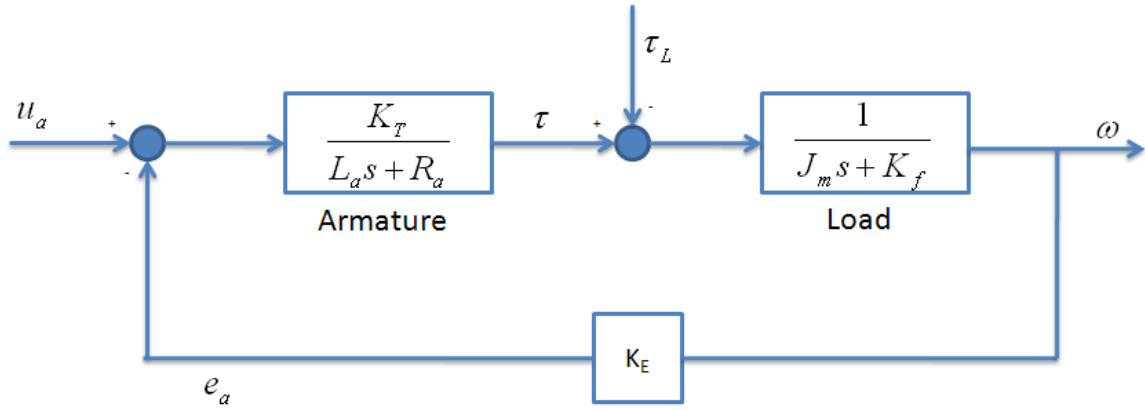


Figure 5.3: Block diagram representation of a DC-motor

Inserting (5.29) into (5.28) give

$$i_a(s) = \frac{u_a(s) - K_E \frac{i_a(s) - \tau_L(s)}{J_m s + K_f}}{L_a s + R_a}$$

$$i_a(s) \left(L_a s + R_a + \frac{K_E}{J_m s + K_f} \right) = u_a(s) + \frac{K_E}{J_m s + K_f} \tau_L(s)$$

The equation for i_a can then be written as

$$i_a(s) = H_1(s)u_a(s) + H_2(s)\tau_L(s)$$

where $H_1(s)$, and $H_2(s)$ is the relationship between i_a and the inputs. The transfer function $H_1(s)$, from the voltage u_a to the current i_a , can then be written as

$$H_1(s) = \frac{i_a(s)}{u_a(s)} = \frac{J_m s + K_f}{L_a J_m s^2 + (K_f L_a + R_a J_m) s + R_a K_f + K_T K_E}. \quad (5.30)$$

Further, the transfer function from the load torque τ_L to the torque τ is given by

$$H_2(s) = \frac{i_a(s)}{\tau_L(s)} = \frac{K_E}{L_a J_m s^2 + (K_f L_a + R_a J_m) s + R_a K_f + K_T K_E}. \quad (5.31)$$

The transfer function from the inputs to the output ω can also be found using the same approach.

Inserting (5.28) into (5.29) give

$$\omega(s) = \frac{\frac{K_T(u_a(s) - K_E \omega(s))}{L_a s + R_a} - \tau_L(s)}{J_m s + K_f}$$

$$\omega(s) \left(J_m s + K_f + \frac{K_E K_T}{L_a s + R_a} \right) = \frac{K_T u_a(s)}{L_a s + R_a} - \tau_L(s),$$

and the equation for the output ω can be written as

$$\omega(s) = H_3(s)u_a(s) + H_4(s)\tau_L(s).$$

The transfer function $H_1(s)$, from the voltage u_a to the angle velocity ω , can then be written as

$$H_3(s) = \frac{\omega}{u_a}(s) = \frac{K_T}{J_m L_a s^2 + (J_m R_a + K_f L_a)s + K_f R_a + K_E K_T}. \quad (5.32)$$

Further, the transfer function from the load torque τ_L to the angular velocity ω is given by

$$H_4(s) = \frac{\omega}{\tau_L}(s) = \frac{L_a s + R_a}{J_m L_a s^2 + (J_m R_a + K_f L_a)s + K_f R_a + K_E K_T}. \quad (5.33)$$

5.3 1 DOF Dynamic Model

The motor dynamics is derived in Section 5.1 and are given as:

$$L_a \dot{i}_a = -R_a i_a - K_E \omega + u_a(t) \quad (5.34)$$

$$J \ddot{\theta} = -K_f \dot{\theta} + \tau - r \cdot f_L. \quad (5.35)$$

The equations given by (5.10), (5.34) and (5.35) represent a state space of dimension \mathbb{R}^5 . The state space can be reduced to \mathbb{R}^3 by introducing the constraint given by (5.12). The mass dynamics in (5.10), with state variables (θ, ω, i_a) , is then obtained as

$$m \cdot r \cdot \ddot{\theta} = mg + f_m - k_1(r \cdot \theta + x_0 - z(t) - y_0) \quad (5.36)$$

Since $f_m = f_L$ the equation (5.35) can be rewritten by adding (5.36), giving

$$J \ddot{\theta} = -K_f \dot{\theta} + \tau - r \left(mr \ddot{\theta} - mg + k_1(r \theta + x_0 - z(t) - y_0) \right) \quad (5.37)$$

$$\rightarrow (J + r^2 m) \cdot \ddot{\theta} = -K_f \cdot \dot{\theta} + \tau - k_1 r^2 \cdot \theta + mg \cdot r - k_1 r (x_0 - z(t) - y_0)$$

Hence, the total dynamic system describing the setup in Figure 5.1, written in 1st order state space form, becomes

$$\dot{\theta} = \omega \quad (5.38)$$

$$\dot{\omega} = \frac{1}{J + mr^2} \left[-k_1 r^2 \theta - K_f \omega + K_T i_a + mgr + k_1 r (z(t) + y_0 - x_0) \right] \quad (5.39)$$

$$\dot{i}_a = \frac{1}{L_a} \left[-K_E \omega - R_a i_a + u_a \right] \quad (5.40)$$

The system above requires that $x_m = x - x_0$ at all times. This means that no slack in the wire between the pulley motor and mass may be accepted. If slack in the wire occurs the equation will no longer be valid, and the ω and x dynamics will not be coupled. An alternative approach may be necessary to decouple the ω and x dynamics to avoid this problem. However, since the simulated mooring force is positive the wire will need to be tensioned at all times and therefore no slack in the wire may occur.

Defining the states as

$$x := [\theta \quad \omega \quad i_a]', \quad (5.41)$$

we can write the dynamic model as

$$\dot{x} = Ax + Bu_a + Gw, \quad (5.42)$$

$$y = Cx, \quad (5.43)$$

with

$$A = \begin{bmatrix} 0 & 1 & 0 \\ \frac{-k_1 r^2}{J_m + mr^2} & \frac{-K_f}{J_m + mr^2} & \frac{K_T}{J_m + mr^2} \\ 0 & -\frac{K_E}{L_a} & -\frac{1}{L_a} \end{bmatrix}, \quad B = \begin{bmatrix} 0 \\ 0 \\ \frac{1}{L_a} \end{bmatrix}, \quad G = \begin{bmatrix} 0 \\ r \\ 0 \end{bmatrix} \quad (5.44)$$

$$C = [0 \quad 1 \quad 0] \quad (5.45)$$

and disturbance $w = mg + k_1(z(t) + y_0 - x_0)$.

The observability and controllability matrix can be found for the state space system above utilizing the same methods as applied for the DC motor dynamics. The controllability matrix and observability matrix to the system above, will have full rank, hence the system will be controllable and observable.

5.4 Motion Controller

The goal is to control the force actuated onto the vessel, this can be achieved by presetting the velocity of the DC motor. A positive velocity of the motor shaft will tension the line connected to the floater. Force measurement can then be used as feedback to determine what velocities the DC motor needs in order to achieve the desired reference forces.

The Faulhaber drive electronics include a motion controller that can be configured to control the velocity of the motor shaft. The Faulhaber Motion manager software sets the configurations of the motion controller. By running on continuous mode (CONTMOD) and the SOR1 operating mode it is possible to preset the velocity to the motor via analog voltage input. Alternatively we can use the SOR2 mode with velocity presetting via a pulse-width-modulation (PWM) signal. It is also possible to run with velocity presetting via RS232, meaning that commands can be sent to the motion controller, for example direction of rotation.

In this thesis the velocity will be preset via analog voltage input. The maximum speed is set to be 10 000 rpm in the Faulhaber motion manager software. 10 V at the analog input will then give 10 000 rpm as target velocity.

A schematic overview of the system included in the Faulhaber motion controller is shown in Figure 5.4. The target velocity due to an analog voltage input is calculated in the ‘‘Target

Velocity Calculations” box. The system also consists of a PI velocity controller that attempts to minimize the difference between the target velocity and actual velocity by adjusting the engine control input u . Figure 12.1 in Appendix 12.1 gives a more detailed view of the system implemented on the Faulhaber motion controller. In the supplied Faulhaber software it is possible to monitor the target velocity, actual velocity and actual current. The data can be stored and used in the system identification process.

The computer software LabVIEW® utilized together with the cRIO module can be used to send analog voltage signals as input to the Faulhaber drive electronics. By controlling the analog input it is possible to control the actual velocity of the motor shaft. Hence, the desired force actuated onto the vessel can be controlled.

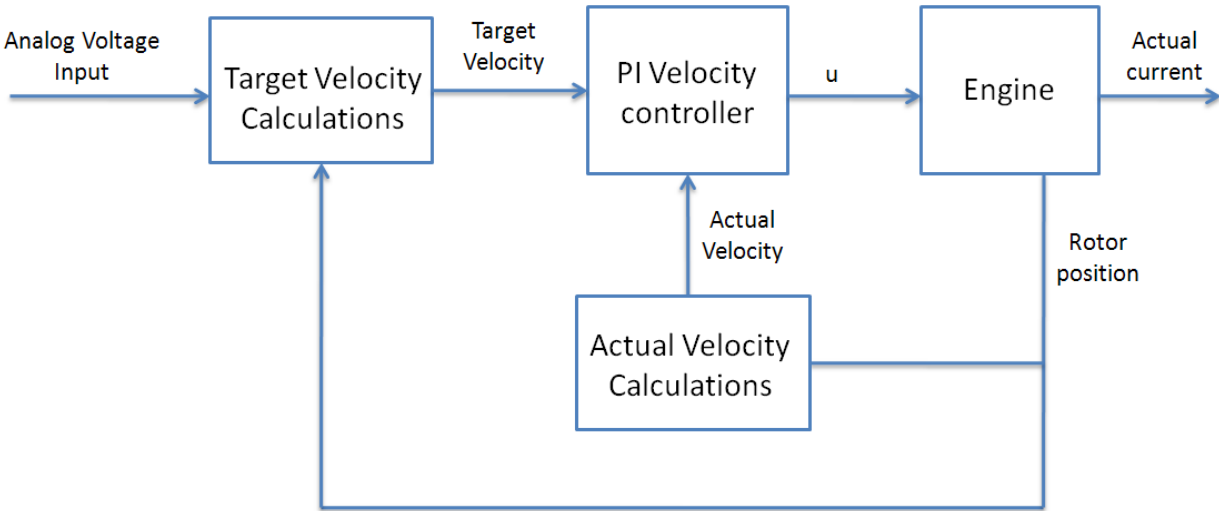


Figure 5.4: Schematic overview of the system implemented on the Faulhaber motion controller.

The physical system of the Faulhaber motion controller is detailed and complex. However, it is possible to use previously derived models of the mass and motor dynamics to describe the main physical properties of the system.

A model describing the dynamics from a given target velocity ω_0 to the actual velocity ω and current i_a can be found. Figure 5.5 shows the block diagram of PI control for a DC motor with angular velocity as feedback. The block shown as “1 DOF dynamic model” in the figure are the previously derived equations from (5.38) to (5.40), which consists of the motor and mass-spring dynamics. The 1 DOF dynamic model can be used to describe the DC motor dynamics, however this model will include the disturbance from the mass-spring dynamics (the disturbance from the mass-spring can be neglected in the model by simply setting the mass and spring value to zero). However, it is convenient to include this dynamics when the DC motor is connected to the mass-spring. A PI controller is included to minimize the difference between a preset target velocity ω_0 and the actual velocity ω . A PI controller is chosen to represent the PI velocity controller on the Faulhaber motion controller.

A function will be necessary to describe the relationship between the current i_a , or actual motor shaft velocity ω , to actuated force f_m . When the motor shaft is connected directly to a spring the force can be described as the distance the pulley will turn multiplied with spring stiffness. This will be explained more in detail later in the section.

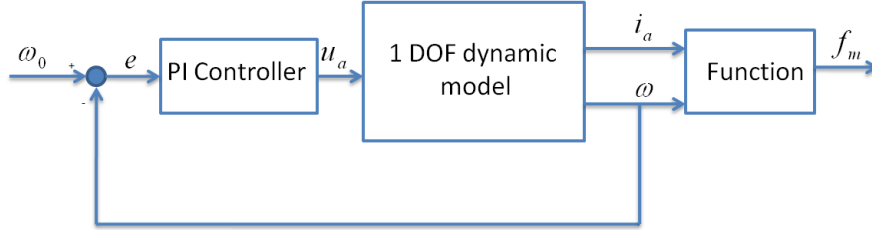


Figure 5.5: Blockdiagram from the target velocity ω_0 to the actuated force f_m .

The mathematical equation for the PI velocity controller in Figure 5.5, in frequency domain, can be written as

$$H_{PI}(s) = k_p + \frac{k_i}{s}, \quad (5.46)$$

where k_p is the proportional constant and k_i is the integral constant.

The control objective is that the tracking error will approach zero. The tracking error is defined as

$$e(t) = \omega_0 - \omega, \quad (5.47)$$

where ω_0 is the target velocity and ω is the output. The control input signal is then given as

$$u_a(s) = e(s) \left(\frac{k_i}{s} + k_p \right). \quad (5.48)$$

The control energy needed to achieve error regulation will then be

$$u_a(t) = k_i \int e(t) dt + k_p e(t). \quad (5.49)$$

Inserting (5.49) into the 1 DOF dynamic model from (5.38) to (5.40) give

$$\dot{\theta} = \omega \quad (5.50)$$

$$\dot{\omega} = \frac{1}{J + mr^2} \left[-k_1 r^2 \theta - K_f \omega + K_T i_a + mrg + k_1 r (z(t) + y_0 - x_0) \right] \quad (5.51)$$

$$\dot{i}_a = \frac{1}{L_a} \left[-K_E \omega - R_a i_a + k_i \int e(t) dt + k_p e(t) \right] \quad (5.52)$$

If $\dot{\xi} = e = \omega_0 - \omega$ the total model, from ω_0 to ω and i_a , can be written as

$$\dot{\xi} = \omega_0 - \omega \quad (5.53)$$

$$\dot{\theta} = \omega \quad (5.54)$$

$$\dot{\omega} = \frac{1}{J + mr^2} \left[-k_1 r^2 \theta - K_f \omega + K_T i_a + mrg + k_1 r(z(t) + y_0 - x_0) \right] \quad (5.55)$$

$$\dot{i}_a = \frac{1}{L_a} \left[-K_E \omega - R_a i_a + k_i \xi + k_p (\omega_0 - \omega) \right], \quad (5.56)$$

since $\int_0^{\infty} e(t) dt = \xi$.

Defining the states as

$$x := [\xi \quad \theta \quad \omega \quad i_a]', \quad (5.57)$$

we can write the dynamic model as

$$\dot{x} = Ax + B\omega_0 + Gw, \quad (5.58)$$

$$y = Cx, \quad (5.59)$$

with

$$A = \begin{bmatrix} 0 & 0 & -1 & 0 \\ 0 & 0 & 1 & 0 \\ 0 & -\frac{k_1 r^2}{J_m + mr^2} & \frac{-K_f}{J_m + mr^2} & \frac{K_T}{J_m + mr^2} \\ \frac{k_i}{L_a} & 0 & -\frac{K_E + k_p}{L_a} & -\frac{R_a}{L_a} \end{bmatrix}, \quad B = \begin{bmatrix} 1 \\ 0 \\ 0 \\ \frac{k_p}{L_a} \end{bmatrix}, \quad G = \begin{bmatrix} 0 \\ r \\ \frac{r}{J_m + mr^2} \\ 0 \end{bmatrix} \quad (5.60)$$

$$C = [0 \quad 0 \quad 1 \quad 1] \quad (5.61)$$

and disturbance $w = mg + k_1(z(t) + y_0 - x_0)$.

The equations given by (5.53) to (5.56) describe the model from the target angular velocity ω_0 to the actual angular velocity ω and the current i_a .

When the DC motor is directly connected to a pretensioned spring connected to a fixed point, the relationship between ω and measured force f_m can be defined to be proportional to the motor shaft angle of rotation θ :

$$f_m = C_1 \int \omega dt = C_1 \theta. \quad (5.62)$$

When the spring is connected directly to the oscillating system actuator, with vertical motion η_3 , the force can be expressed as:

$$f_m = C_1 \theta + C_2 \eta_3. \quad (5.63)$$

The force can also be expressed using the current:

$$f_m = K \cdot i_a \quad (5.64)$$

A second model needs to be derived in order to find the relationship between the analog voltage and the target velocity, shown in Figure 5.4. Earlier it was mentioned that 10 V as analog input will result in 10 000 rpm as target velocity, assuming the maximum speed is set to 10 000 rpm. However, the relationship is not proportional and a model is needed to describe it. The black box shown as “target velocity calculation” in Figure 5.4 from the analog voltage input u_{ai} to the target velocity ω_0 must therefore be determined. The model, shown in Figure 5.6, is assumed to be a PI controller that attempts to minimize the difference between a reference $\omega_{r,0}$ and the target velocity ω_0 .

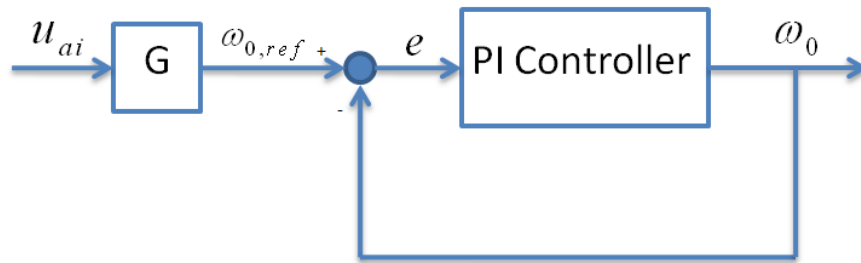


Figure 5.6: Block diagram from the analog voltage u_{ai} input to the target velocity ω_0 .

The relationship, between a target velocity ω_0 and it's reference velocity $\omega_{r,0}$, can be written as

$$\omega_0 = \int k_{ui}(\omega_{r,0} - \omega_0)dt + k_{up}(\omega_{r,0} - \omega_0), \quad (5.65)$$

where k_{ui} and k_{up} are some unknown constants. Further, it is assumed that the relationship between an analog voltage u_{ai} and its reference $\omega_{r,0}$ is proportional

$$\omega_{r,0} = Gu_{ai}, \quad (5.66)$$

where G is a unknown constant. Inserting this relationship into (5.65) give

$$\omega_0 = \int k_{ui}(Gu_{ai} - \omega_0)dt + k_{up}(Gu_{ai} - \omega_0). \quad (5.67)$$

The derivative of ω_0 can be written as

$$\begin{aligned} \dot{\omega}_0 &= k_{ui}(Gu_{ai} - \omega_0) + k_{up}(G\dot{u}_{ai} - \dot{\omega}_0) \\ \rightarrow \dot{\omega}_0(1 + k_{up}) + k_{ui}\omega_0 &= k_{ui}Gu_{ai} + k_{up}G\dot{u}_{ai} \end{aligned} \quad (5.68)$$

Assuming that the initial conditions are zero the Laplace transfer function in frequency domain, describing the relationship between target velocity and analog voltage, may be written as

$$\frac{\omega_0}{u_{ai}}(s) = \frac{k_{up}Gs + k_{ui}G}{(1 + k_{up})s + k_{ui}}. \quad (5.69)$$

The model can be used to find the target velocity from a given voltage input. The transfer function have one pole and one zero.

6 System Identification

In this chapter the unknown parameters in the derived models are determined. Measured input and output data from experiments are used to determine the parameter values. The parameters are tuned so that the model output fit the measured output using the same input.

In the first section the parameter values in the derived model from analog voltage to target velocity are determined. The System Identification Toolbox is used to tune the parameters to fit the data in best feasible way.

In the second section the parameter values in the model describing the relationship between target velocity, current and actual velocity are determined. The input data is selected to be the measured target velocity while the outputs are selected to be the current and actual velocity of the motor shaft. Measured input and output data are used to tune the initial DC motor parameters using the System Identification Toolbox. The last part of the section describes how the control gains in the model are determined.

Finally, the relationship between a measured force ring voltage and an actual force is discussed.

6.1 Parameter Identification in the Model from Analog Voltage to Target Velocity

The analog voltage input is set to be a white noise signal with 0.1 [s] zero-order hold sample time. The analog voltage input to the Faulhaber motion controller will then be a piecewise-constant white noise signal. Figure 6.1 shows the measured target velocity due to this applied voltage.

To determine the parameters in the model between analog voltage u_{ai} to target velocity ω_0 the measured input and output data in Figure 6.1 can be used. To find the unknown parameters in (5.69), the first half of the measurement data can be used for identifying the model, while the last half can be used for validation. Since the derived model have 1 pole and 1 zero (P1Z) it is possible to use System Identification toolbox to identify an optimal P1Z that fits the measured data.

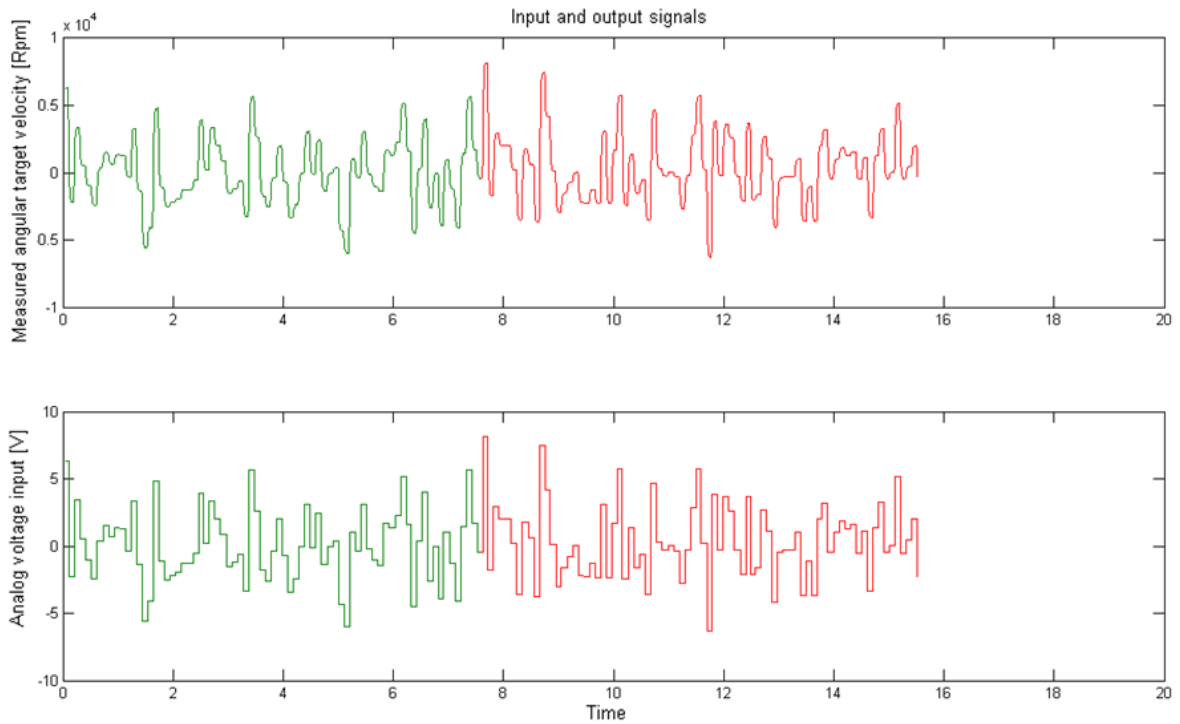


Figure 6.1: Measurement of the target velocity (top) due to a white noise analog voltage input (bottom).

From the calculations performed by system identification toolbox the optimal PIZ will be:

Process model with transfer function

$$G(s) = PIZ(s) = Kp * \frac{1+Tz*s}{1+Tp1*s}$$

with

$$Kp = 988.63+-2.8207$$

$$Tp1 = 0.010566+-0.00025546$$

$$Tz = 0.0047011+-0.00014818$$

Estimated using PEM using SearchMethod = Auto from data set z
Loss function 32296.3 and FPE 32553.3

The unknown parameters in (5.69) can therefore be selected to be:

$$Kp = G, \quad Tz = \frac{k_{up}}{k_{ui}}, \quad Tp1 = \frac{1+k_{up}}{k_{ui}}. \quad (6.1)$$

6.2 Parameter Identification in the Model from Target Velocity to Current and Actual velocity

In this section the parameters in the derived model from (5.53)-(5.56) are determined. First the control parameters in the model are found using a DC motor with optimal PID control. The section ends with describing how the unknown DC motor parameters are found.

The mass is set to be equal to zero since collected measurements are performed with the motor connected directly to a spring fixed to the roof. Measurement data are also collected when the pulley, connected to the shaft, runs freely; the stiffness and mass are then set to be zero. The other parameters in the model are set to be equal to:

Description		Unit
Distance from “roof” to stationary oscillator	$z_0 = 0.5$	[m]
Distance from “roof” to mass	$x_0 = 0.8$	[m]
Pulley radius	$r = 0.04$	[m]
Distance from stationary oscillator to mass	$y_0 = 0.3$	[m]

Table 6.1: Parameter values in the model.

6.2.1 Determination of the Control Gains

When the motor runs freely it is possible to look at a DC motor with angular velocity as feedback to determine optimal controller gains. Figure 6.2 shows the block diagram of optimal PID control for a DC motor with angular velocity as feedback. The transfer function $H_3(s)$ of the DC motor from the applied voltage u_a (control input) to the angular velocity ω is derived in (5.32).

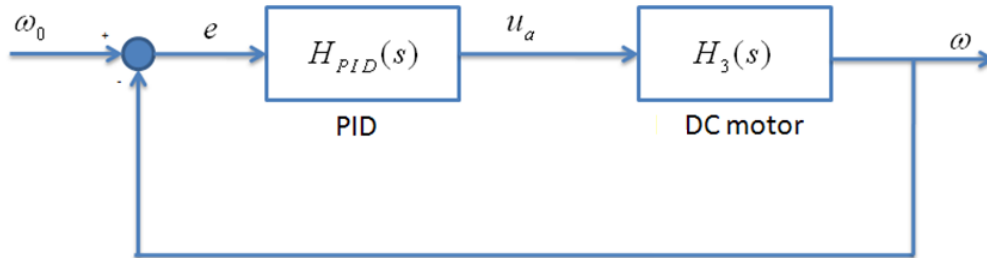


Figure 6.2: Block diagram of PID control of a DC motor

$H_3(s)$ can then be defined as in Yu & Hwang (2004):

$$\frac{\omega(s)}{u_a(s)} = \frac{c}{s^2 + as + b} \quad (6.2)$$

where the constants a, b and c are given by $H_3(s)$ previously derived. The mathematical equation of a PID controller in frequency domain is

$$H_{PID}(s) = k_p + \frac{k_i}{s} + k_d s, \quad (6.3)$$

where k_p is the proportional constant, k_d is the derivative constant and k_i is the integral constant.

The control objective is that the tracking error will approach zero. The tracking error is defined as

$$e(t) = \omega_0 - \omega, \quad (6.4)$$

where ω_0 is the velocity command and ω is the output. The control input signal is then given as

$$u_a(s) = e(s) \left(\frac{k_i}{s} + k_p + k_d s \right). \quad (6.5)$$

The control energy needed to achieve error regulation will then be

$$u_a(t) = k_i \int e(t) dt + k_p e(t) + k_d \frac{d}{dt} e(t). \quad (6.6)$$

To find optimal value of k_p, k_d and k_i the approach described in Yu & Hwang (2004) can be used. The augmented state vector is introduced and its differential equation is given as

$$\dot{z}(t) = \begin{bmatrix} \dot{e}(t) \\ \ddot{e}(t) \\ \ddot{e}(t) \end{bmatrix} = \bar{A}z(t) + \bar{B}\dot{u}_a(t), \quad (6.7)$$

where

$$\bar{A} = \begin{bmatrix} 0 & 1 & 0 \\ 0 & 0 & 1 \\ 0 & -b & -a \end{bmatrix} \text{ and } \bar{B} = \begin{bmatrix} 0 \\ 0 \\ -c \end{bmatrix}. \quad (6.8)$$

Further, in Yu & Hwang (2004) the performance measure is given as

$$J_p = \int_0^{\infty} \left(z^T(t) Q z(t) + \dot{u}_a^T(t) R \dot{u}_a(t) \right), \quad (6.9)$$

where Q and R are symmetric weighting matrices. The matrices should be selected to minimize the performance measure. From Yu & Hwang (2004) it is shown that the optimal control input is given as:

$$\begin{aligned} \dot{u}_a^*(t) &= -R^{-1} \bar{B} S z(t) \\ &= -K z(t) \\ &= -[K_1 \quad K_2 \quad K_3] z(t) \\ &= [k_i \quad k_p \quad k_d] z(t) \end{aligned} \quad (6.10)$$

where S needs to satisfy the algebraic Riccati equation

$$\bar{A}^T S + S \bar{A} - S \bar{B} R^{-1} \bar{B}^T S + Q = 0. \quad (6.11)$$

The motor parameters are assumed to be the same as the ones given in the motor datasheet:

Parameters	Values	Unit
R_a	1.2	Ω
K_E	0.02012	V/(rad/s)
K_f	$2.2918 \cdot 10^{-6}$	Nm/(rad/s)
L_a	$1.94 \cdot 10^{-4}$	H
K_T	$20.12 \cdot 10^{-3}$	Nm/A
J_m	$3.4 \cdot 10^{-6}$	kgm ²

Table 6.2: Initial DC motor parameters, ref. (DC Motor Specifications).

The augmented matrices will then be

$$\bar{A} = \begin{bmatrix} 0 & 1 & 0 \\ 0 & 0 & 1 \\ 0 & -(R_a K_f + K_T K_E) / L_a J_m & -(J_m R_a + K_f L_a) / L_a J_m \end{bmatrix} \text{ and } \bar{B} = \begin{bmatrix} 0 \\ 0 \\ -K_T / L_a J_m \end{bmatrix}$$

The weighting matrices are selected to be

$$Q = \begin{bmatrix} 100 & 0 & 0 \\ 0 & 5000 & 0 \\ 0 & 0 & 0 \end{bmatrix}, \quad R = 1 \quad (6.12)$$

Solving the Riccati equation (6.11) for S and substituting into (6.10) give the optimal gains

$$[k_i \quad k_p \quad k_d] = [10.0000 \quad 70.6907 \quad 0.0020], \quad (6.13)$$

with roots of the closed-loop characteristic equation calculated as $-3298.1 \pm 3269.9i$ and -0.1414 .

The derived controller gains can be used in the model describing the relationship between the target velocity, actual velocity and current.

6.2.2 Determination of the DC motor parameters

The unknown DC motor parameters in the differential equations described by (5.53) - (5.56) needs to be determined. In order to do so proper experimental data needs to be measured and stored. The target velocity and actual velocity can be measured and stored using the Faulhaber software manager. The experimental target velocity and actual velocity is shown Figure 6.3. The figure shows that the actual velocity has a delay compared to the target velocity.

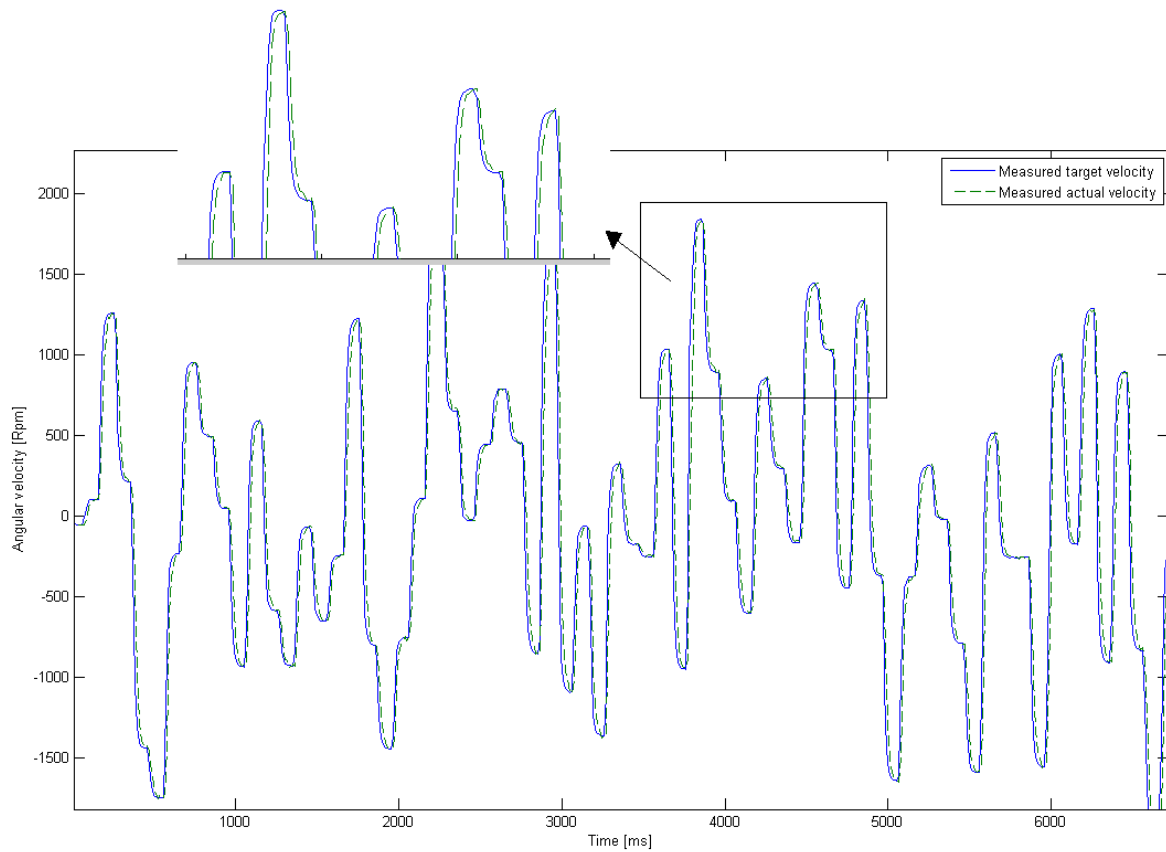


Figure 6.3: The actual velocity (dashed) of the motor shaft due to a measured target velocity (solid).

Measurement of the current can also be found using the Faulhaber software manager. The current was measured using a sinusoidal voltage as input, and a pretensioned spring connected directly to the roof and motor shaft. The measured input-output data, with current mean removed, are shown in Figure 6.4.

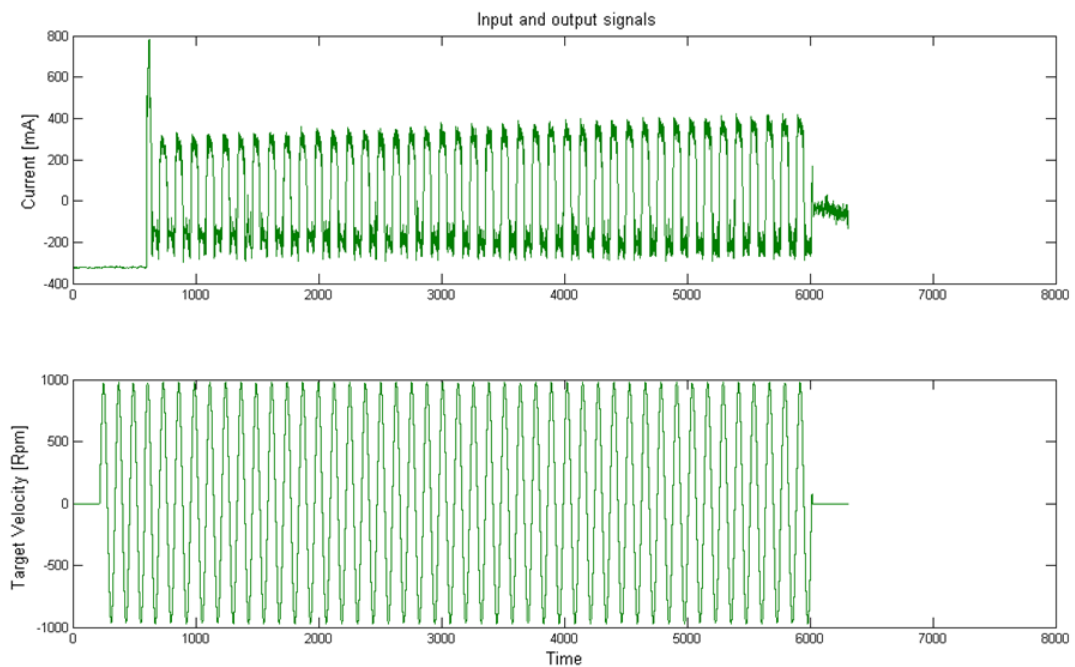


Figure 6.4: Current measurement (top) due to a sinusoidal target velocity (bottom).

The derived differential equations (5.53) - (5.56) can be used to describe the model from the target velocity ω_0 to the actual velocity ω and the current i_a . The System Identification Toolbox can find the unknown parameters using the given differential equations by comparing it to the input and output measurements.

The initial DC motor parameters are set to be equal to the parameters given in Table 6.2. The initial parameters are however changed by trial and error and by running the System identification program together with different measured data.

In Appendix 12.2 the system identification toolbox calculations are given. The parameters are found using target velocity as input and actual current/velocity as output. From the calculation the following DC motor parameters are obtained:

Parameters	Values	Unit
R_a	0.3915	Ω
K_E	0.0309	V/(rad/s)
K_f	0.4611	Nm/(rad/s)
L_a	0.0042	H
K_T	1.5120	Nm/A
J_m	0.00213	kgm ²

Table 6.3: DC motor parameters.

The Matlab® “pem” function used to estimate the model parameters uses optimization to minimize the cost function, defined as follows for scalar outputs (The MathWorks):

$$V_G(G, H) = \sum_{t=1}^N e^2(t), \quad (6.14)$$

where $e(t)$ is the difference between the measured output and the predicted output of the model.

6.3 Relationship between measured voltage and actual force

Different weights are used to establish a relationship between the measured voltage, in the force ring, and the corresponding force. The weights are connected to the force ring fixed to the roof. The measured force due to the mass m can then be expressed as $F = mg$, where g is the gravitational constant. The voltage measurements due to different weights are shown in Figure 6.5.

Voltage [mV]	Force [N]
-254	0
-335	1.160523
-404	2.337723
-464	3.122523
-557	4.495923
-667	6.065523
-721	6.850323
-801	7.929423
-933	9.989523
-1068	11.951523
-1180	13.423023
-1279	14.894523
-1408	16.856523

Figure 6.5: Voltage measurement in the force ring to a force.

The principle of least squares can be used in a fast and efficient manner to find the best fitting straight line passing through the data given by Figure 6.5. The unknown parameters in a linear equation $\hat{f} = \theta_1 U + \theta_2$ can be found using this method, where U is the experimental voltages and \hat{f} is the computed force. From (Åström & Wittenmark, 1997) the unknowns θ should be chosen in such a way that the sum of the squares of the difference between the actually observed and the computed values multiplied by a degree of precision is a minimum.

If all the measurements are assumed to have the same precision, the least square principle says that the parameters should be selected so that the following loss function given in (Åström & Wittenmark, 1997)

$$J(\theta) = \frac{1}{2} \sum \mathcal{E}_i^2,$$

is minimal. $\mathcal{E}_i = f_i - \hat{f}_i$, where f_i is the measured values of the force, and $\hat{f} = \theta_1 U + \theta_2$ is the computed force. The loss function is minimal for parameters θ such that

$$f = V\theta \tag{6.15}$$

where

$$V = \begin{bmatrix} U_1 & 1 \\ \vdots & \vdots \\ U_n & 1 \end{bmatrix} \text{ and } \theta = [\theta_1 \quad \theta_2]^T. \tag{6.16}$$

To find θ , we premultiply (6.15) with V^T and multiply with the inverse of $V^T V$ on both sides

$$\theta = (V^T V)^{-1} V^T f = V^+ f, \tag{6.17}$$

where V^+ is the pseudo-inverse of V . Figure 6.6 show the best fitting line for the data set given by Figure 6.5.

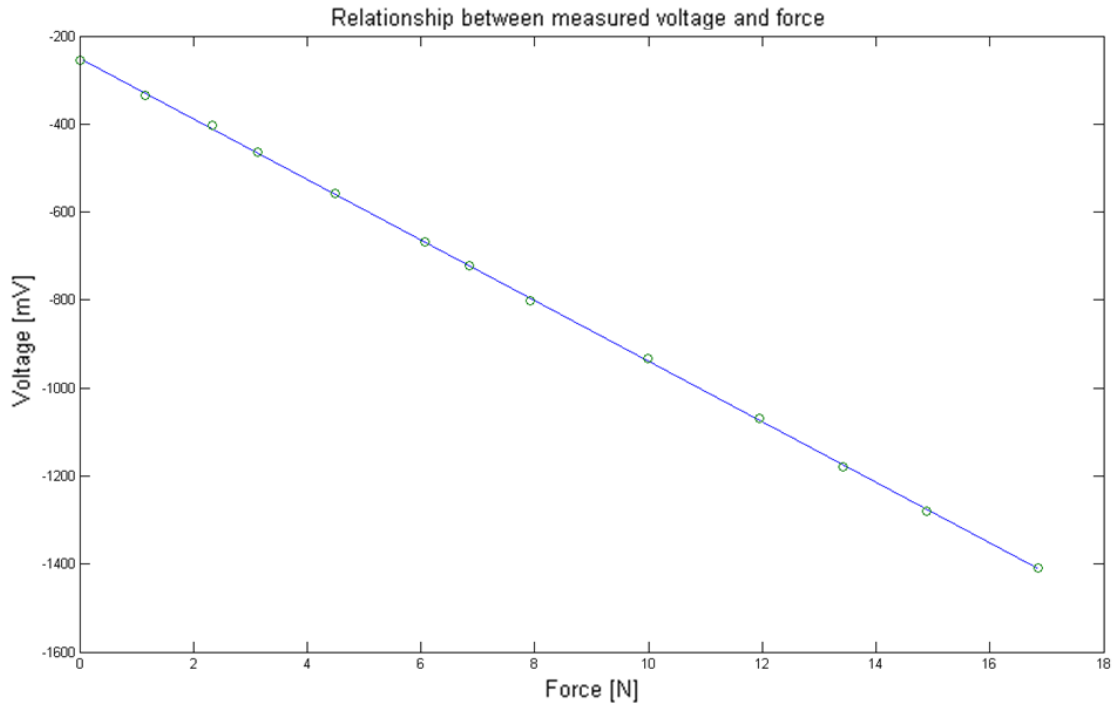


Figure 6.6: Best fit linear equation of observed data for voltage and force. Found using least square method.

The best fit equation is found to be

$$\hat{f} = -0.01453U - 3.6343 \quad (6.18)$$

where U is the force ring voltage and \hat{f} is the best fit computed force.

6.4 Discussion

The results obtained in the system identification process use measured data with a DC motor connected to a pretensioned spring and with a freely rotating pulley. Preferably, the measured data used in the system identification of the model should have been collected using a mass and spring together with the vertical oscillating motion. The parameters will therefore be un-optimized when the mass is included. The vessel mass will induce vertical motion and a disturbance load at the motor shaft.

The vertical motion to the oscillating system can be accounted for by considering its force impact. When the vertical motion measurements to the oscillating actuator are known, its force impact can be found by multiplying the displacement with the spring stiffness. The force due to the oscillating motion can then be added to the spring force generated by the DC motor to obtain the total measured “force ring” force, assuming the spring is connected directly to the oscillating system and the mass is neglected.

7 Model Validation

In this chapter the simulated outputs from the derived model are compared with measured data. The parameters in the model are found in the system identification chapter. Using the known parameters the chapter starts with comparing the simulated target velocity to the measured target velocity. In the second section the simulated actual velocity/current are compared to measured data. Finally, the measured force and the simulated force are compared.

7.1 Model Validation between Analog Voltage to Target Velocity

Figure 7.1 shows the comparison between the measured and simulated target velocity ω_0 due to a given voltage input. The transfer function in (5.69) using calculated parameters gives an 85.6 % fit to the measured output data. A transfer function with 2 poles (P2) is also shown in the figure, the P2 transfer function gives an 82 % fit. The fit is calculated using the following equation (The MathWorks):

$$fit = 100 \cdot \frac{1 - norm(y_{out} - y)}{norm(y - mean(y))} \quad (7.1)$$

where y is the measured output and y_{out} is the simulated.

The established model from the analog voltage to the target velocity, gives a satisfactory fit to the experimental measured data.

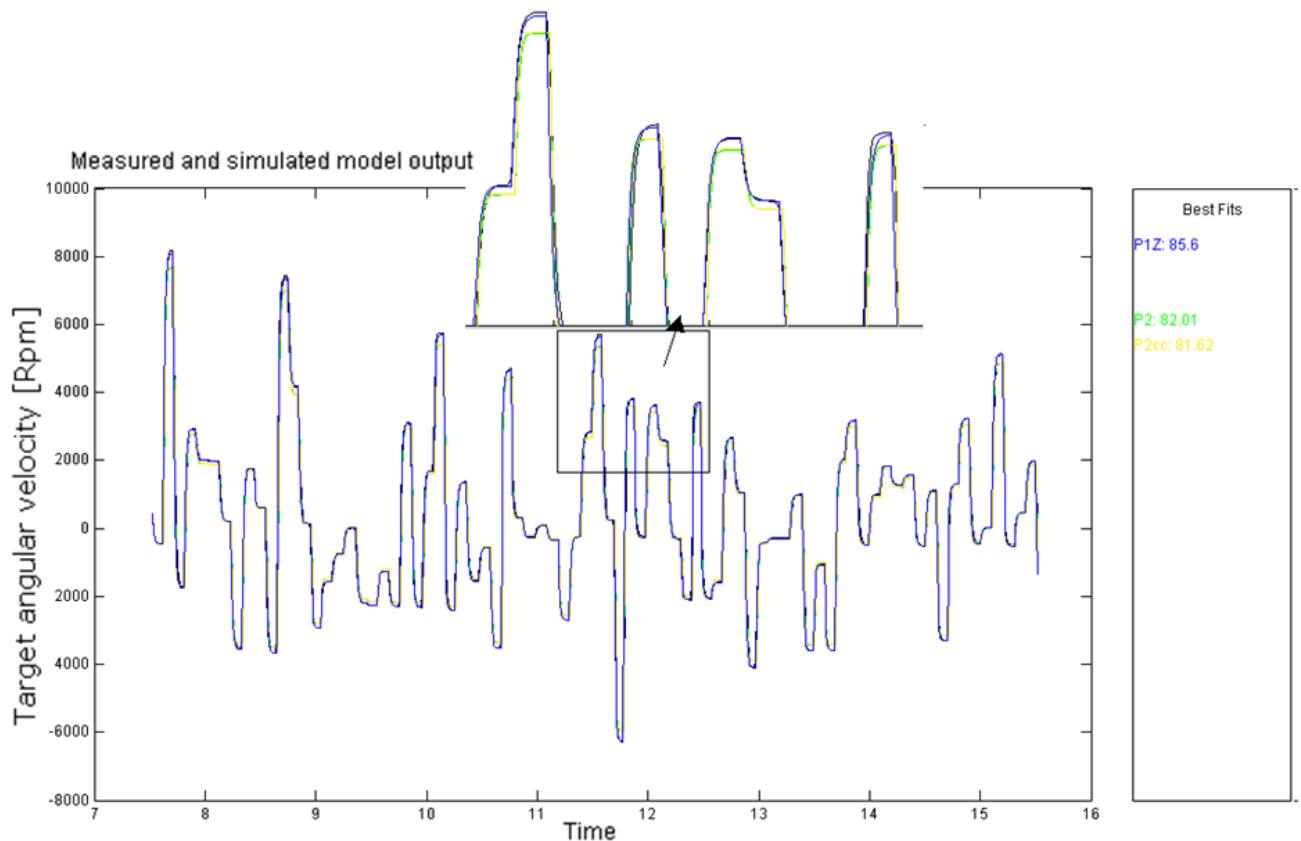


Figure 7.1: Comparison between the measured and simulated target velocity using an optimal one pole-one zero transfer function, and a two pole transfer function.

7.2 Model Validation from Target Velocity to Current and Actual Velocity

The comparison between the simulated actual velocity ω and the measured actual velocity is shown in Figure 7.2. The figure shows that the simulated velocity has a 90.26 % fit to measured velocity from experiment.

The parameters work relative well if the target velocity input is white noise. However, the model does not necessarily work well for all types of input signals. In order to test how well the model performs, a relative unfavorable input signal is used. The input signal is set to be a pulse signal with amplitude close to maximum, in this case pulses at ± 9000 rpm. The result comparing the simulated ω and experimental angular velocity output is shown in Figure 7.3. The fit in this case will be 77.3 %. A worse fit is expected for this case since the amplitude is close to maximum and the model is tuned for lower amplitudes. The comparison is established using a freely running motor shaft.

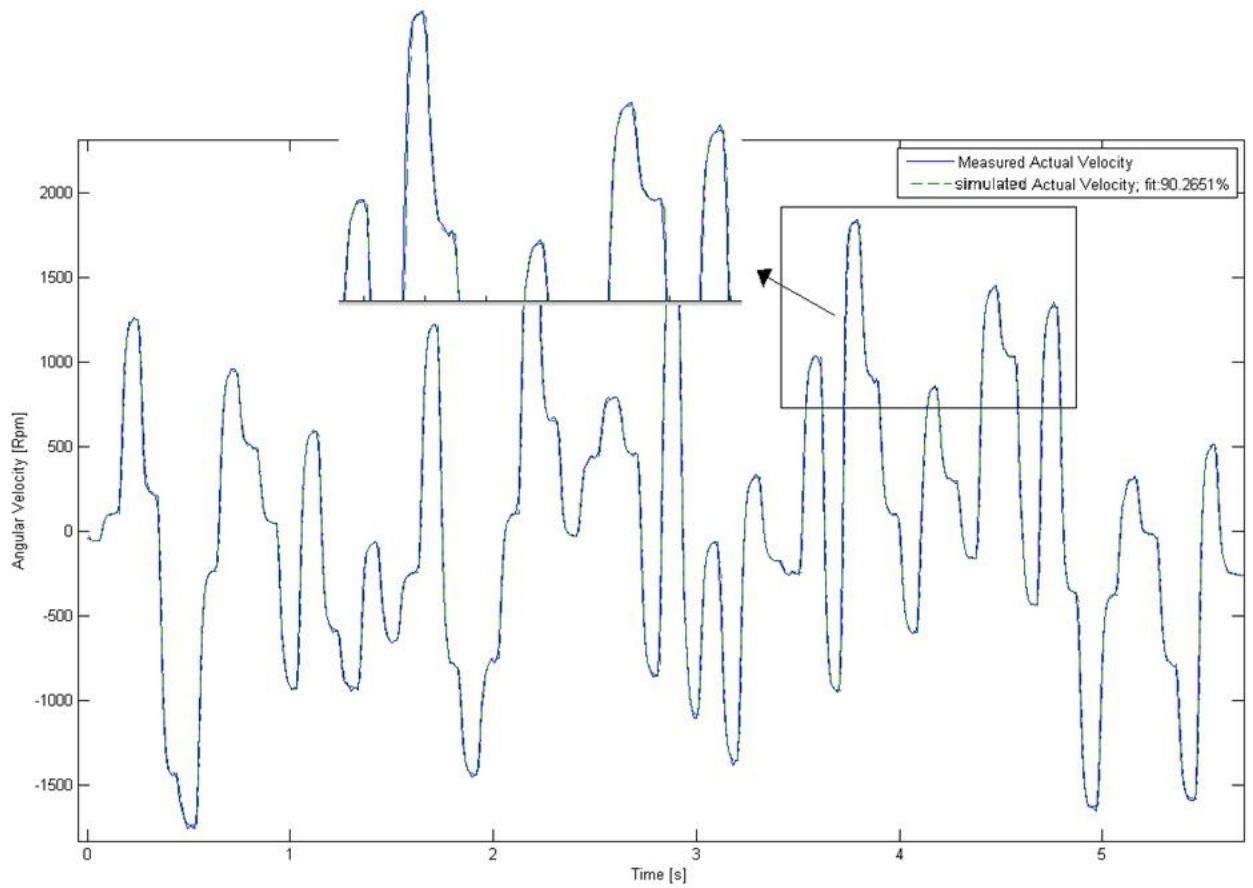


Figure 7.2: Comparison between the measured (solid) and simulated actual velocity (dashed) due to a white noise analog voltage input.

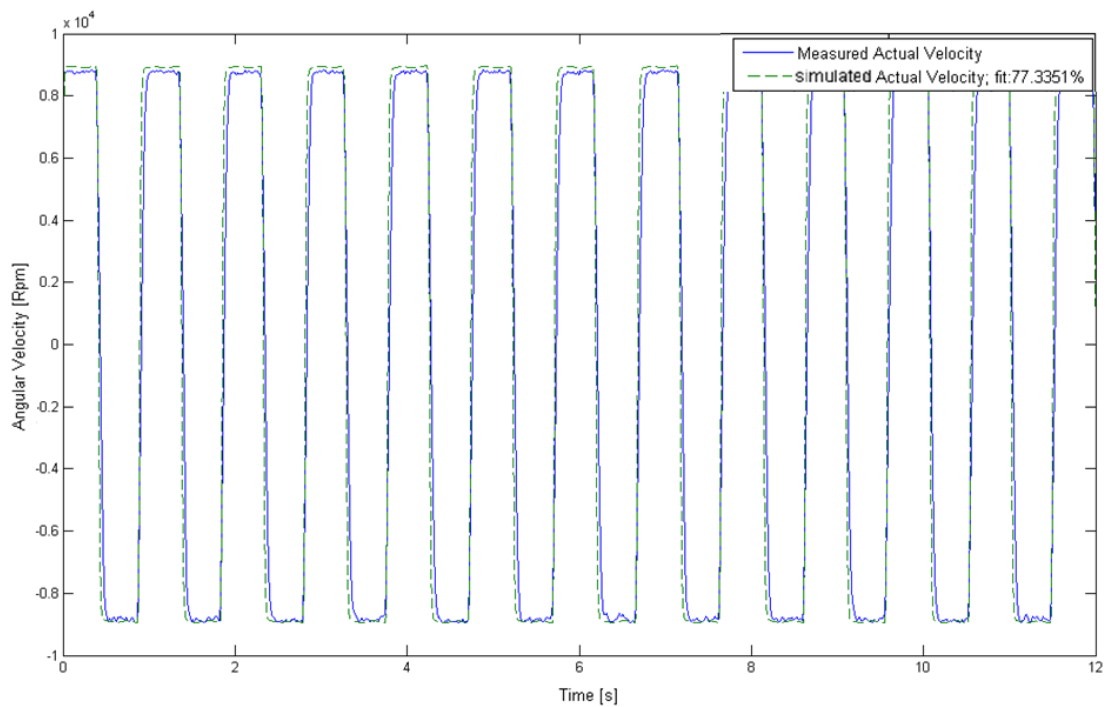


Figure 7.3: Comparison between the measured (solid) and simulated actual velocity (dashed) using established DC motor parameters given in Section 6.2.2, and pulses as analog voltage input.

In Figure 7.4 the measured current from experimental data is compared to the simulated current. The current is simulated using the parameters found in the system identification chapter. The measurements are done using a pretensioned spring fixed to the roof and an analog sinusoidal voltage as input. The simulated model current gives a 59 % to the measured current.

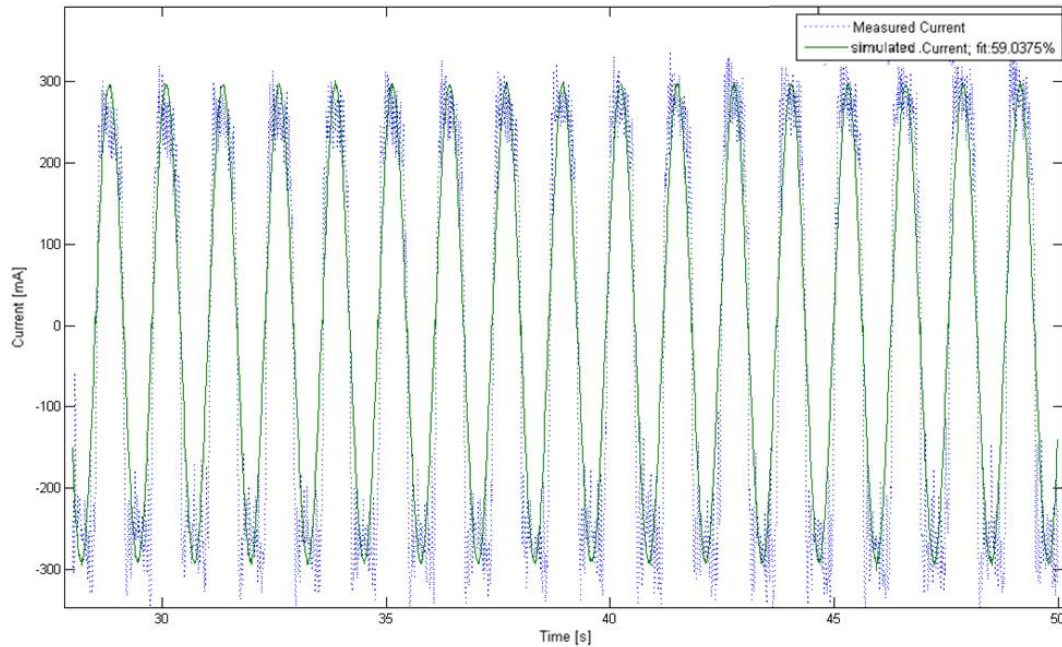


Figure 7.4: Comparison between the measured (dashed) and simulated current (solid), using established DC motor parameters given in Section 3, sinusoidal voltage as input and a pretensioned spring connected directly to the roof.

7.3 Comparison between the Simulated Force and Measured Force

The measured force due to a sinusoidal analog voltage input is monitored and stored. The DC motor is connected to a spring that is fixed to the roof. The input voltage and its corresponding force are shown in Figure 7.5. The force ring measurements, in Volt, are found in Newton using (6.18). The input voltage has initial amplitude high, hence a high initial velocity. The positive velocity in the beginning will therefore tension the spring even more. This is done to keep the spring tensioned when the voltage becomes negative again.

The force measurements from experiment due to the sinusoidal voltage input are shown in Figure 7.5. In this case the DC motor is connected directly to a spring fixed to the roof. The force due to the analog voltage is then measured.

If the analog voltage is used as input in the derived model of the system a simulated actual velocity can be used to describe the force in the spring. Since the DC motor is connected directly to the pretensioned spring the simulated force can be expressed as $f_m = K \int \omega dt$, where ω is the actual velocity and K is a constant. When K is selected to be 0.086 the simulated forces will correspond well to the measured forces from experiment.

The simulated force is shown together with the measured force in Figure 7.6. The simulated force differs from the measured forces the first four seconds. This is due to the fact that the initial force in the experiment is positive since the spring is pretensioned. In the model the simulated force will be zero since the voltage is zero.

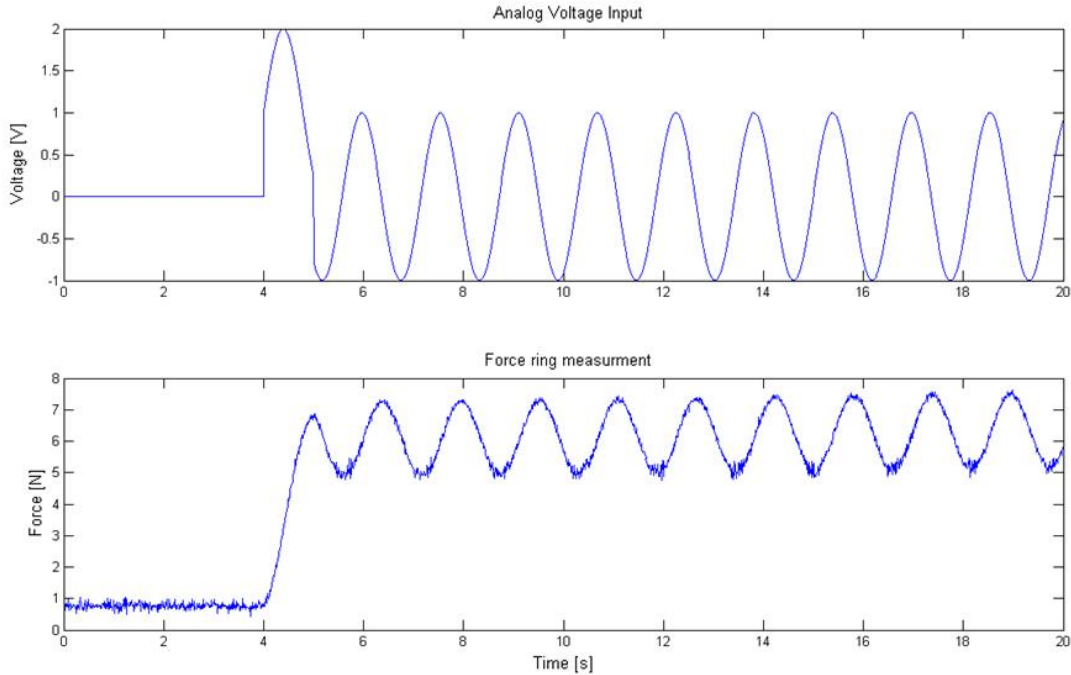


Figure 7.5: Analog voltage input (top) and the corresponding measured force (bottom).

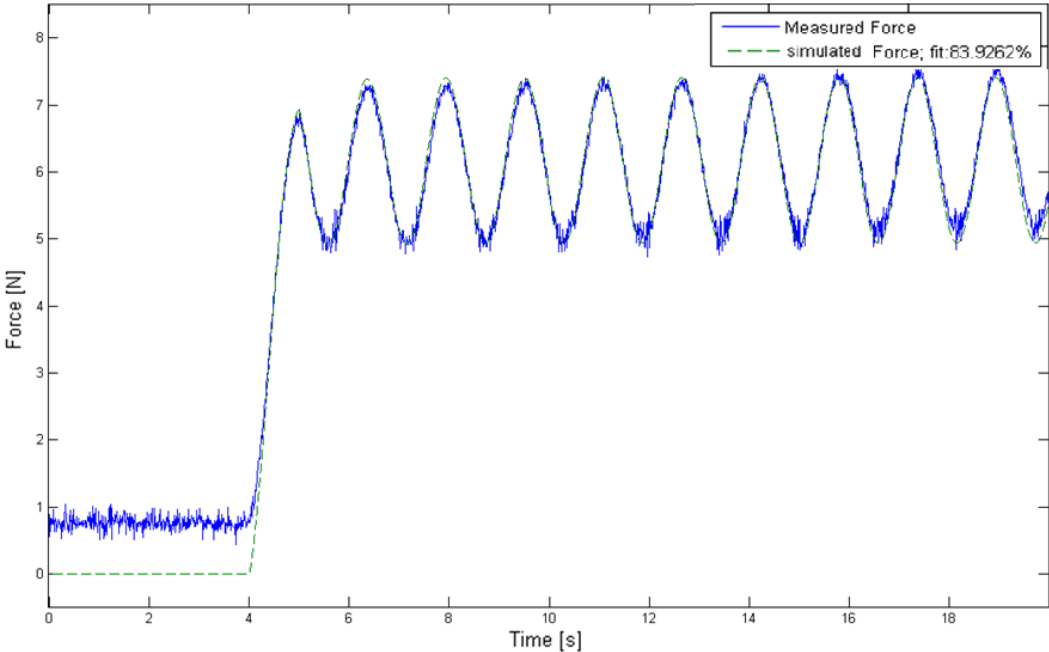


Figure 7.6: Simulated force (dashed) from model compared to the measured force (solid) from experiment, using the same voltage input given by Figure 7.5.

7.4 Discussion

A model from a given analog voltage input to the actual measured force is established. There is a good accordance between the simulated actual velocity and the measured velocity due to the same voltage input. The match between simulated current and measured current is also satisfactory. The parameters in the model are established for a DC motor connected to a pretensioned spring, and for a DC motor running freely.

The vertical motion from the oscillating generator can be accounted for by adding its contributing force. The force due to the vertical motion can be found by multiplying the vertical motion with the spring stiffness. A good model is therefore established when the spring is connected directly to the oscillating system.

If a mass is included in-between the spring and rope connected to the oscillating system the vertical motion due to the mass will induce disturbance in to the system. Preferably, optimal model parameters should have been established for this case.

8 Control Design

The objective is for the mooring force acting on the vessel to track given desired reference signals. The corresponding feedback controller must then track the reference. The objective for the controller will be to actuate these equivalent forces in each time step on to the vessel model. If the reference force is defined as f_{ref} , and the output is the measured force f_m . The main objective will be to design a control law ensuring that $f_m \rightarrow f_{ref}$.

This can be achieved by controlling the velocity of the motor shaft; hence the analog voltage input to the real process must be controlled. The difference between the force reference and measured force must be minimized. The force measurements will include white noise, or disturbances. Hence, filtering this signal must be carried out. An estimated force that removes the noise in the measured force must be used as feedback.

8.1 Control Design

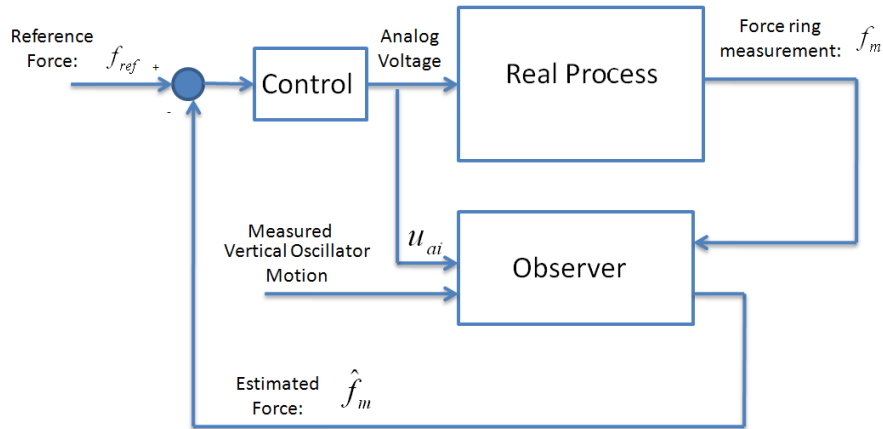


Figure 8.1: Blockdiagram from the force reference to the measured force.

The control strategy is to design a control law ensuring that $f_m \rightarrow f_{ref}$. A PID controller can be used for this purpose. The mathematical equation of a PID controller in frequency domain is

$$H_{PID}(s) = k_{p1} + \frac{k_{i1}}{s} + k_{d1}s, \quad (7.2)$$

where k_{p1} is the proportional constant, k_{d1} is the derivative constant and k_{i1} is the integral constant.

The control objective is that the tracking error will approach zero. The tracking error is defined as

$$e(t) = f_{ref} - \hat{f}_m, \quad (7.3)$$

where f_{ref} is the force command and \hat{f}_m is the estimated force. The control input signal is then given as

$$u_{ai}(s) = e(s) \left(\frac{k_{i1}}{s} + k_{p1} + k_{d1}s \right). \quad (7.4)$$

The control energy needed to achieve error regulation will be

$$u_{ai}(t) = k_{i1} \int e(t) dt + k_{p1} e(t) + k_{d1} \frac{d}{dt} e(t). \quad (7.5)$$

8.2 Observer Design

The main purpose of an observer is to reconstruct unmeasured or absent signals and to provide noise filtering of measured signals. The filtered or reconstructed signals are then used as feedback to the control system. In this case the measured force will be noisy and a filtered force signal must be used as feedback to the control system.

An estimator that copies the model from ω_0 to f_m exactly can be expressed as

$$\begin{aligned} \dot{\hat{\xi}} &= \hat{\omega}_0 - \hat{\omega} + K_1 \tilde{f}_m \\ \dot{\hat{\theta}} &= \hat{\omega} + K_2 \tilde{f}_m \\ \dot{\hat{\omega}} &= \frac{1}{J + mr^2} \left[-k_1 r^2 \hat{\theta} + K_f \hat{\omega} + K_T \hat{i}_a + mrg + k_1 r (z(t) + y_0 - x_0) \right] + K_3 \tilde{f}_m \\ \dot{\hat{i}}_a &= \frac{1}{L_a} \left[-K_E \hat{\omega} - R_a \hat{i}_a + k_i \hat{\xi} + k_p (\hat{\omega}_0 - \omega) \right] + K_4 \tilde{f}_m \\ \hat{f}_m &= K \cdot \hat{\theta} + C \cdot \eta_3 \end{aligned}$$

The deviation error $\tilde{f}_m = f_m - \hat{f}_m \in \mathbb{R}^1$ is taken between noise corrupted real measurement of the force and estimated values. K_1 , K_2 , K_3 and K_4 are the observer gains.

In Figure 8.2 the estimated force due to sinusoidal voltage inputs is compared to the measured force from experiment with measured vertical motion η_3 to the oscillating system set to zero.

The observer gains are chosen to be:

$$K_1 = 400, \quad K_2 = 320, \quad K_3 = 310 \quad \& \quad K_4 = 200. \quad (7.6)$$

The estimated force is also compared to the measured force from experiment when the input voltage is a white noise signal. Figure 8.3 shows the estimated force and measured force for this case. The observer removes the unwanted noise in the signal.

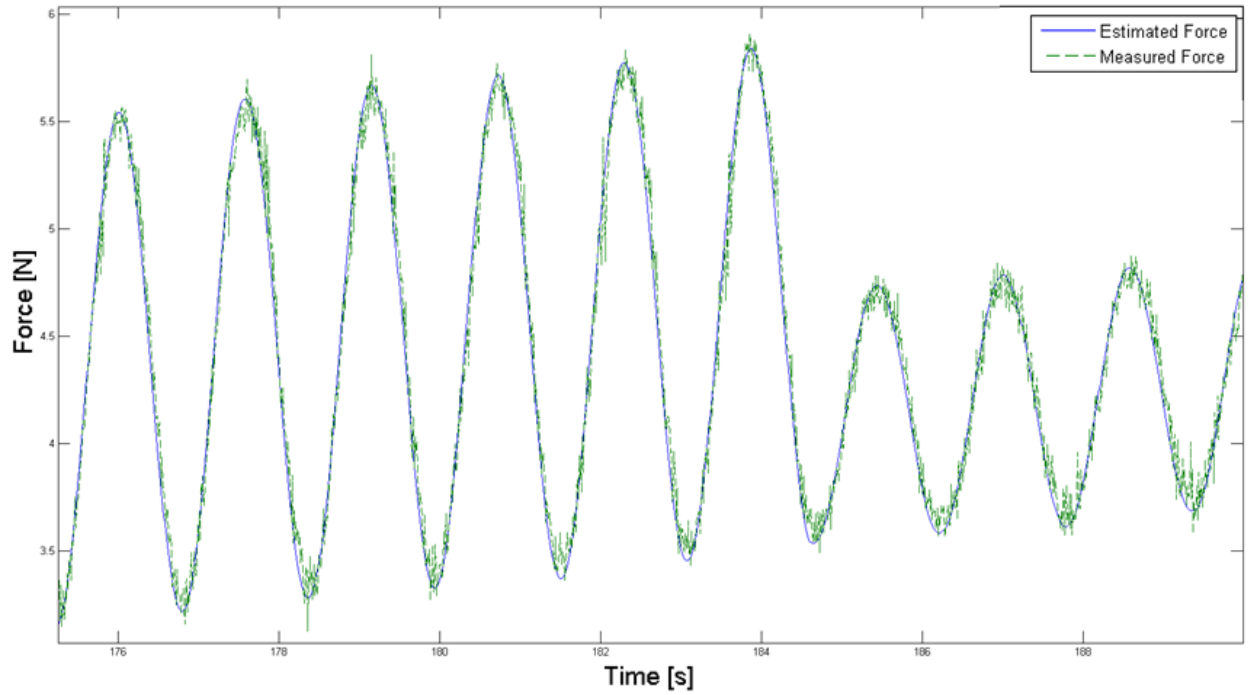


Figure 8.2: Estimated force compared to the measured force due to sinusoidal voltage inputs.

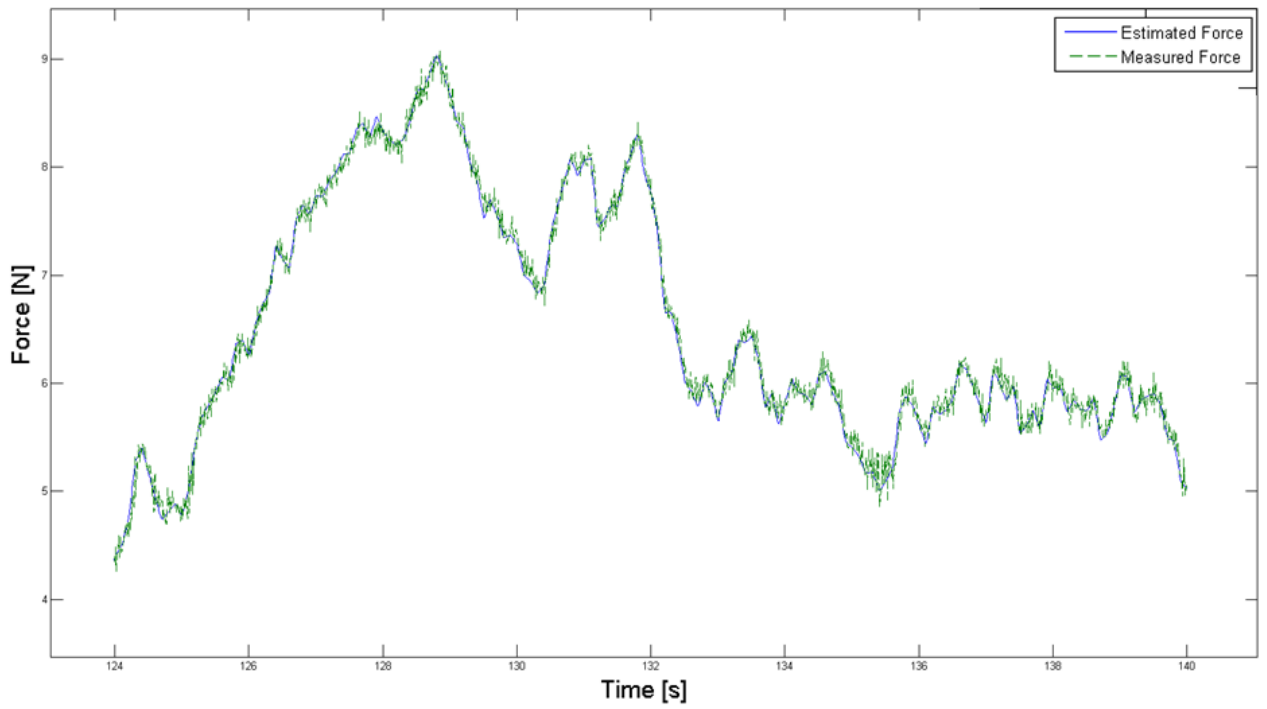


Figure 8.3: Estimated force compared to the measured force.

8.3 Mooring Line Calculations

To simplify the mooring line calculations a sinusoidal heave motion of the vessel model is considered. The corresponding force in the mooring line due to this vertical motion is calculated using RIFLEX by co-student Stian Garlid. The force corresponds to the top node vertical mooring line force. In Figure 8.4 the vertical force in one mooring line is given for a sinusoidal heave motion with amplitude $\zeta_{aM} = 0.057$ [m] and period $T_M = 1.55$ [s]. The force and heave motion are given using 1:70 as model scale, corresponding to a full scale amplitude $\zeta_a = 4$ m and period $T = 13$ s.

In lack of an equation describing the relationship between a vertical motion and corresponding force a lookup table in Simulink® is used. When the measured vertical motion is known the corresponding mooring line force can be found from the calculated data. However, as seen in Figure 8.4 a vertical displacement will correspond to two different force values. To separate these two values it is possible to look at the derivative of the vertical motion. When the derivative is positive the first section of the corresponding force is used in the lookup table, and when the derivative is negative the second section is used. The calculated data in the lookup table use the steady state heave motion over one period as seen in Figure 8.4. When the vertical displacement is in-between two given values the lookup table uses linear interpolation to find the corresponding force. Desired force references are now established for a given heave period and amplitude.

The specific heave motion can therefore be used to calculate the desired reference force as shown in Figure 8.5. The calculated mooring line forces are then utilized as reference in the control system.

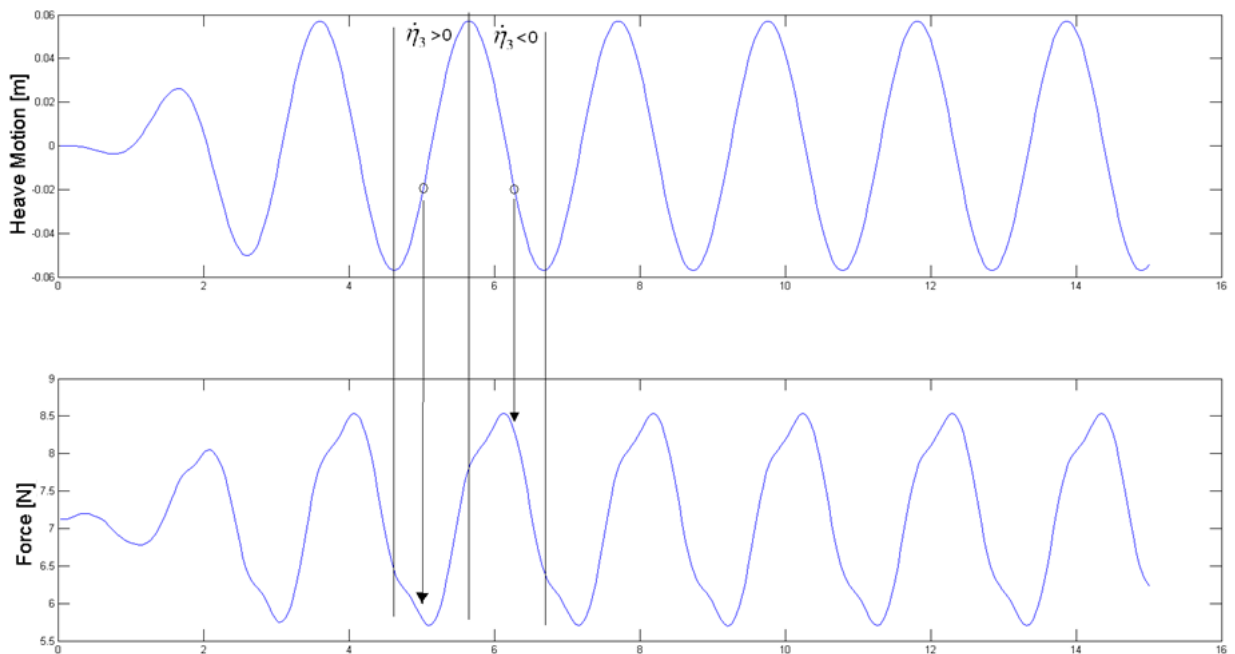


Figure 8.4: Top node vertical force in one mooring line(bottom) and the corresponding vertical motion(top).

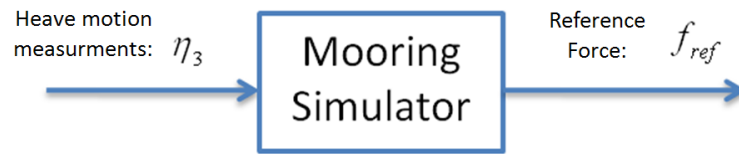


Figure 8.5:Blockdiagram from measured heave motion to desired mooring line force.

9 Experiments

A series of model tests were performed in order to investigate the performance to the control system using various force reference inputs. The Marine Cybernetics (MC) laboratory was used as testing site, and an experimental setup consisting of a Faulhaber engine, oscillating system, spring and mass, was used in the execution of the experiments. In the experiments a 100 Hz sampling frequency is used, the sampling frequency is set in the “configuration parameter “ panel in the Simulink® model.

The experimental testing is performed using two different experimental setups. The first case include a setup were the force ring is connected directly to the oscillating unit. The spring is then connected in-between the force ring and a rope running down to the Faulhaber engine. Measurements of the vertical displacement to the oscillating unit, representing the heave motion, are then used to calculate the desired mooring line force. The Faulhaber engine will then try to pull the spring and line so that it achieves the same force. Tests are conducted using sinusoidal motions of the oscillating unit as well as zero displacement.

A second test case is conducted by connecting the spring in-between the oscillating unit and a mass. The force ring is connected directly to the underside of the mass and a rope running down to the Faulhaber engine. Tests are conducted to see whether the Fulhaber engine manages to actuate correct forces corresponding to given reference values. The vertical motions of the oscillating unit are set to be sinusoidal and zero.

This chapter describes the experimental setups, and present some of the main results obtained. A discussion regarding the control system performance and practical issues connected to the accomplishment of the experiments concludes the chapter.

9.1 Case 1

In this case the vessel is considered to be the oscillating system as shown in Figure 9.1. The vertical motion will therefore correspond to the heave motion of the vessel. The heave motion measurements can be used to calculate the desired reference forces using the approach given in Section 8.3. Figure 9.1 shows the experimental setup consisting of the oscillating system, force ring, spring and Faulhaber engine. A pulley is attached to the Faulhaber engine shaft pulling the “mooring line”. The mooring line consists of a line and a spring. The spring is connected in between the line and force ring fixed to the oscillating system.

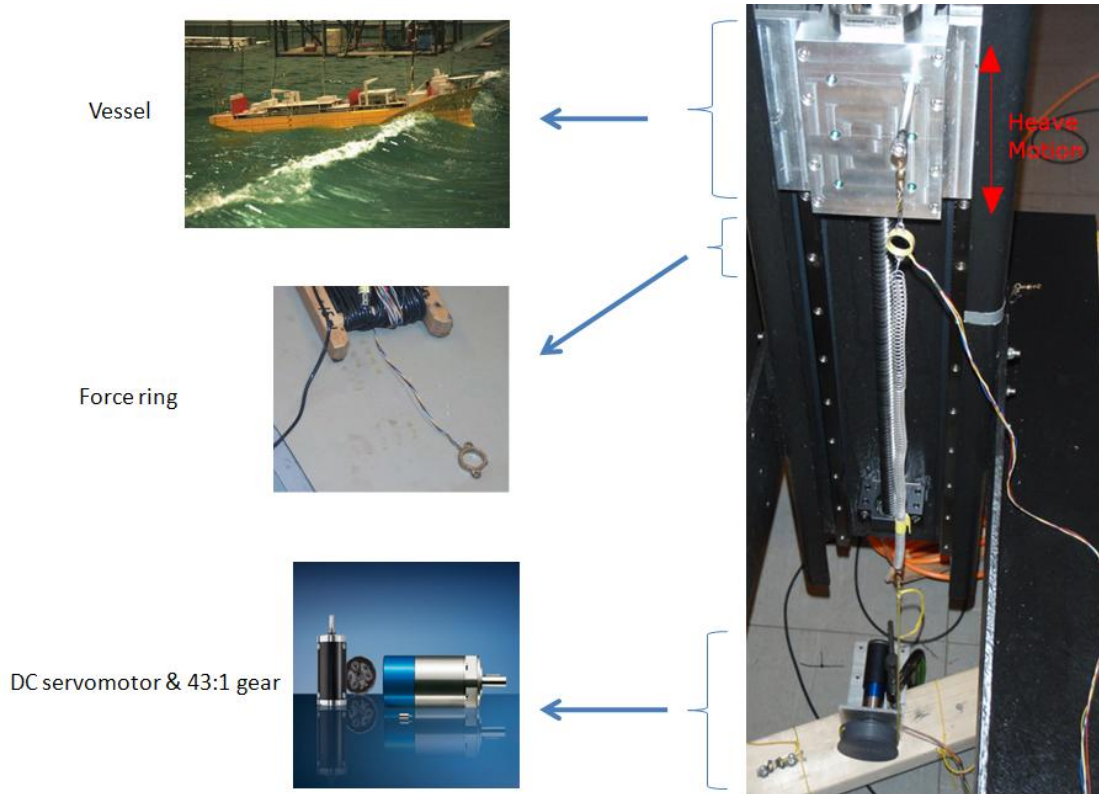


Figure 9.1: Experimental setup case 1.

The measured heave motion to the oscillating system can be used as input to the control system to calculate the desired reference forces as shown in Figure 8.4. The heave motion is sent to the cRIO module as an analog voltage signal. With 0 volt as input the oscillator is in its top position. However, as a default the oscillating system is lowered with 0.2 m corresponding to 2 volt as input. The relationship between vertical motion and voltage is given as

$$\eta_3 = \frac{1}{10}(u_\eta - 2), \quad (7.7)$$

where η_3 is the measured heave motion in meter and u_η is the voltage input.

The heave motion to the oscillating system is set to be equal to the steady state motion given by Figure 8.4 with amplitude $\zeta_{aM} = 0.057$ [m] and $T_M = 1.55$ [s]. The parameters in the control system are set to be equal to the values given by Table 9.1. The mass is not considered in this case and its value is set to be zero.

The estimated force in the control system is set to be equal to $\hat{f}_m = K \cdot \hat{\theta} + C \cdot \eta_3$. K and C are found by experimental testing and their values are set to be equal to 0.005 and 4.85 respectively.

The experimental result using the parameters given in Table 9.1 is shown in Figure 9.2. The plot shows a good resemblance between the reference and measured force. Hence, the control system will be able to actuate the desired mooring line forces for a vessel moving in the given heave motion. However, there is some disturbance in the measured force especially at the peak amplitudes.

The estimated force filters the signal quite well. However, by reducing the observer gains the noise in the estimated force can be reduced even more. Due to the rapid motion, 1.55 seconds from top to bottom, the observer gains needed to be set high.

Observer gains	Controller gains	Mass	Sinusoidal Heave Motion
$K_1=7000$	$k_p=11$	$m=0$ [kg]	Amplitude=0.057 [m]
$K_2=4300$	$k_i=3$		Period=1.55 [s]
$K_3=3300$	$k_d=0.02$		Frequency=0.64 Hz
$K_4=7000$			

Table 9.1: Parameter values.

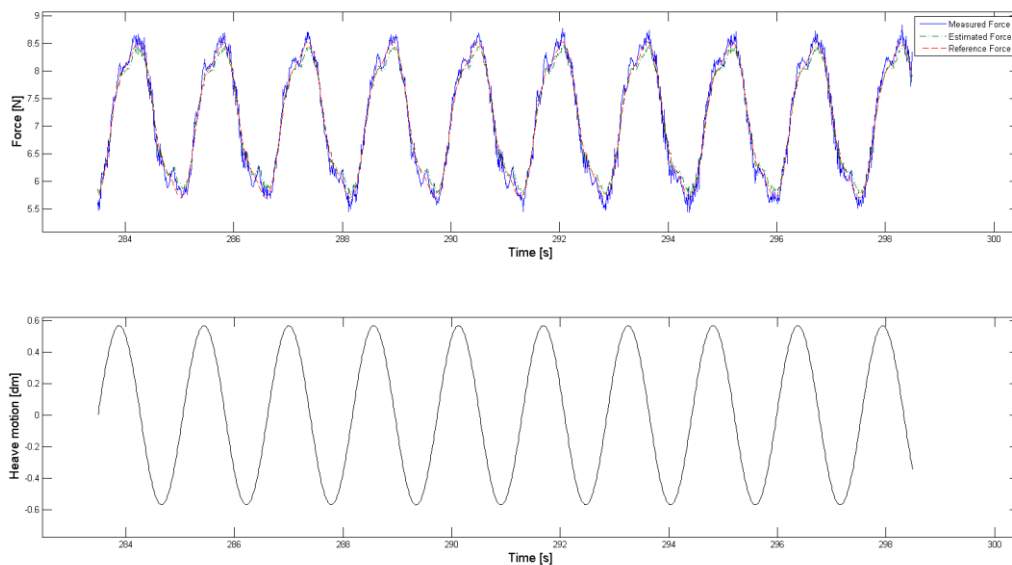


Figure 9.2: Experimental result using parameter values in Table 9.1. Mooring line force reference shown together with estimated and measured force (top) and heave motion (bottom).

The 1:70 in model scale give a relative small heave period (time is scaled with the square root of the model scale). Preferably a larger model scale should be utilized when model testing, resulting in a larger heave period. Experiments assuming higher heave periods are therefore conducted. In the experiments using higher heave periods, the observer gains may be reduced. The result using the parameters in Table 9.2 is shown in Figure 9.4.

The noise at the peak amplitudes are now reduced and the measured force follow the force reference better. Some disturbance is still present, however this is hard to remove due to the constant white noise disturbance present in the measurements.

Observer gains	Controller gains	Mass	Sinusoidal Heave Motion
$K_1=1500$	$k_p=11$	$m=0$ [kg]	Amplitude=0.057 [m]
$K_2=1900$	$k_i=3$		Period=5 [s]
$K_3=1800$	$k_d=0.02$		Frequency=0.2 Hz
$K_4=1500$			

Table 9.2: Parameter values.

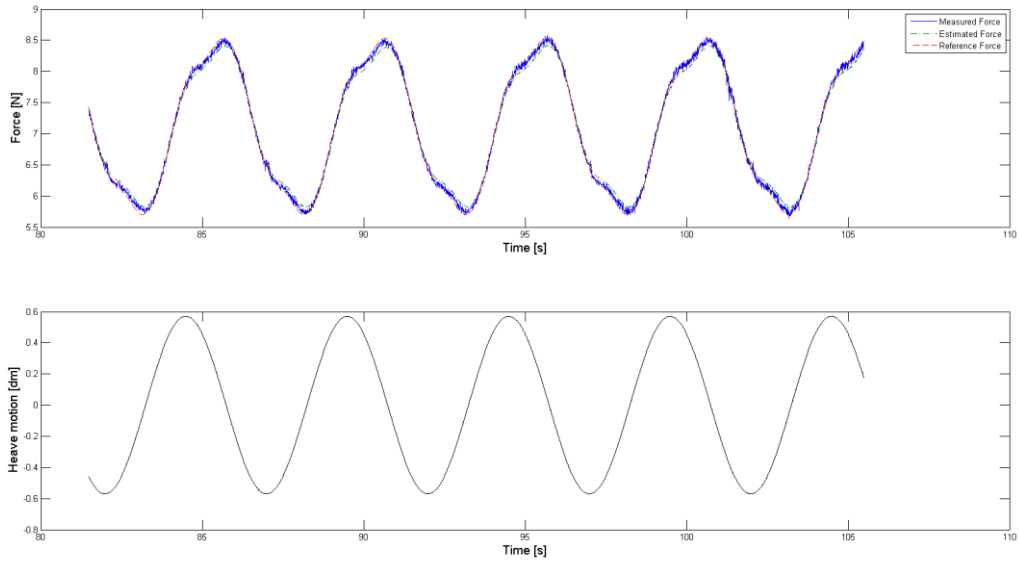


Figure 9.3: Experimental result using parameter values in Table 9.2. Force reference shown together with estimated and measured force (top) and heave motion (bottom).

The desired force is now changed to a random sinusoidal reference. The amplitude and bias to this reference signal is then changed during the experiment. The heave motion is set to be a sinusoidal motion with amplitude $\zeta_{aM} = 0.057$ [m] and period $T_M = 3.3$ [s]. The result is shown in Figure 9.4. The control system will be able to follow the sinusoidal references using different bias and amplitude values.

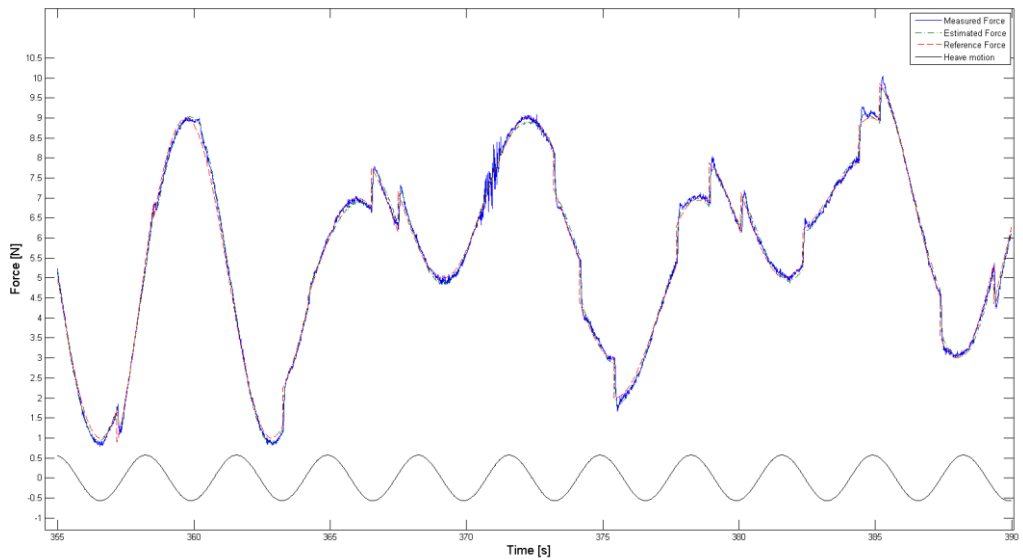


Figure 9.4: Random sinusoidal force reference with different amplitude and bias values changed under simulation. Sinusoidal force reference shown together with estimated and measured force (top) and heave motion (bottom).

Figure 9.5 shows a close up view when the bias to the sinusoidal reference force is changed. From the figure the settling time is found to be $T_s = 0.12$ [s]. This is the time it will take for

the measured force to reach its reference value. The estimated force filters the unwanted disturbance in the measured force properly.

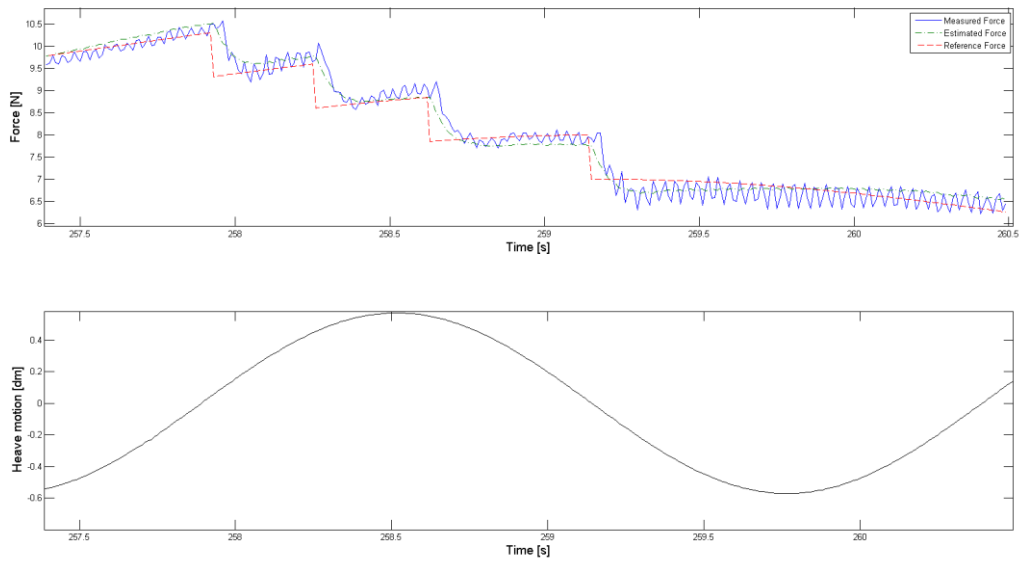


Figure 9.5: Sinusoidal force reference with different bias values changed under experiment shown together with estimated and measured force (top). The plot is shown together with the corresponding heave motion (bottom).

Figure 9.6 show a piecewise constant force reference plotted together with the measured and estimated force. From the figure the settling time is found to be $T_s = 0.15$ [s]. In this case there will be no heave motion of the oscillating system.

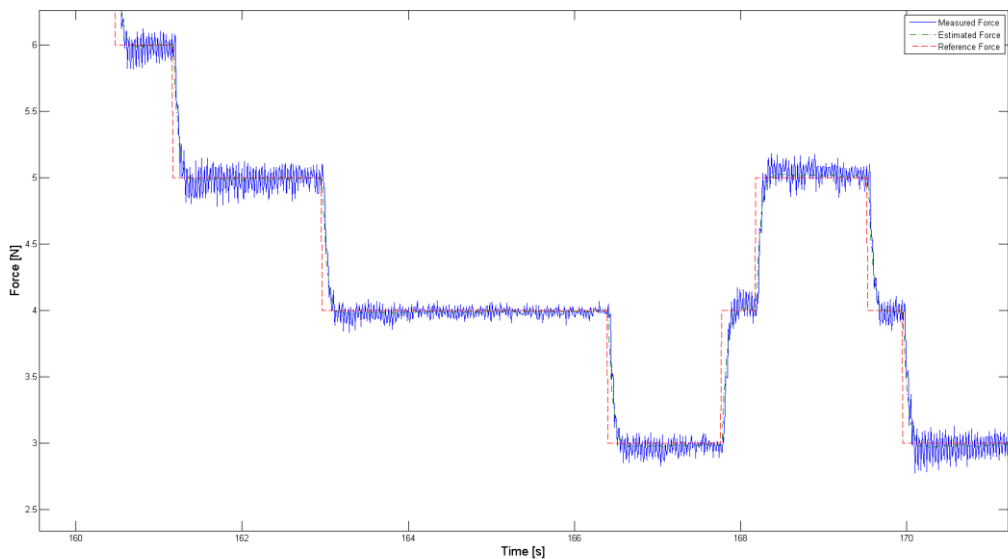


Figure 9.6: Force reference shown together with its measured and estimated force. The vertical motion from the oscillating system is set to be zero.

Several additional experimental results using a pretensioned spring without vertical heave motion are shown in Appendix 12.4. The experiments were done using a sinusoidal force reference and a zero order hold element, meaning that the signal is kept constant until the next sample instant. The Sample time in the zero order hold element is then gradually decreased.

With 10 ms sampling time the force reference will be a piecewise constant signal with 10 ms steps. The result using 10 ms sampling time is presented in Figure 9.7. The figure shows that the measured force have a good fit to the desired reference.

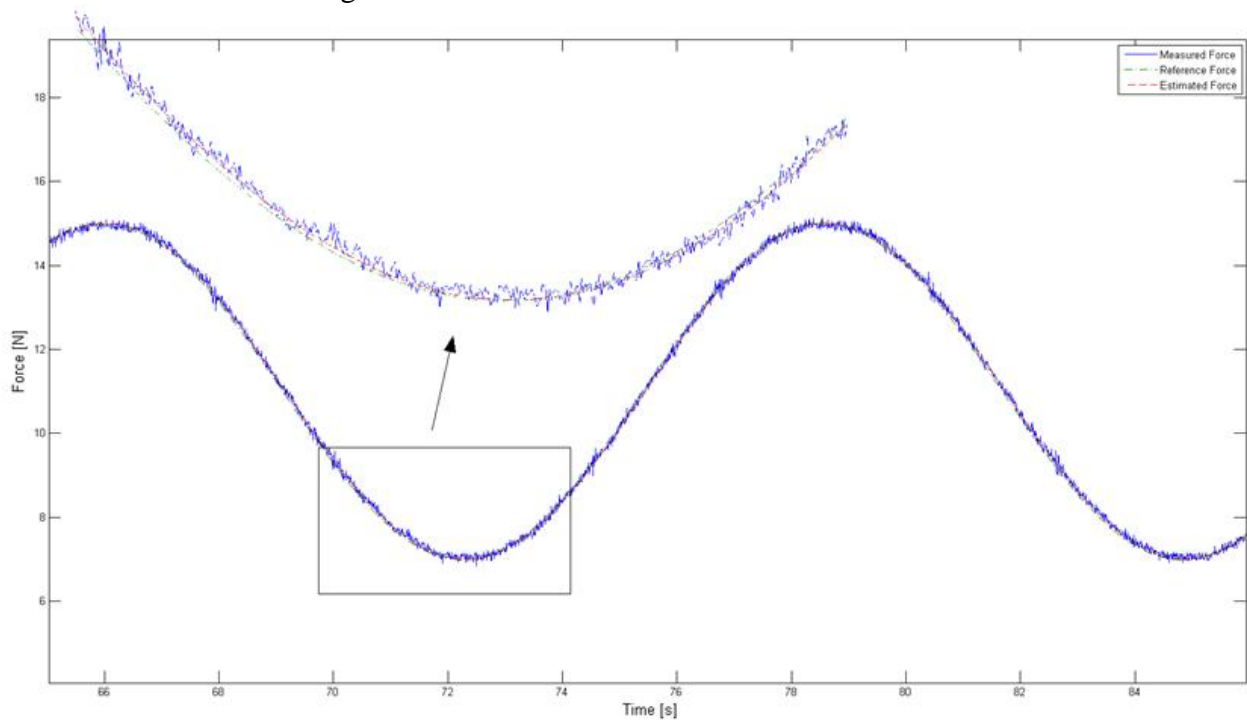


Figure 9.7: Estimated and measured force compared to a sinusoidal force reference with 10 ms zero order hold.

9.2 Case 2

The experimental setup for case two is shown in Figure 9.8. The “vessel in waves” will consist of the mass (vessel), spring and an oscillating system. The oscillating system will induce vertical motion representing the wave motion.

Figure 9.9 shows a detailed view of the key components in the experimental setup. The force ring is connected in-between the mass and a rope. The rope is then connected to the Faulhaber engine. Guidelines are used to guide the mass in the vertical direction and to prevent it from spinning and hitting the oscillating system frame.

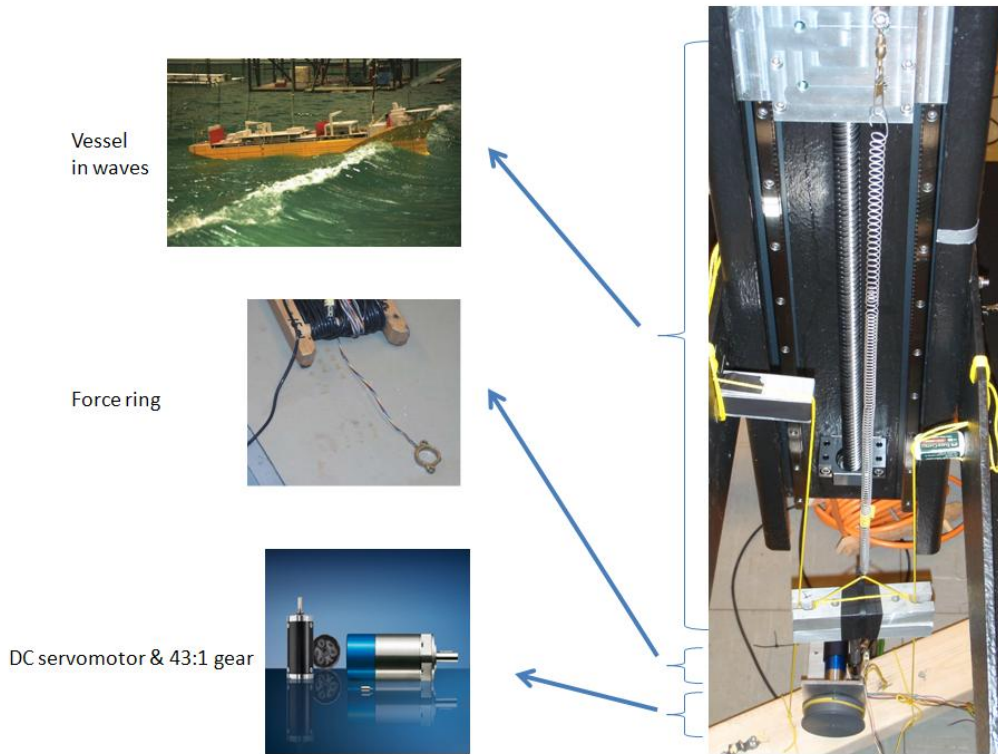


Figure 9.8: Experimental setup case 2.

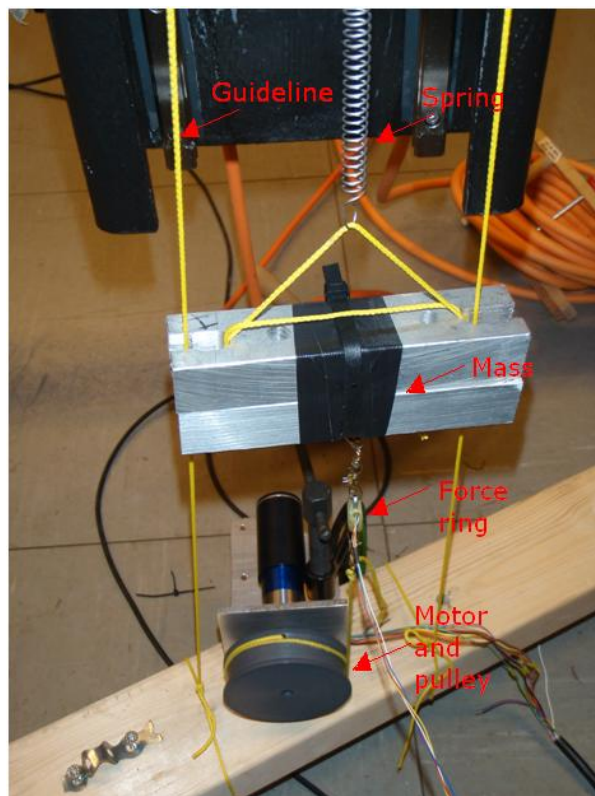


Figure 9.9: Detailed view of the experimental setup showing key components.

The estimated force used as feedback in the control system is set to be equal to $\hat{f}_m = K \cdot \hat{\theta} + C \cdot z$. K and C are found by experimental testing and their values are set to be equal to 0.005 and 4.85 respectively. z will represent the measured vertical wave motion to the oscillating system and is given as

$$z = \frac{1}{10}(u_\eta - 2) \quad (7.8)$$

where u is the voltage input from the oscillating system.

In Figure 9.10 a sinusoidal reference force is presented together with the measured force and estimated force using parameters given by Table 9.3. As seen from the figure the measured force is noisy but it follows the reference quite well. The vertical motion to the oscillating system is set to be a fixed sinusoidal motion with amplitude 0.057 m and frequency 0.1 Hz.

The bias to the sinusoidal force reference is then changed during the experiment. The force references together with the measured and estimated force are presented in Figure 9.11. The settling time is found to be $T_s = 1.2$ [s].

The controller manages to follow a random sinusoidal force reference quite well for low frequency vertical oscillating motions. A 1.2 second settling time is needed to reach the new sinusoidal reference when the bias in the reference is changed. As illustrated by Figure 4.3 given in J.M. Heurtier et al. (2001) the mooring line top tension is sinusoidal. The mooring line top tension has no discontinuity like the reference given by Figure 9.11. The control system should therefore be able to follow a sinusoidal reference of the form presented in J.M Heurtier et al. (2001). However, if the vertical oscillating motion frequency is set to be too high disturbances in the system gets significant, this will be a limiting factor.

Experiments using zero vertical oscillating motion are also conducted. A piecewise constant signal is used as force reference. The measured and estimated forces from the experiment are presented with its force reference in Figure 9.12. The settling time is found to be $T_s = 0.95$ [s], and the measured signal has a transient. The mass included in the system will induce disturbances into the system, but as seen in the figure the estimated force will filter away much of this disturbance.

Observer gains	Controller gains	Mass	Sinusoidal vertical motion generated by the oscillating system
$K_1=1500$	$k_p=0.4$	$m=0.64$ [kg]	Amplitude=0.057 [m]
$K_2=1900$	$k_i=2$		Period=10 [s]
$K_3=1800$	$k_d=0$		Frequency=0.1 Hz
$K_4=1500$			

Table 9.3: Parameter values.

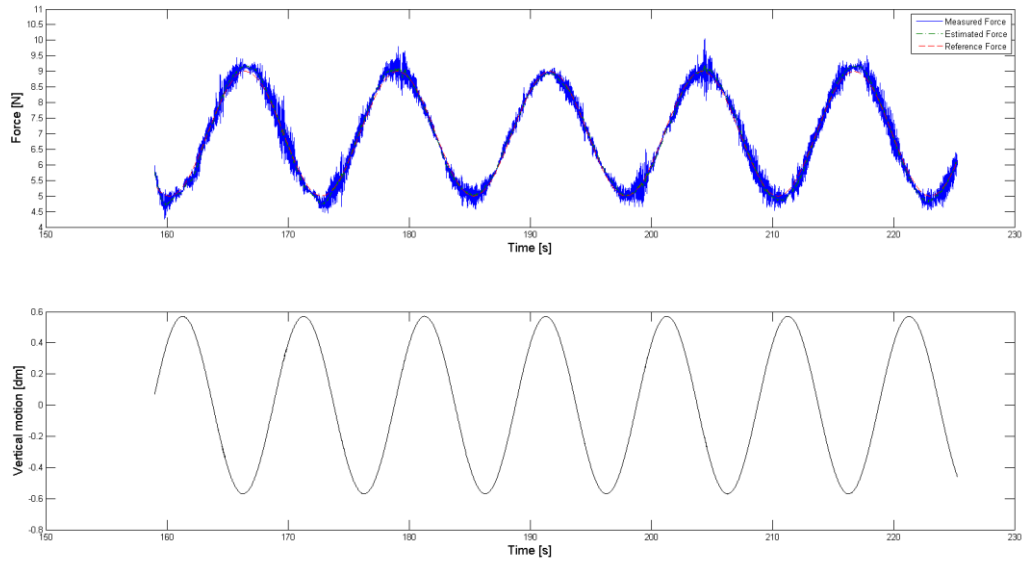


Figure 9.10: Experimental result using parameter values in Table 9.3. The sinusoidal reference, measured and estimated force (top) are shown together with the vertical motion to the oscillating system (bottom).

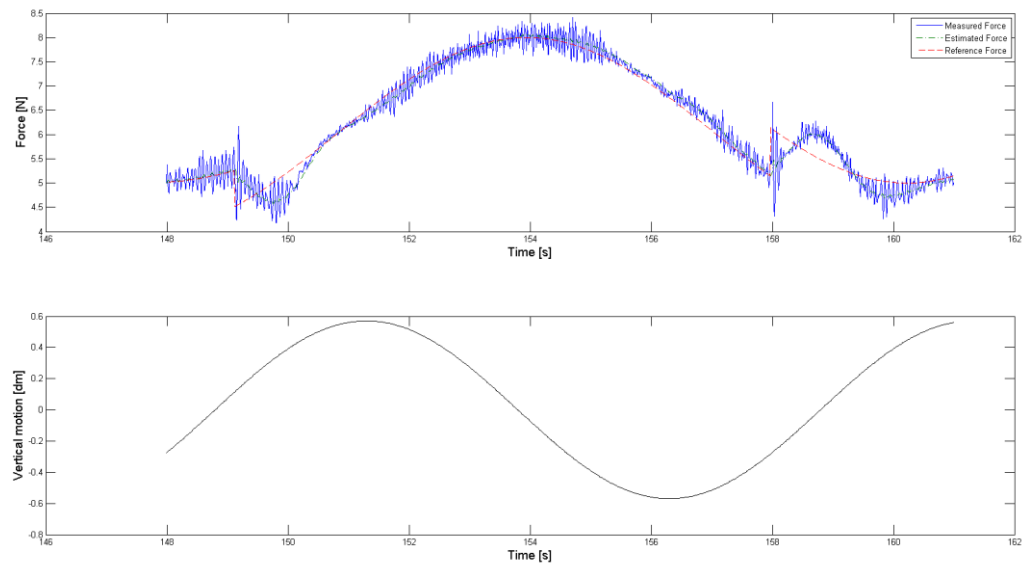


Figure 9.11: The sinusoidal reference, measured and estimated force (top) are shown together with the vertical motion to the oscillating system (bottom), using different bias in the sinusoidal reference force.

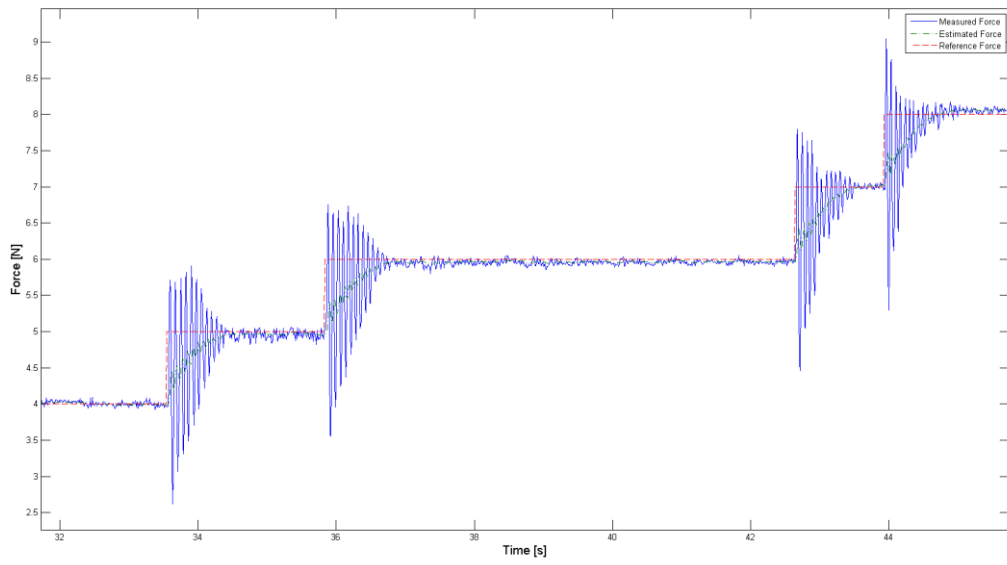


Figure 9.12: Force reference shown together with the measured and estimated force. The vertical motion from the oscillating generator is set to zero.

9.3 Discussion

The model tests indicate that the control system in case two is able to follow a sinusoidal force reference when the frequency of the vertical oscillating motion generated is low. When the frequency gets higher, more disturbance is introduced due to the vertical motion of the mass, a modified controller with smaller proportional gain and a relative high integral effect is needed. The need for high integral effect compared to the proportional gain is to compensate for the increased disturbance.

The calculated mooring line vertical forces, for a given heave motion, show good accordance to the measured force from experiments in case one. The vertical motion to the oscillating system is set to be equal to the desired heave motion. The Faulhaber engine will then try to actuate the calculated forces due to this motion, on to the oscillating system, or vessel in this case. The result shows good resemblance between the calculated mooring forces and actuated forces, although some disturbances are induced at the top peaks. A better result is achieved for a vertical heave motion with lower frequency, and lower observer gains.

9.3.1 Challenges

The mass and spring stiffness chosen in the experiments do not correspond to the model scale water plane stiffness and model scale mass for a realistic vessel model. A realistic vessel model built in scale 1:70 has a length of 1.2 meter and a mass of approximately 15 kg, ref Corneliussen, J. , (2003) - Cybership 2. To use a model like this in the experiments proved to be difficult to achieve.

During the experiments, some problems were discovered. One of the problems was that it was difficult to store the information in the Simulink® model real-time for 100 Hz fundamental sampling frequency. If too many *.mat files were used to store signals in the Simulink® diagram an error in the LabVIEW® interface will occur. The loop will have problem running if too many *.mat files are stored on to the cRIO hard drive when running the compiled Simulink® model in LabVIEW® .

A second problem discovered was that the mass will not be constrained to only vertical motion. In an attempt to avoid this problem guidelines were used to guide the mass in the vertical direction. However, this method should be improved.

At first the force measurements were noisy and corrupted. A wire that grounded the negative cord was needed to achieve proper force measurements.

To assume that the spring force in the experiment will be a simple linear approximation will be a strong assumption. In most instances Hook's law is not precise and the spring behavior will not always be elastic.

The DC motor parameters are not optimized for case two when the mass is included. Preferably, proper input output data should have been collected using this setup. However, the observer will filter away much of the disturbance introduced due to the mass.

The observer and controller gains are found by trial and error. Optimal gains should preferably have been established.

10 Conclusions

This chapter summarizes the results obtained in this master's thesis, and proposes areas that need further investigation and analysis.

10.1 Conclusion

This thesis has focused on the experimental setup and control of the mooring line forces actuated on to a simplified vessel model. More specifically, it is considered how desired forces can be induced correctly in real time on to a vessel model moving in 1 DOF. The main conclusion is that it may be possible to follow desired simulated mooring forces for a sinusoidal heave motion of the vessel.

The method of actuating forces onto a vessel model with 6 DOF using a motor-winch configuration was modified in order to make it easier to study. A simplified 1 DOF dynamic system, including an actuator representing the mooring line, was developed to investigate the performance of the control system actuating the mooring line forces.

The simplified vessel model moving in heave direction is mathematically modeled. The mass dynamics and motor dynamics to the system are derived and explained. The unknown parameters in the model have been found, and the simulated outputs from the model are compared to measurement data from experiment. The simulated model outputs show good resemblance with the measured. However, proper model parameters with a mass included in the system should be looked further into.

Further, an experimental setup of the system is developed and appropriate procurement of parts necessary has been obtained. To induce correct mooring line forces, in model scale, reasonable peak values for the expected mooring line top tension has been used in the decision process to find an appropriate actuator. The actuator, or Faulhaber electrical motor, has no problems inducing the desired peak values. The drive electronics for the electrical motor has a wide variety of control options, and control of the motor shaft torques, necessary to obtain desired forces, is possible. However, there will be a limitation in how fast these desired forces are reached. The frequency to the vessel heave motion will be a critical factor.

Experiments show that the control system is able to actuate the correct mooring line vertical component on to a vessel model moving in a specific sinusoidal heave motion, although some disturbances are induced at the top peaks. A lowered heave motion frequency will reduce this disturbance. The model scale considered is chosen to be 1:70, the frequency will then be high (small period) since time is scaled with the square root of the model scale. A more favorable heave motion frequency using for example 1:40 as model scale would be preferred.

Real time measurements of the heave motion are used to find the corresponding mooring line forces. The corresponding mooring line forces are calculated in forehand using RIFLEX, such that a lookup table can be used to find the corresponding force for a given real time heave motion, however this puts a constraint on the vessel heave motion. Preferably, RIFLEX should be connected to the system to calculate these forces real time using an UDP or Ethernet connection. Correct mooring line forces may then be calculated when the vessel

heave motion is changed to a sinusoidal movement different from the specific heave motion used in the experiment.

Experiments using given mooring force references were also conducted to investigate the performance to the control system. A given force reference will give a good indication on whether the induced force reference from the control system manage to follow the mooring force reference appropriately, despite the fact that the force reference to a real mooring line will be different. With a lowered heave motion frequency the induced force by the actuator follow the force reference better. When the sinusoidal reference is changed instantaneously to a different set point it will take about 120 ms for the control system to follow the new sinusoidal reference.

In case one the control system is able to actuate the desired forces within 150 ms for a piecewise constant reference, assuming the vertical heave motion is set to zero. For case two the vertical disturbance due to the mass will increase this settling time to 950 ms. When the force reference is set to be sinusoidal and the vertical generator motion is set to be different from zero, the actuator will be able to actuate the desired sinusoidal forces used in the experiments. When the mass is included more disturbances will occur in the system, and a lower proportional gain, as well as a relative high integral gain is needed to counter act the disturbance. The estimated force will filter away much of the induced disturbance due to the mass, hence avoiding a jagged motion at the motor shaft.

Finally, an assessment of the necessary sampling frequency has been conducted. A 50 Hz sampling frequency will be necessary to recreate the continuous time responses for a vessel model moving in three DOF exposed to force inputs. The vessel model is considered to be a barge exposed to a regular wave with 7 seconds period and 2 meter amplitude. A frequency response analysis from the force inputs to the vessel responses are used to determine the highest frequency in the system (bandwidth). The bandwidth is then used to determine the necessary sampling frequency to recreate the signals without loss of information.

10.2 Recommendations for Further Work

The LabVIEW® program interface must be modified using a custom I/O. The custom I/O must be programmed to send the measured heave motion as an output signal. RIFLEX must then be set to receive this signal calculate the desired mooring force due to this motion and send the calculated mooring force signal back to LabVIEW®. Calculated mooring line forces will then be available for different vessel heave motion. The calculated mooring force must be used as reference in the control system. UDP can be used to communicate between LabVIEW® and RIFLEX.

As a next step the system can be expanded to three DOF. The actuator motor-winch configuration can then be arranged as proposed in Figure 2.5. An oscillating system moving in three DOF must then be used. The surge, pitch and heave motion measurements must be sent to RIFLEX to calculate desired resulting forces. The motor-winch configuration applied together with a control allocation scheme, in the vertical plane, can then be utilized to actuate the calculated resulting forces on to the oscillating system. An oscillating system that is able to move in three DOF must then be utilized. The oscillating system actuator mounted on the MC carriage may be a possible solution.

When considering the mass connected to the spring and oscillating system, optimal model parameters should preferably be established using measurement data for this system. The controller and observer gains can be found using optimization methods. A realistic vessel mass and spring stiffness should have been used, hence a more accurate model.

RS232 communication can be used to set the velocity of the motor shaft instead of the analog voltage input as used in this thesis. The velocity can then be preset by sending commands from LabVIEW® to the Faulhaber drive electronics.

11 Bibliography

- Aarsnes, J. V., & Steen., S. (2008). Lecture Notes UK-2008-4. In *Experimental Methods in Marine*. Department of Marine Technology, The Norwegian University of Science and Technology.
- Argyros, A., Langley, R. S., & Ahilan, R. V. (2009). New Study Aims to Simplify Mooring Analysis for Deepwater Systems. *Scandinavian Oil and Gas Magazine* , 37, 52-54.
- Åström, K. J., & Wittenmark, B. (1997). *Computer Controlled Systems: Theory and Design* (Third ed.). Prentice-Hall International.
- Balchen, J. G. (1990). Rational transfer function approximations to transport delay. In *Modeling, Identification and Control* (Vol. 11, pp. 127-140).
- Balchen, J. G., Andresen, T., & Foss, B. A. (2003). *Reguleringsteknikk*. Trondheim: Tapir.
- Buchner, B. (1999). Model test challenges for deep water floaters. *MARIN, The Netherlands* .
- Buchner, B., Wichers, J., & de Wilde, J. (1999). Features of the State-of-art Deepwater Offshore Basin. *OTC paper no. 10814*. Houston: Offshore Technology Conference.
- Chen, C.-T. (1999). *Linear systems Theory and Design*. New York: Oxford university press.
- Corneliussen, J. (n.d.). Retrieved from http://www.itk.ntnu.no/ansatte/Fossen_Thor/MSc/JorgenCorneliussen.pdf
- DC Motor Specifications*. (n.d.). Retrieved from Faulhaber: http://www.faulhaber.com/uploadpk/EN_3564B_MIN.pdf
- DNV. (2007). DNV-RP-C205 Environmental Conditions and Environmental Loads. *Recommended Practice*.
- Egeland, O. (1993). *Servoteknikk*. Trondheim: Tapir.
- Faltinsen, O. M. (1990). *Sea loads on ships and offshore structures*. Trondheim: Cambridge ocean technology series.
- Fossen, T. I. (2002). *Marine Control Systems - Guidance, Navigation, and Control of Ships, Rigs and Underwater Vehicles*. Trondheim: Tapir Trykkeri.
- Gear Specifications*. (n.d.). Retrieved from Faulhaber: http://www.faulhaber.com/uploadpk/EN_301_MIN.pdf
- Hesphana, J. P. (2009). *A Course in Linear Systems Theory*. Princeton, New Jersey: Prinecton Press.
- Hüche, E. (1996). *Digital Signal Handling*. Århus: Teknisk Forlag A/S.
- Huse, E., Kleiven, G., & Nielsen, F. G. (1998). Large Scale Model Testing of Deep Sea Risers. *OTC Paper no. 8701*. Houston.

- Instruction Manual*. (n.d.). Retrieved from Faulhaber:
http://www.faulhaber.com/uploadpk/EN_MCxx3003-06S_im_Rev4_DFF.pdf
- J.M. Heurtier, P. L. (2001). Coupled Dynamic Response of Moored FPSO with Risers. *International Offshore and Polar Engineering Conference*, (p. 8). Stavanger.
- MARINTEK, & Chevron. (2008). *MARINTEK and Chevron Energy Technology Company extend the limits of ultra-deepwater model testing*. Retrieved from
<http://www.sintef.no/Home/Marine/MARINTEK/MARINTEK-Publications/MARIN...>
- Ormberg H. and Larsen, K. (1998). Coupled analysis of floater motion. *Applied Ocean*, 20, pp. 55-67.
- Perdikaris, G. A. (1991). *Computer Controlled Systems: Theory and Application*. Springer.
- Pettersen, B. (2007). *Hydrodynamikk* (Vols. UK-2004-75). Trondheim: Tapir.
- Sagatun, T. I. (n.d.). Retrieved from Vessel-Crane Moonpool Specifications:
<http://www.itk.ntnu.no/research/HydroLab/reports/specrevised.pdf>
- SNAME. (1950). The Society of Naval architects and Marine Engineers. Nomenclature for Treating the motion of Submerged Body Through a Fluid. In *Technical and Research Bulletin No. 1-5*.
- Søgaard, M. (n.d.). *Staubo Elektro-Maskin AS*. Retrieved February 2010, from
<http://www.staubo.no/kontakt.html>
- Stansberg, C. T., Ormberg, H., & Oritsland, O. (2002). Challenges in Deep Water Experiments: Hybrid Approach. *Journal of Offshore Mechanics and Arctic Engineering* , 124, 90-96.
- Stansberg, C., Karlsen, S., Wichers, J., & Irani, M. (2004). Model Testing for Ultradeep Waters. *OTC paper no. 16587* .
- The MathWorks*. (n.d.). Retrieved February 2010, from
<http://www.mathworks.com/access/helpdesk/help/toolbox/control/getstart/f1-1010549.html#f1-1011876>
- The MathWorks*. (n.d.). Retrieved from <http://www.mathworks.com/>
- Watts, S. (1999). Hybrid Hydrodynamic Modelling. *Offshore Technology* (7), 13-17.
- Yu, G.-R., & Hwang, R.-C. (2004). Optimal PID control of Brushless DC Motors Using LQR Approach. *IEEE International Conference on Systems, Man and Cybernetics*.

12 Appendix A

12.1 Motion controller and Computer Software

An overview of the Faulhaber motion controller circuit for the DC motor running in speed mode is shown in Figure 12.1.

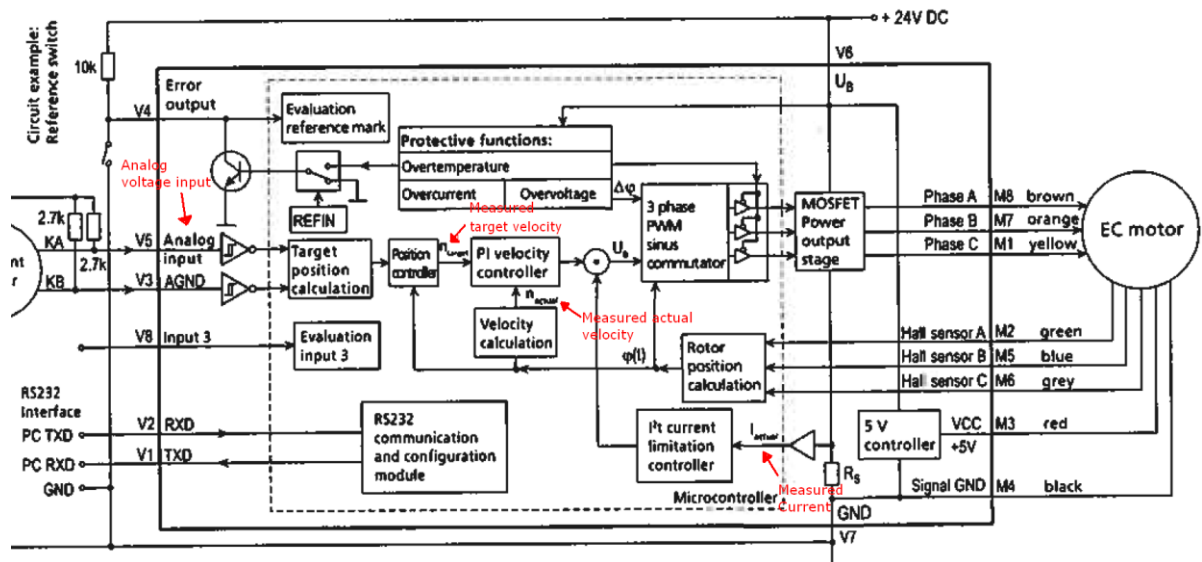


Figure 12.1: Circuit for the Overview - MCBL 3003S

The LabVIEW® interface is shown in Figure 12.10.

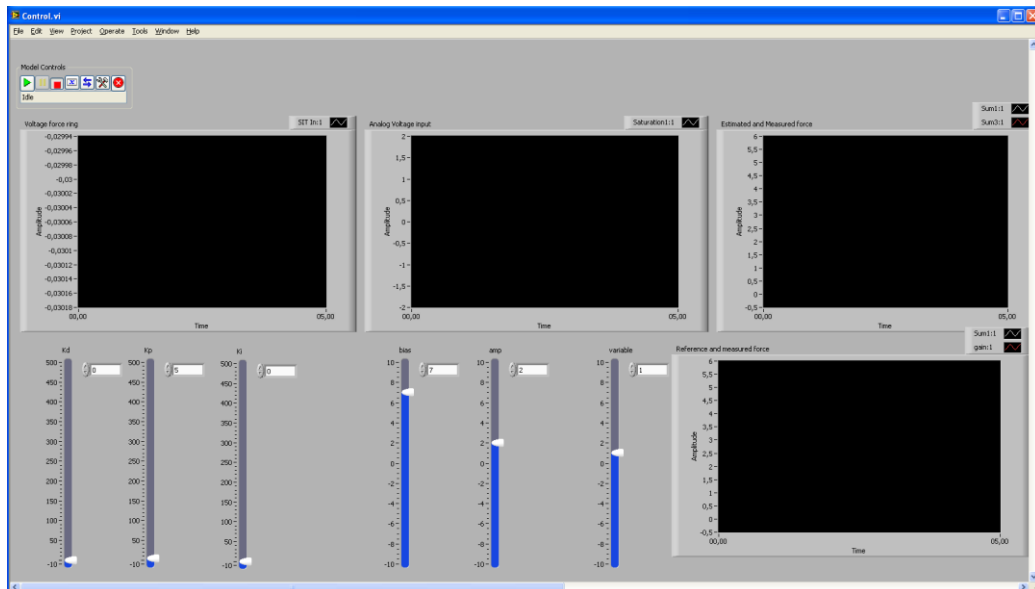


Figure 12.2: LabVIEW® VI used for control of DC motor.

12.2 Parameter DC motor Calculations using System Identification Toolbox

Calculations performed by Matlab® system identification toolbox, to find appropriate DC parameters in the model to fit the output data. Calculations performed by Matlab® are shown in

Time-continuous nonlinear state-space model defined by 'twobodies_m' (m-file):

$$\begin{aligned} dx/dt &= F(t, u(t), x(t), p1, \dots, p6) \\ y(t) &= H(t, u(t), x(t), p1, \dots, p6) + e(t) \end{aligned}$$

with 1 input, 4 states, 2 outputs, and 6 free parameters (out of 6).

Input:

u(1) Target Velocity(t) [rad/s]

States:

Initial value

x(1) error(t) [-]	xinit@exp1	-0.990949	(est) in [-Inf, Inf]
x(2) angle(t)	xinit@exp1	-893.588	(est) in [-Inf, Inf]
x(3) Actual velocity(t)[rpm]	xinit@exp1	12.4466	(est) in [-Inf, Inf]
x(4) Current(t) [mA]	xinit@exp1	3.25606	(est) in [-Inf, Inf]

Outputs:

y(1) Actual velocity(t) [rpm]
y(2) Current(t) [mA]

Parameters:

	value	standard dev	
p1 Jm [kgm^2]	0.0021399	0.000641746	(est) in [-Inf, Inf]
p2 Kt [Nm/A]	1.51175	0.719261	(est) in [-Inf, Inf]
p3 Kf [Nm/(rad/s)]	0.461112	0.220075	(est) in [-Inf, Inf]
p4 Ra [Ohm]	0.391492	0.33844	(est) in [-Inf, Inf]
p5 Ke [V/(rad/s)]	0.0309026	0.244718	(est) in [-Inf, Inf]
p6 La [H]	0.00416976	0.00238501	(est) in [-Inf, Inf]

The model was estimated from the data set 'twobodies_m', which contains 501 data samples.

Loss function 2.34775e+007 and Akaike's FPE 2.40398e+007

Created: 06-Jun-2010 14:03:13

Last modified: 06-Jun-2010 14:12:55

The model was estimated from the data set 'twobodies_m', which contains 501 data samples.

Loss function 2.36408e+007 and Akaike's FPE 2.42071e+007

Last modified: 06-Jun-2010 13:59:31

Table 12.1: Model parameter estimation from given input output data.

Criterion: Trace minimization
 Scheme: Trust-Region Reflective Newton (LSQNONLIN,
 LargeScale = 'On')

Iteration	Norm of Cost	First-order step	optimality
0	6615.14	-	-
1	6466.95	10	2.74e+008
2	6464.44	20	9.4e+007
3	6463.15	40	5.06e+006
4	6462.28	80	5e+007
5	6460.62	160	5.24e+006
6	6459.35	162	1.58e+007
7	6457.77	162	3.91e+007
8	6454.74	162	6.68e+006
9	6454.74	162	6.68e+006
10	6454.73	40.5	3.87e+007
11	6454.36	10.1	1.05e+007
12	6453.78	20.2	1.01e+007
13	6453.7	40.5	6.77e+006
14	6453.7	10.1	6.77e+006
15	6453.7	2.53	6.77e+006
16	6453.7	0.632	6.77e+006
17	6453.7	0.158	6.77e+006
18	6453.7	0.0395	6.77e+006
19	6453.7	0.00988	6.77e+006
20	6453.7	0.00247	6.77e+006

Table 12.2: Trace minimization performed by Matlab®.

12.3 Sesam

The Sesam software developed by DNV(Det Norske Veritas) give the hydrodynamic data. The panel model was made using Genie and the analysis using Hydro-D.

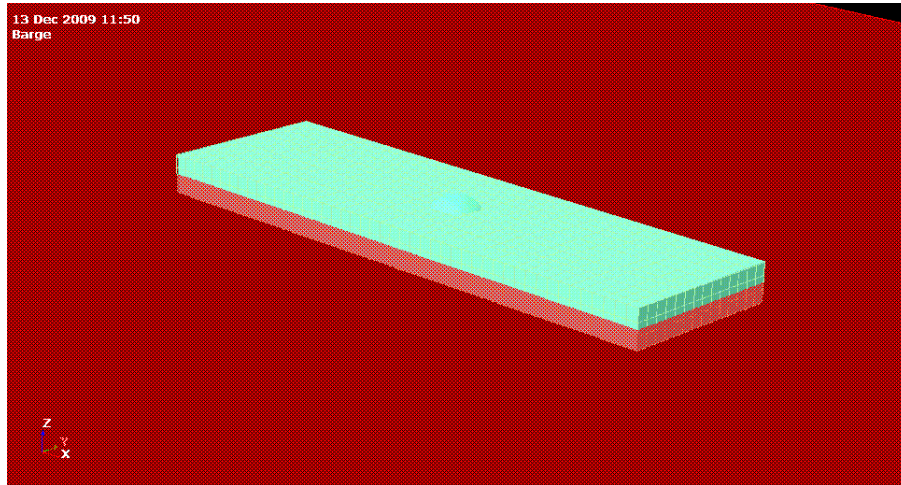


Figure 12.4: Genie model in Hydro-D.

Property	Value	Denomination
Frequency set	0.5:0.5:20	s
Depth	2000	m
Kinematic viscoisity	1.19e-6	m/s^2
Gravity	9.080665	m/s^2
Direction	0	rad
Density	1025	kg/s^2
Quadratic element mesh	2*2	m
Number of elements	1648	-

Figure 12.5:Parameter input for Hydro-D.

We used the parameters in Figure 12.5 to find the transfer functions, phases to find the necessary matrixes for the given case with wave amplitude $\zeta_a = 2$ m and wave period $T = 7$ s.

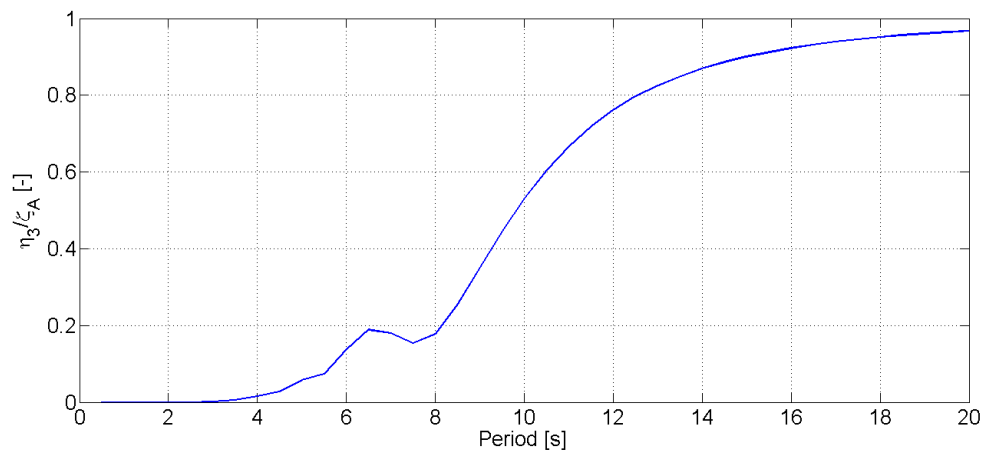


Figure 12.6: Hydrodynamic transfer function in heave.

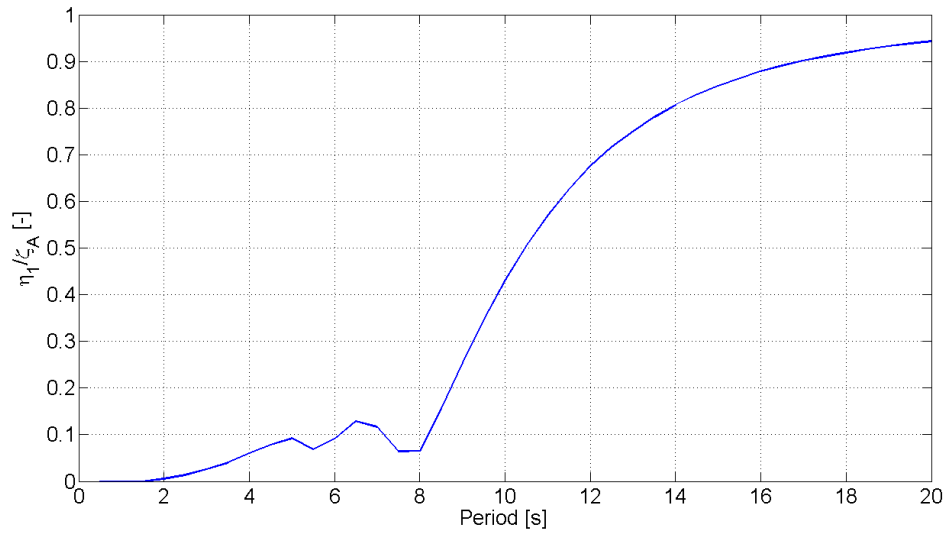


Figure 12.7: Hydrodynamic transfer function in surge.

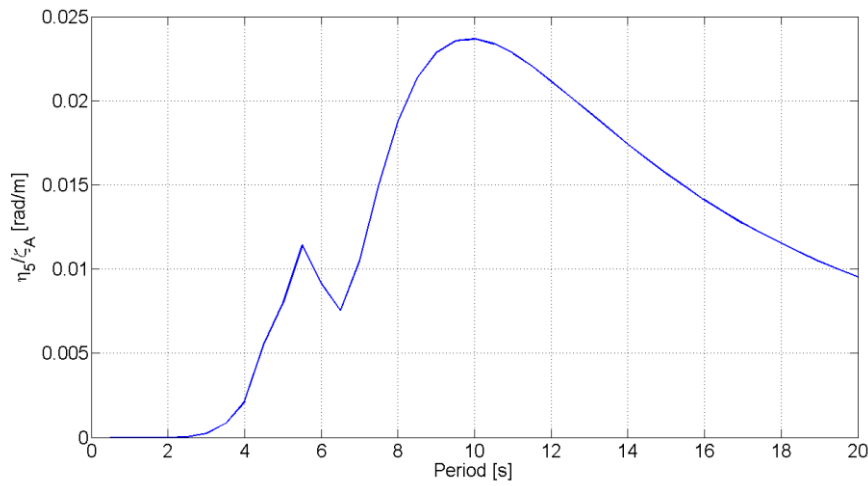


Figure 12.8: Hydrodynamic transfer function in pitch.

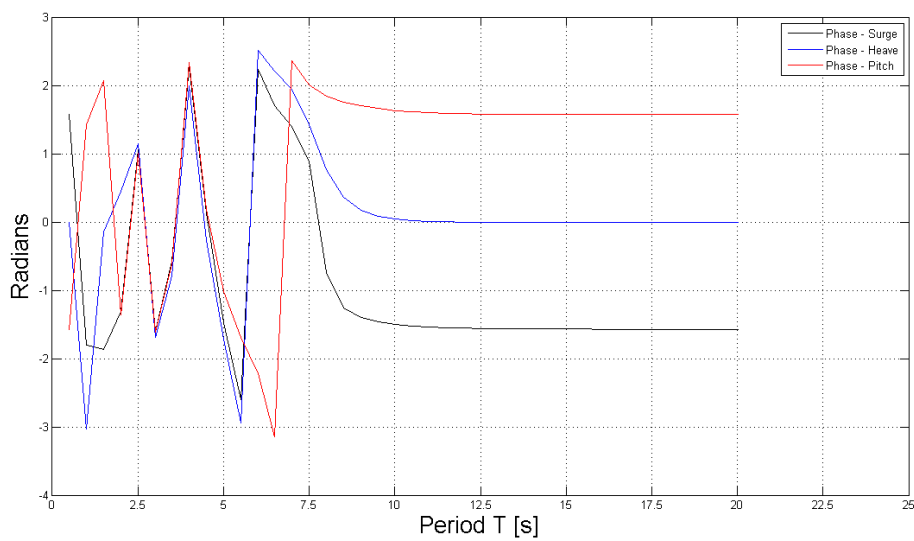


Figure 12.9: Hydrodynamic transfer function phase.

12.4 Piecewise Constant References

The wave motion is set to be zero, and the DC motor is connected to a pretensioned spring in the roof. The plots below show the measured, reference and estimated force. The control parameters are set to be equal to $k_{p1} = 5$, $k_{i1} = 0$ & $k_{d1} = 0$ and the observer parameters are set to be $K_1 = 400$, $K_2 = 320$, $K_3 = 310$ & $K_4 = 200$. The force reference is chosen to be a sinusoidal signal with a zero order hold element. With zero order hold sampling time set to 2 seconds the piecewise constants signal change its set point to a new value after 2 seconds, as presented in the figure.

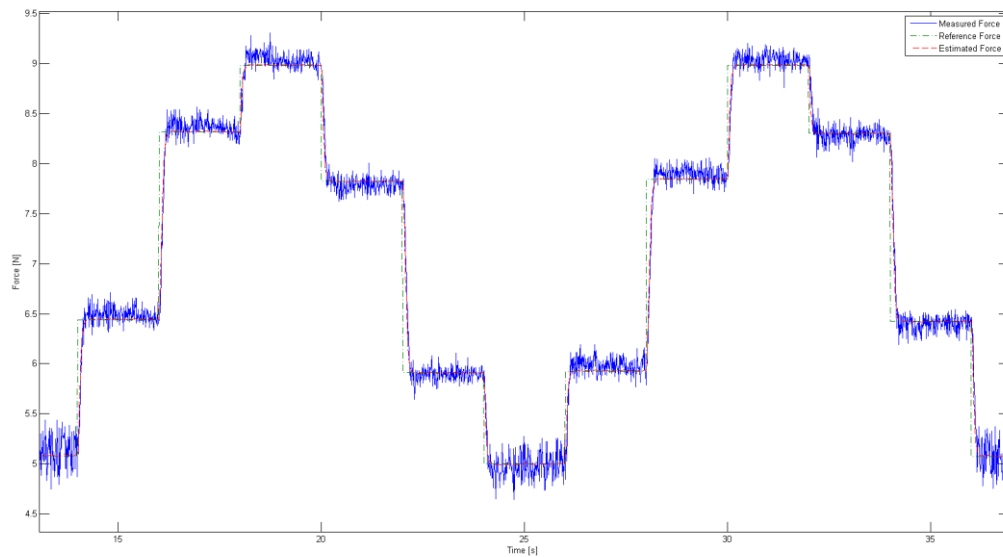


Figure 12.10: Estimated and measured force compared to a sinusoidal reference force with 2 sec zero order hold.

The zero order hold element is increased to 500 ms. The piecewise constant reference is shown together with the measured and estimated force.

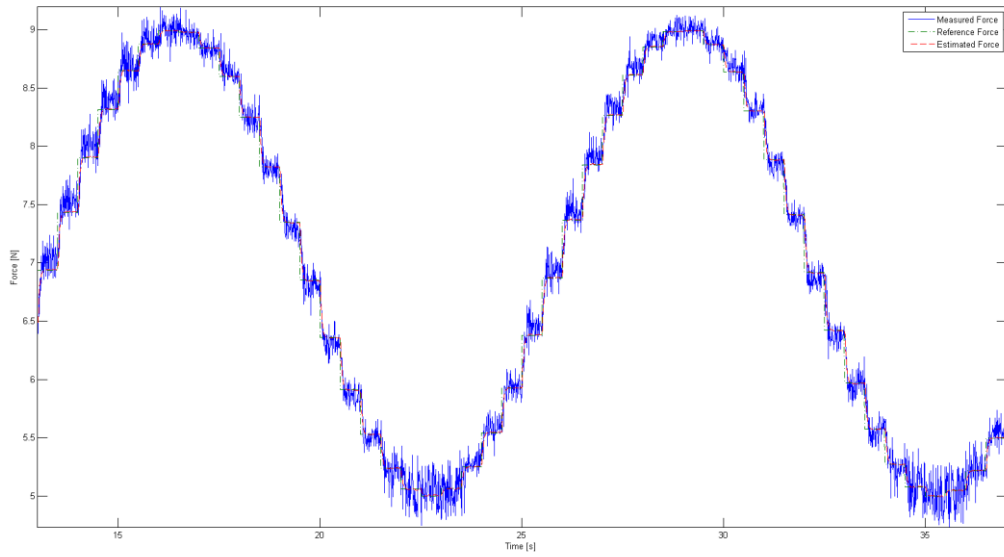


Figure 12.11: Estimated, measured force compared to a sinusoidal force reference with 500 ms zero order hold.

The zero order hold element sampling time is lowered even more to 250 ms and 100 ms in the following figures.

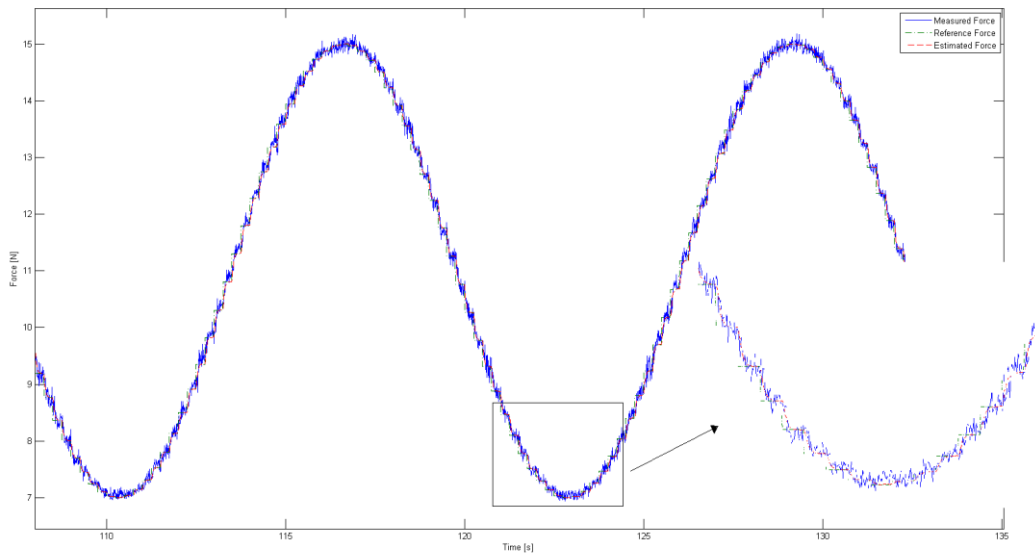


Figure 12.12: Estimated, measured force compared to a sinusoidal force reference with 250 ms zero order hold.

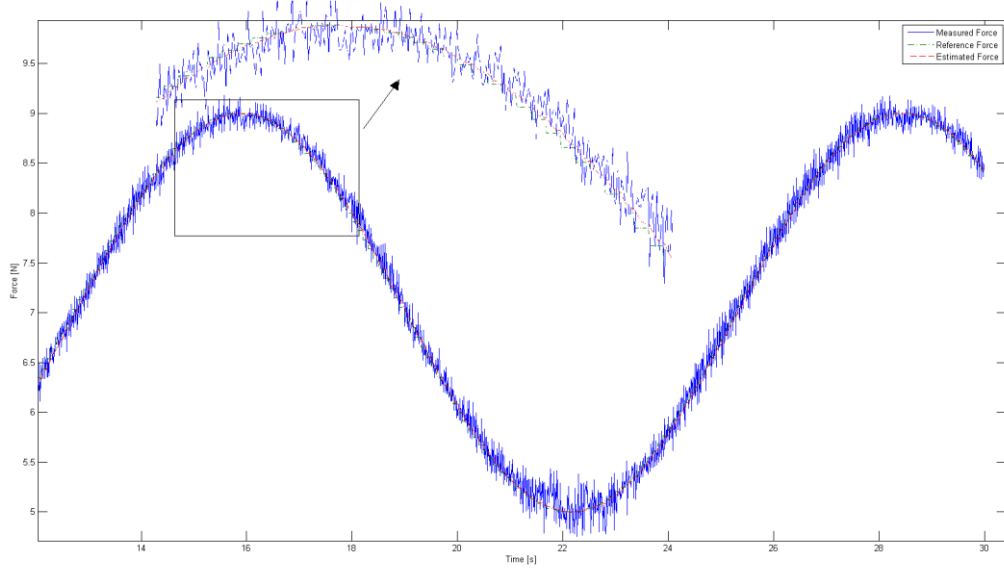


Figure 12.13: Estimated, measured force compared to a sinusoidal force reference with 100 ms zero order hold.

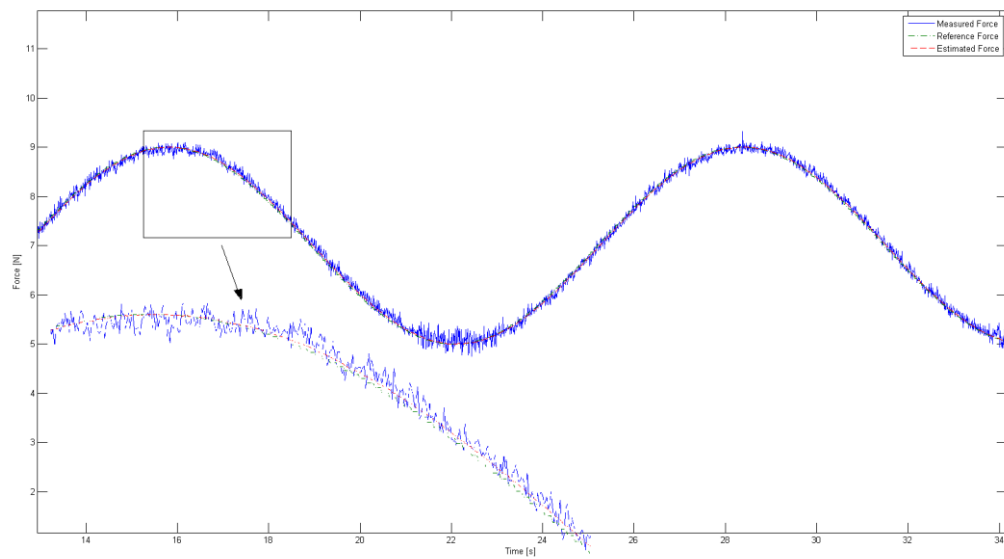


Figure 12.14: Estimated, measured force compared to a sinusoidal force reference with 50 ms zero order hold.

12.5 Frequency Responses

The frequency response from the force inputs X , Z and moment M to the surge velocity u are shown in Figure 12.15. By looking on the figures the DC gains and the systems bandwidths can be found.

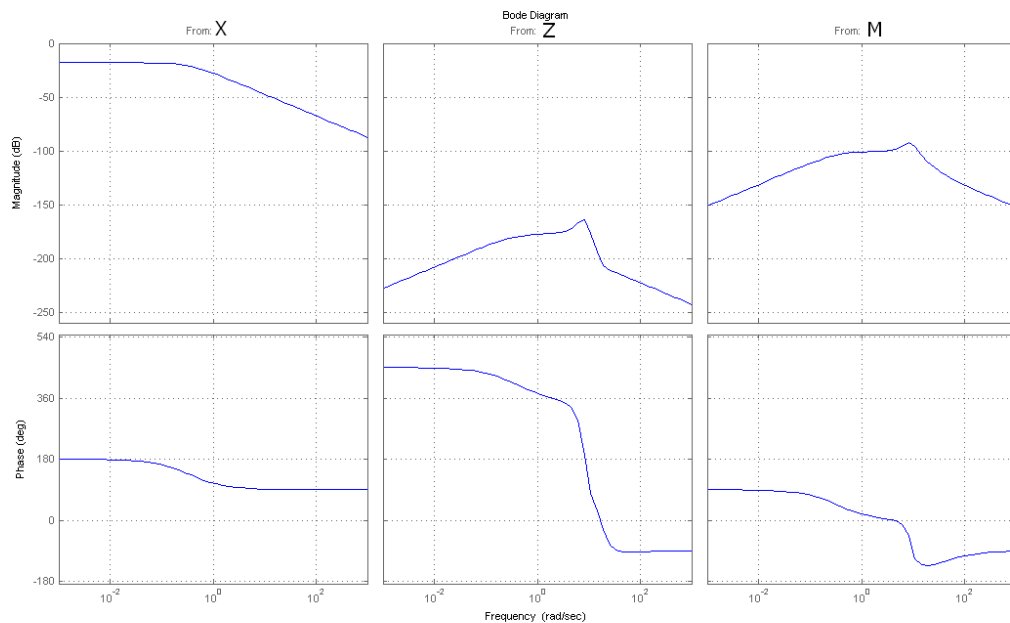


Figure 12.15: Frequency response for the transfer functions from the force inputs to the surge velocity.

When $\mathbf{C} = [0 \ 0 \ 0 \ 0 \ 1 \ 0]$ the output will be $y = w$ and the frequency response can be found. Figure 12.16 show the frequency response from the three inputs $\mathbf{u} = [X \ Z \ M]^T$ to the velocity output in heave w . All the DC gains are zero in this case.

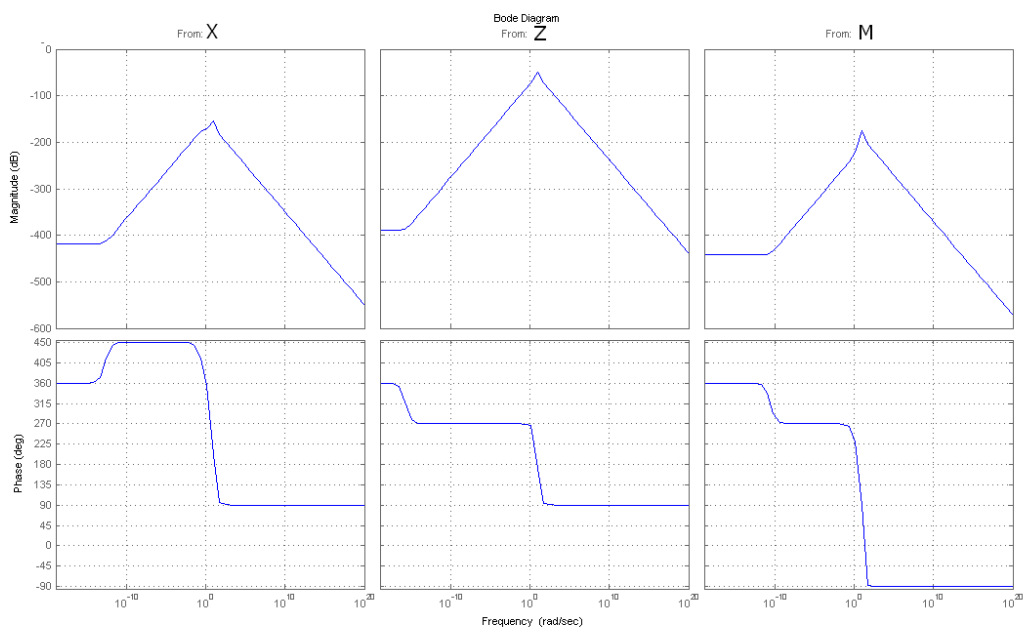


Figure 12.16: Frequency response for the transfer functions from the force inputs to the heave velocity.

The poles and zeros to the system with input \mathbf{u} and output w are shown in Figure 12.17. Implying that the system is stable since all its poles are in the L.H.P.

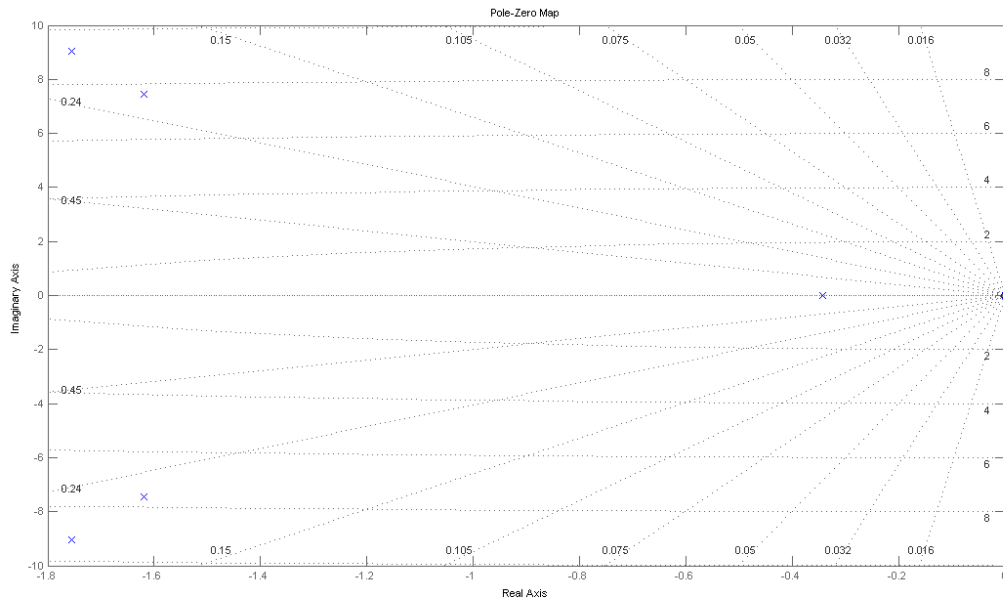


Figure 12.17: Poles ‘x’ and zeros ‘o’ for the system with heave velocity as output.

With, $\mathbf{C}=[0 \ 0 \ 0 \ 0 \ 0 \ 1]$, the output will be $y = q$. The frequency response from the three inputs $\mathbf{u}=[X \ Z \ M]^T$ to the output q are shown in Figure 12.18.

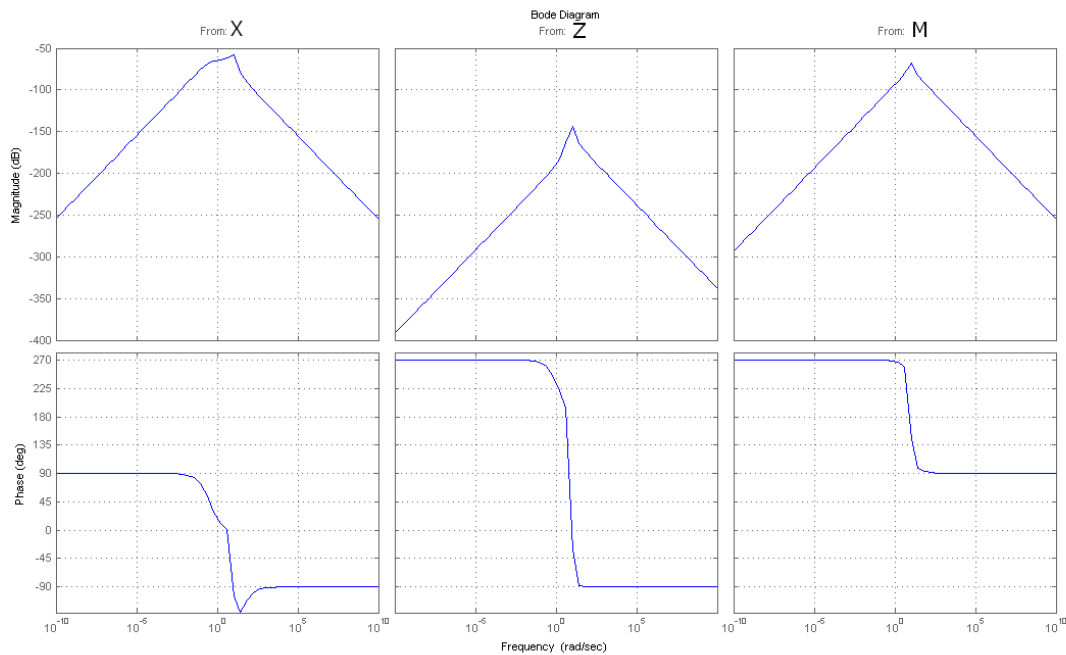


Figure 12.18: Frequency response for the transfer functions from the force inputs to the angular velocity in pitch.

In this case the DC gain will be zero and the bandwidth frequency will be high. The poles and zeros are given in Figure 12.19. The system is stable since it has all the poles in the L.H.P.

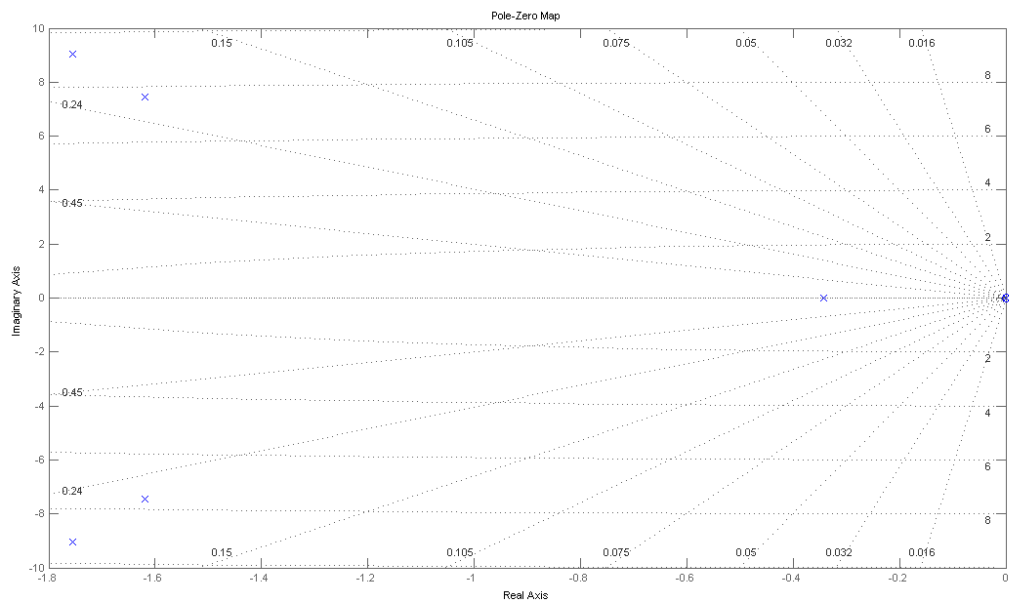


Figure 12.19: Poles 'x' and zeros 'o' for the system with angular velocity in pitch as output.